



UNIVERSITÀ DEGLI STUDI DI TRIESTE

**XXX CICLO DEL DOTTORATO DI RICERCA IN
NANOTECNOLOGIE**

**INNOVATIVE APPROACH FOR THE TREATMENT
AND THE DIAGNOSIS OF RHEUMATOID
ARTHRITIS EXPLOITING POLYMERIC
BIODEGRADABLE NANOPARTICLES
TARGETING SYNOVIAL ENDOTHELIUM**

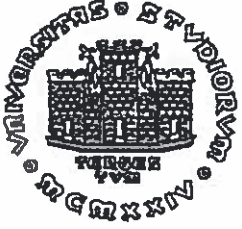
Settore scientifico-disciplinare: **MED/04**

DOTTORANDO
Federico Colombo

COORDINATORE
Prof.ssa Lucia Pasquato

SUPERVISORE DI TESI
Paolo Macor, PhD

ANNO ACCADEMICO 2016/2017



UNIVERSITÀ DEGLI STUDI DI TRIESTE

XXX CICLO DEL DOTTORATO DI RICERCA IN

NANOTECNOLOGIE

**INNOVATIVE APPROACH FOR THE TREATMENT
AND THE DIAGNOSIS OF RHEUMATOID
ARTHRITIS EXPLOITING POLYMERIC
BIODEGRADABLE NANOPARTICLES
TARGETING SYNOVIAL ENDOTHELIUM**

Settore scientifico-disciplinare: MED/04

DOTTORANDO
Federico Colombo

Federico Colombo

COORDINATORE
Prof.ssa Lucia Pasquato

Lucia Pasquato

SUPERVISORE DI TESI
Paolo Macor, PhD

Paolo Macor

ANNO ACCADEMICO 2016/2017

*To my family,
I will always be grateful to you*

Abstract

Rheumatoid arthritis (RA) is an autoimmune disease affecting joints due to the persistent inflammation of the synovial tissue. It affects 1% of the worldwide population with high socioeconomic costs. Patients usually require lifetime treatments in order to prevent late stage of the disease, which leads to a condition of disability and pain. Despite the introduction of biological drugs, Methotrexate (MTX) is still the gold standard. However, it shows some weakness such as inefficacy or adverse events after long term usage. For this reason, there is the need to develop drugs with an improved safety profile and higher therapeutic efficacy. Moreover, it is of primary importance to develop diagnostics with enhanced sensitivity and tissue specificity.

In order to meet these needs, the purpose of this work is to develop a nanotechnological agent capable to delivery its content, such as drugs or diagnostic tracers, specifically into pathological joints, avoiding healthy tissues.

These aims have been achieved exploiting peculiar features of biodegradable nanoparticles (BNPs), such as improved pharmacokinetic and bioavailability, associated with a peptide specific for the inflamed synovia. Recently, the heterogeneity of the molecules present in the endothelium has allowed to develop peptides capable to target vessels of specific tissues. In this project, a cyclic peptide able to target the microvasculature of the inflamed synovia has been exploited to drive BNPs only into inflamed joints.

BNPs have been characterized for their physicochemical features, polymers' toxicity and drug release. Targeted polymeric nanoparticles (tBNPs) demonstrated, both *in vitro* and *in vivo*, to preferentially bind inflamed synovial tissue, and their accumulation depends on the degree of inflammation.

Targeted BNPs loaded with MTX showed higher efficacy compared to free MTX in two different animal models of RA. In addition, a reduced dose of tBNPs-MTX demonstrated to maintain its efficacy, showing fewer side effects compared with systemic administration of free MTX. This new therapeutic approach provided a new mechanism of action from approved therapy and suggest potential application in non-responding patients.

All these evidence highlight the potential use of tBNPs as a biocompatible and adaptable tool for the diagnosis and the treatment of RA showing important efficacy, reduced side effects and with the potential to enhance the sensitivity of several imaging technologies.

Table of contents

1. Introduction.....	1
1.1. Rheumatoid arthritis.....	2
1.1.1. Aetiology	3
1.1.2. Genetics.....	4
1.1.3. Environmental factors	5
1.1.4. Epigenetics	6
1.1.5. Pathophysiology	6
1.1.6. Local inflammation.....	9
1.1.7. From local to systemic inflammation	11
1.1.8. Adaptive immunity.....	13
1.1.9. Innate immunity	13
1.2. Neoangiogenesis.....	14
1.3. Animal models of rheumatoid arthritis	16
1.3.1. Collagen induced arthritis (CIA).....	16
1.3.2. Antigen-induced arthritis (AIA)	17
1.3.3. Other models of RA	17
1.4. Treatment of rheumatoid arthritis	18
1.4.1. Synthetic DMARDs and glucocorticoids	19
1.4.2. Methotrexate	19
1.4.3. Biological DMARDs	20
1.4.4. Targeted synthetic DMARDs	21
1.4.5. Side effects of RA therapies	21
1.5. Nanotechnology and Nanomedicine	22
1.5.1. Nanocarriers.....	23
1.5.2. Biodegradable polymers	26
1.5.3. Properties and rational design of nanoparticles	27
1.6. Passive and active targeting.....	30
1.6.1. Passive targeting	31
1.6.2. Active targeting	31
1.7. Targeting agents for rheumatoid arthritis	32
1.7.1. Recombinant antibodies and their fragments	33
1.7.2. Peptides.....	34

1.7.3.	Targeting the vasculature.....	35
2.	Aim and rationale of the thesis	36
3.	Materials and methods	39
3.1.	Production of the targeting molecule	40
3.2.	Purification of the targeting molecule	40
3.3.	SDS page and Western blot of the target molecule.....	41
3.4.	Nanoparticles production.....	41
3.5.	Characterization of nanoparticles by DLS, Nanoparticles tracking, TEM and STEM.	42
3.6.	MTT viability assay.....	42
3.7.	Release of MTX from nanoparticles.....	43
3.8.	Labelling of the targeted molecule and nanoparticles	43
3.9.	Staining of tissue sections	44
3.9.1.	Preparation of paraffin embedded sections of human synovial tissues	44
3.9.2.	Preparation of frozen sections of AIA and CIA	45
3.9.3.	Staining of frozen sections with antibodies	45
3.9.4.	Staining of frozen sections with nanoparticles	46
3.9.5.	Staining of viable EA.hy926 cells with nanoparticles	47
3.9.6.	Microscopes used in this work	47
3.10.	Imaging flow cytometer	47
3.11.	ELISA on EA.hy926	48
3.12.	Antigen induced arthritis (AIA).....	48
3.13.	Collagen induced arthritis (CIA).....	50
3.14.	Hematoxylin Eosin staining	51
3.15.	Blood analysis	52
3.16.	ELISA mouse anti-collagen antibodies	52
3.17.	ELISA rat anti-mBSA antibodies	52
3.18.	Number of polymorphonuclear (PMN) leukocytes.	53
3.19.	Multiplex ELISA	53
4.	Results and discussion	54
4.1.	Design and characterization of biodegradable nanoparticles.....	55
4.1.1.	Design and characterization of the targeting molecule	55
4.1.2.	Design and characterization of targeted nanoparticles for rheumatoid arthritis	59
4.1.3.	Biocompatibility of nanoparticles and MTX release kinetics.....	64
4.2.	Targeting the endothelial tissue of the inflamed synovia	66

4.2.1.	Binding and internalization of BNPs and tBNPs with EA.hy926 cell line	66
4.2.2.	<i>In vivo</i> biodistribution of BNPs and tBNPs in a AIA rat model.....	72
4.2.3.	<i>In vivo</i> biodistribution of BNPs and tBNPs in CIA mouse model.....	74
4.3.	Preclinical studies in a model of polyarthritis	77
4.3.1.	Efficacy of tBNPs-MTX in CIA mouse model	77
4.3.2.	Evaluation of toxic effects in CIA mice treated with tBNPs-MTX	80
4.3.3.	Cytokines multiplex analysis.	81
4.4.	Mechanism of action of MTX encapsulated into tBNPs.....	84
4.4.1.	Efficacy and side effects of tBNPs-MTX therapy in AIA rat model.	84
4.4.2.	tBNPs-MTX reduce neoangiogenesis of the inflamed synovia	87
5.	Conclusion	90
6.	References.....	94
	Acknowledgement	111

List of figures

Table 1: Classification criteria for rheumatoid arthritis 2010 ACR/EULAR	3
Figure 1: Role of the adaptive immunity in RA.....	5
Figure 2: Pathogenetic model of RA.....	8
Figure 3: Early immune response.....	10
Figure 4: Joint and synovial tissue.....	11
Figure 5: Basic structure of organic nanocarriers.....	26
Figure 6: Biodistribution of nanoparticles.....	29
Figure 7: Passive and active targeting.....	32
Figure 8: Antibodies and their fragments used as targeting molecules.....	35
Figure 9: Targeting molecule.....	56
Figure 10: Study of colocalization.	58
Figure 11: Schematic representation of polymeric nanoparticles.	60
Figure 12: 3D model of the targeting molecule.	62
Figure 13: Nanoparticles characterization.	64
Figure 14: Evaluation of nanoparticles' toxicity in vitro.....	66
Figure 15: Target the inflamed synovial tissue.....	68
Figure 16: Binding and internalization of BNPs and tBNPs with EA.hy926.	71
Figure 17: In vivo biodistribution of tBNPs and BNPs in a model of rat AIA.....	74
Figure 18 In vivo biodistribution of tBNPs and BNPs in a model of mouse CIA.....	76
Figure 19. Haematoxylin Eosin staining.	77
Figure 20: Efficacy of tBNPs-MTX in CIA model.....	79
Figure 21: Blood analysis and gain growth in CIA mouse.....	81
Figure 22: Multiplex cytokine profiles in CIA mice.....	83
Figure 23: Efficacy and blood analysis in AIA rat treated with tBNPs.	86
Figure 24: C3 staining of AIA rats' synovial tissues.....	87
Figure 25: vWF staining in AIA rats' synovial tissues.....	89

List of abbreviations

A2	Adenosine receptor 2
ACPAs	Antibodies to citrullinated protein antigens
AIA	Antigen induced arthritis
AICAR	5-aminoimidazole-4-carboxamide ribonucleotide
APCs	Antigen presenting cells
APRIL	A proliferation inducing ligand
APS	Ammonium persulfate
ARA	American Rheumatism Association
BALT	Bronchus-associated lymphoid tissue
BCIP	5-Bromo-4-Chloro-3-Indolyl-phosphate
Bcl-2	B-cell lymphoma 2
bDMARDs	Biological disease-modifying antirheumatic drugs
bFGF	Basic fibroblast growth factor
BLyS	B-lymphocyte stimulator
BNPs	Biodegradable nanoparticles
BRM	Biological response modifier
BSA	Bovine serum albumin
C	Constant domain
CAIA	Collagen antibody-induced arthritis
cAMP	Cyclic adenosine monophosphate
CD14	Cluster of differentiation 14
CD20	Cluster of differentiation 20
CD44	Cluster of differentiation 44
CD68	Cluster of differentiation 68
CD80	Cluster of differentiation 80
CD86	Cluster of differentiation 86
CDR	Complementarity determining region
CFA	Complete Freud Adjuvant
CHO	Chines Hamster Ovary

CIA	Collagen induced arthritis
CME	Clathrin-mediated endocytosis
CRP	C-reactive protein
CTRL	Control
CXCL12	C-X-C Motif Chemokine ligand 12
CXCL8	C-X-C Motif Chemokine ligand 8
CXCR1	C-X-C Motif Chemokine receptor 1
CXCR2	C-X-C Motif Chemokine receptor 2
CXCR4	C-X-C Motif Chemokine receptor 4
DAPI	4',6-diamidino-2-phenylindole
DAS	Disease activity score
DHFR	Dihydrofolate reductase
DLS	Dynamic light scattering
DMARDs	Disease-modifying antirheumatic drugs
DMEM	Dulbecco's Modified Eagle's Medium
DMSO	Dimethyl Sulfoxide
EDTA	Ethylene diamine tetra acetic acid
EES	Extravascular extracellular space
ELISA	Enzyme-linked immunosorbent assay
EMA	European Medicines Agency
EPR	Enhanced permeability retention
ESR	Erythrocyte sedimentation rate
EULAR	European League Against Rheumatism
Fab	Fragment antigen-binding
FasL	Fas ligand
FBS	Fetal bovine serum
Fc	Fragment crystallisable
FDA	Food and Drug Administration
FGF-2	Fibroblast growth factor-2
FITC	Fluorescein Isothiocyanate
FLS	Fibroblast-like synoviocytes
GRA	Granulocytes

H	Heavy chain
HA	Hyaluronic acid
HIF	Hypoxia inducible factors
HLA	Human leucocyte antigen
HRP	Horseradish peroxidase
i.p	Intra peritoneal
i.v	Intra venous
iBALT	Induced bronchus-associated lymphoid tissue
ICAM-1	Intercellular adhesion molecule-1
IFA	Incomplete Freund Adjuvant
IL-1 β / α	Interleukin 1 β / α
IL1 / 2 / 6/....	Interleukin 1 / 2 / 6/
JAK	Janus kinase
KC	Keratinocyte-derived cytokine
L	Light chain
LYM	Lymphocytes
M-CSF	Macrophages colony-stimulating factor
M-CSF	Granulocytes colony-stimulating factor
MAP44	MBL-associated protein of 44kDa
MBL	Mannose-binding lectin
mBSA	Methylated bovine serum albumin
MCP-1	Monocyte chemotactic protein 1
MG-CSF	Granulocytes-macrophages colony-stimulating factor
MHC	Major histocompatibility complex
MIP-1 α	Macrophage Inflammatory Proteins 1 α
MIP-1 β	Macrophage Inflammatory Proteins 1 β
MLS	Macrophages like synoviocytes
MMP1	Matrix metalloproteinases 1
MMP10	Matrix metalloproteinases 10
MMP3	Matrix metalloproteinases 3
MMP8	Matrix metalloproteinases 8
MMP9	Matrix metalloproteinases 9

MMPs	Matrix metalloproteinases
MON	Monocytes
MPS	Mononuclear phagocyte system
MRI	Magnetic Resonance Imaging
MTT	1-(4,5-Dimethylthiazol-2-yl)-3,5-diphenylformazan
MTX	Methotrexate
MWCO	Molecular weight cut-off
MWNTs	Multi-walled nanotubes
NBT	Nitro Blue Tetrazolium
NC	Normalized counts
NETs	Neutrophil extracellular traps
NHS	N-Hydroxysuccinimide
NLRs	Nucleotide-binding oligomerization domain (NOD) like receptors
NOD	Nucleotide-binding oligomerization domain
NPs	Polymeric nanoparticles
NSAIDs	Non-steroidal anti-inflammatory drugs
NTA	Nanoparticle tracking analysis
OD	Optical Density
PAD	Peptidyl arginine deaminase
PBS	Phosphate buffered saline
PCL	Poly (ϵ -caprolactone)
PDGF	Platelet-derived growth factor
PDGF- β	Platelet-derived growth factor β
PDI	Polydispersity index
PEG	Polyethylene glycol
PEG-b-PLA	COOH-poly(ethylene glycol)-b-polylactide
PET	Positron emission tomography
PFA	Paraformaldehyde
PLA	Poly (lactide)
PLGA	Poly (lactide-co-glycolide) copolymers
PLT	Platelets
PMMA	Poly (methyl methacrylate)

PMN	Polymorphonuclear cells
PTPN22	Protein tyrosine phosphatase non-receptor type 22
PTX	Paclitaxel
RA	Rheumatoid arthritis
RANKL	Receptor activator of NF-κB ligand
RBC	Red blood cells
RF	Rheumatoid Factor
RT	Room temperature
scFv	Single chain fragment variable
SDF-1	Stromal-derived factor 1
SDS-PAGE	Sodium Dodecyl Sulphate - PolyAcrylamide Gel Electrophoresis
STAT	Signal transducer and activator of transcription
STEM	Scanning transmission electron microscopy
SWNTs	Single-walled nanotubes
TB	Tuberculosis
tBNPs	Targeted biodegradable nanoparticles
TBS	Tris-buffered saline
TCRs	T-cell receptors
TEM	Transmission electron microscopy
TEMED	N,N,N',N'tetrametiletilendiamina
TGF-beta	Transforming growth factor-beta
TGFβ	Transforming growth factor β
Th	T-helper
Th17	T-helper 17
TMB	3,3',5,5'-Tetramethylbenzidine
TNF-α	Tumor necrosis factor α
Treg	Regulatory helper T-cell
TRITC	Tetramethylrhodamine
TRLs	Toll-like receptors
V	Variable domain
VCAM-1	Vascular cell adhesion molecule-1
VEGF	Vascular endothelial growth factor

vWF	Von Willebrand factor
WBC	White blood cells
ζ	Zeta potential

1. Introduction

1.1. Rheumatoid arthritis

Rheumatoid arthritis (RA) is a systemic autoimmune disease (Firestein 2003)(Smolen et al. 2007) characterized by the chronic inflammation of joint and bone destruction (Aletaha et al. 2010)(Smolen et al. 2016). Despite new therapies improve patients' outcomes with RA, complete remission is still a challenge and patients are treated throughout their life. Historically the term "Rheumatoid arthritis" was coined by Alfred Bering Garrod in 1859 and approved by the American Rheumatism Association (ARA) in 1941 (Todesco S 2002). Cases of osteoarthritis and ankyloses spondylitis, but not of RA, were reported from skeletal remains in Europe and north Africa (Aceves-Avila et al. 1998). Differently, characteristic RA lesions were found in palaeopathological specimens in Native American tribes in North America (19). Interestingly, in these regions the incidence of RA remains really high with 5% of disease incidence. Instead, the worldwide incidence is 0.5-1%, becoming the most common autoimmune inflammatory arthritis in adults (Helmick et al. 2008). Compared with the general population, patients with RA show an increased risk of mortality, mainly due to an increased risk of cardiovascular death (Gabriel 2008). Depending on the studied population, the average age of the onset for rheumatoid arthritis ranges from early 40s to late 50s (Innala et al. 2014)(Symmons et al. 2002). The disease is more frequent in woman than in men with a ratio of 3 to 1 suggesting a pathological role of hormonal factors (Scott et al. 2010). The RA burden is characterized by direct and indirect costs. The direct costs associated with the treatments have increased in the last 20 years due to the introduction of biological drugs. Despite these drugs improve patients' quality of life, the indirect costs are still high due to the loss of productivity (absence from work). In Italy, according to the recent literature, the total social cost associated with RA is €3.5 billion per year with a mean of €13.595 per adult patient. In particular, 21% of the total costs are direct costs while 79% are indirect costs. These costs are in line with the other European countries and the total mean annual cost is estimated at about €25.1 billion (Benucci et al. 2016). RA is characterized by the chronic inflammation of the synovial membrane, which leads to its hyperplasia. During the disease, the small diarthrodial joints of hands and feet are affected first in a symmetric manner (Firestein 2003). The main clinical symptoms associated with RA are swelling of joints, morning stiffness and pain due to the progressive cartilage degradation and bone erosion. These symptoms together with radiological data and the serological presence/absence and type of autoantibodies are needed

to diagnose the disease, its degree and to choose the right treatment strategy. To this aim, the American College of Rheumatology (ACR) and the European League Against Rheumatism (EULAR) developed classification criteria to define the RA severity (Table 1). According to these criteria, which provides a score from 0 to 10, the score of ≥ 6 is indicative of the presence of definite RA (Aletaha et al. 2010).

ACR/EULAR 2010 criteria	SCORE
1. Joint involvement	
• One medium to large joint	0
• Two to ten medium to large joints	1
• One to three small joints (large joints not counted)	2
• Four to ten small joints (large joints not counted)	3
• More than ten joints (at least one small joint)	5
2. Serology	
• Negative RF and negative ACPA	0
• Low positive RF or low positive ACPA	2
• High positive RF or high positive ACPA	3
3. Acute phase reactants	
• Normal CRP and normal ESP	0
• Abnormal CRP or abnormal ESP	1
4. Duration of symptoms	
• Less than 6 weeks	0
• 6 weeks or more	1

Table 1: Classification criteria for rheumatoid arthritis 2010 ACR/EULAR.

1.1.1. Aetiology

The leading cause of rheumatoid arthritis is still unclear, however several studies suggest that environmental factors and genetic predisposition increase the probability to develop RA (McInnes & Schett 2011a). Usually, patients are divided into seropositive and seronegative regarding the presence or absence of autoantibodies specific for citrullinated autoantigens (antibodies to citrullinated protein antigens (ACPAs)) and autoantibodies specific for self IgG-

Fc (rheumatoid factor (RF)). Two-thirds of the patients are seropositive and show worst clinical symptoms compared to seronegative patients. Moreover, the aetiology for the seronegative is less well understood compared to the seropositive, probably because of a lack of homogeneous features (Malmström et al. 2016). Despite the fact that both the RF and the ACPAs are present in the blood before the first symptoms of the disease, the RF is less specific (Aggarwal et al. 2009). Indeed, it occurs in other inflammatory conditions, while the ACPAs are detected in less than 2% in healthy individuals (Malmström et al. 2016).

1.1.2. Genetics

As previously mentioned, genetic factors have a key role in the pathogenesis of RA. Indeed, very interesting epidemiological studies, linking the genetic features to the pathology, demonstrated that native American-Indian populations have high occurrence of RA (5.3-6.8%)(Del Puente et al. 1989)(Harvey et al. 1981) whereas rural African populations (Beighton et al. 1975)(A. J. Silman et al. 1993) and some populations from south-east Asia(Dans et al. 1997), China(Zeng et al. 1997) and Japan(Shichikawa et al. 1999) show low occurrence (0.2-0.3%). Other studies have proved a fourfold increased risk of RA in monozygotic twins compared to dizygotic twins (MacGregor et al. 2000)(A J Silman et al. 1993). Moreover, it is known that a positive family history increases the risk of RA from three to five times (Smolen et al. 2016). Recently, genome-wide association studies have identified more than a hundred loci associated with rheumatoid arthritis (Consortium 2007)(Stahl et al. 2010). Among these loci, the major histocompatibility complex (MHC) class II, known in human as human leucocyte antigen (HLA) class II and responsible for the antigen presentation to T-helper (Th) cells, was extensively studied. Particular HLA alleles like HLA-DR1 and HLA-DR4 were found with high frequencies in the seropositive patient affected by RA if compared with healthy individuals. These alleles share a common aminoacid sequence (known as the shared epitope) (Gregersen et al. 1987) in the third hypervariable region (called pocket 4 (P4)) of the beta chain in the peptide binding groove. Aminoacids found in position 11, 71 and 74 (Raychaudhuri et al. 2012) confer a positive charge to the P4, which is not able to accommodate peptides containing arginine due to its positive charge (Scally et al. 2013). However, when an arginine is converted in a neutral citrulline the peptide is able to fit in the P4 and so it can be presented to the T-helper cell (Figure 1). The conversion of arginine to citrulline is performed by an enzyme called peptidyl arginine deiminase (PAD). Indeed, it has been demonstrated that PAD is overexpress

or miss-regulated during lung exposure to smoke (Padyukov et al. 2004), silica particles (Stolt et al. 2010) and textile dust (Too et al. 2016). Usually, in patients affected by RA, the citrulline able to specifically bind the pocket P4 was found in peptides from vimentin, aggrecan (Scally et al. 2013), fibrinogen (James et al. 2010), α -enolase (Gerstner et al. 2016) and type II collagen (Chemin et al. 2016). Another gene associated with the increased risk to develop RA is the PTPN22 (protein tyrosine phosphatase non-receptor type 22) gene. A mutation in this gene increases the T-cell activation threshold leading, during the thymic selection, to a thymocytes failure to delete autoreactive T-cells (Rieck et al. 2007).

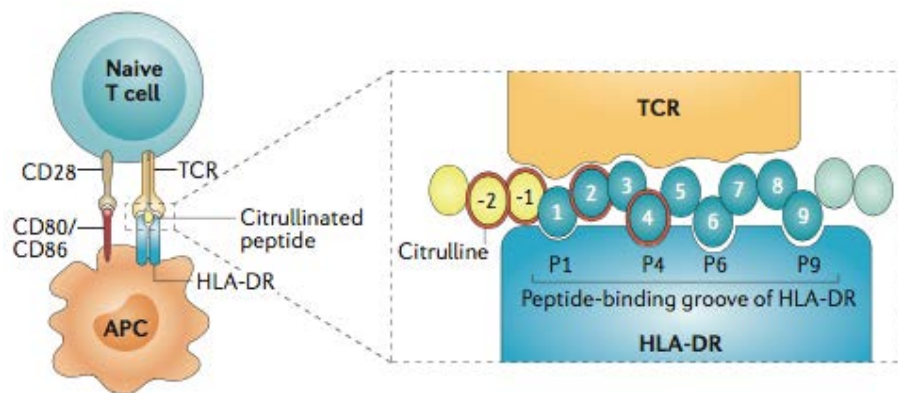


Figure 1: Role of the adaptive immunity in RA.

The figure shows the antigen presentation of citrullinated peptides in complex with the HLA-DR molecules. HLA-DR alleles are associate with rheumatoid arthritis and are known as the shared epitope. In particular, the pocket 4 (P4) is positively charged and, usually, cannot bind positively charged aminoacids such as arginine. Although, citrullinated aminoacids (red rings) have a neutral charge thus can be accommodated into the P4, with the consequent antigen presentation to the TCR on a T-cell. Moreover, TCR can directly recognizes citrulline in position -2, -1 and 2 of other peptides, such as collagen II and α -enolase. Figure taken from Malmstrom V. et al. Nat Rev Immunol, 2016. (Malmström et al. 2016).

1.1.3. Environmental factors

Up to now several environmental factors associated with the pathogenesis of RA have been identified. Among these, cigarette smoking is known to be one of the most important factors which may trigger the onset of the disease (Silman et al. 1996). Recent meta-analysis study has reported a two-fold increased risk of developing RA for male smokers compared with non-smokers. For women, the risk for smokers is 1.3 times higher than non-smokers (Sugiyama et al. 2010). There are many different hypotheses to explain the mechanism by which cigarette smoke enhance the risk to develop the disease. In 2008 have been demonstrated that smoking increases the expression of peptidylarginine deiminase 2 (PAD2) enzyme in the lung mucosa, which in turn increases the process of citrullination (Makrygiannakis et al. 2008). Nevertheless, in addition to cigarette smoking, bacterial infections can increase the protein citrullination. Indeed, it is well known the link between RA and infections by *Porphyromonas Gingivalis*. As a

matter of fact, patients with RA have higher antibody titre for *P. Gingivalis* which correlates with higher concentration of C-reactive protein and RA-associated autoantibodies (Mikuls et al. 2009). Moreover, this bacterium has its own PAD enzyme able to switch arginine in citrulline. For this reason, a model of molecular mimicry has been hypothesized. According to this model, when the immune system reacts against *P. Gingivalis* infection, antibodies against its citrullinated peptides are produced and, due to the high similarity, the immune system tolerance is compromised inducing the epitope spreading to self citrullinated proteins leading to a strong autoimmune response (Hajishengallis 2014)(Wegner et al. 2010). Other infectious agents like Epstein-Barr virus and *Escherichia coli* are known to trigger RA by molecular mimicry and, recently, gut microbiome has been studied for its role for the priming and progression of the disease.

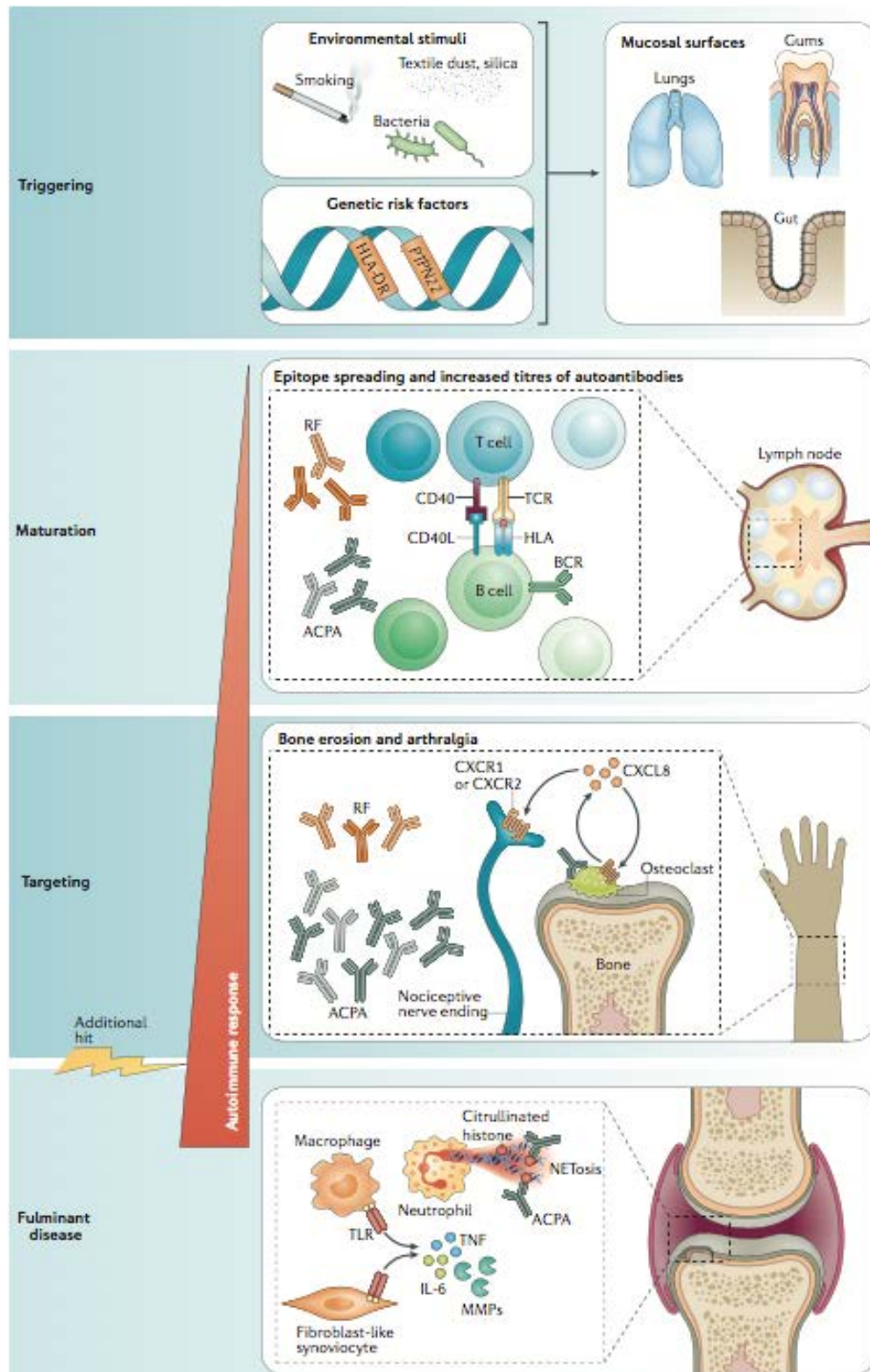
1.1.4. Epigenetics

Epigenetic processes are heritable changes in the gene expression without modification in the DNA sequence. This is possible due to DNA methylation or histones and chromatin associated proteins post-translational modifications such as acetylation, methylation and phosphorylation. These processes lead to a very complex network where genes are finely regulated through their activation or silencing. Epigenetic contributions to the onset and progression of RA have been recently highlighted. Indeed, ten different methylated positions were identified as responsible to increase the risk to develop RA (Liu et al. 2013). Moreover, it was demonstrated that knee and hip RA fibroblast-like synoviocytes (FLS) show different DNA methylation signature of genes encoding the JACK-STAT pathway, explaining, partly, the different degree of inflammation between joints (Ai et al. 2016). Another mechanism of epigenetic regulation is represented by many microRNAs. They can target mRNAs leading to an additional regulation of different genes in different cells type such as lymphocytes, macrophages and FLS (Blüml et al. 2011).

1.1.5. Pathophysiology

As already mentioned above, the cause of the disease is still unclear. What we know is that environmental factors, a characteristic genotype, post-translational modification and other kinds of gene expression regulations contribute to the onset of the disease. According to one of the latest review published on Nature Review Rheumatology by V. Malmstrom et al.

(Malmström et al. 2016) during the development of the pathology, there are four phases (Figure 2). The first phase is called "triggering". At this stage, the mucosal surfaces, such as the lining of the lungs, gums and intestinal mucosa, together with environmental stimuli and genetic risk factors trigger the immune response against self-peptides. In the second phase, called "maturation", the immune system matures and spreads its epitopes, enhancing the antibody titre of RF and ACPA. This immune response does not occur in the joints but into lymph nodes and/or into other secondary lymphoid tissue where T-cells and B-cells are activated and proliferate. The third phase called "targeting" is characterized by the presence of the clinical signs, such as bone loss and joint pain. Specifically, ACPAs may directly bind osteoclasts, which in response produce C-X-C Motif Chemokine Ligand 8 (CXCL8) known as interleukin 8 (IL8). It can acts as growth factor for osteoclasts or as pain inducer when it binds their receptors, C-X-C Motif Chemokine receptor 1 (CXCR1) and CXCR2, expressed on nociceptive nerves. The last phase, called "fulminant disease", is characterized by the synovitis. Indeed, ACPAs can bind citrullinated histones causing the neutrophil extracellular traps (NETosis). Moreover, other citrullinated proteins can be bound by Toll-like receptors (TRLs) expressed on synovial cells and APCs, which in turn produce pro-inflammatory cytokines like tumor necrosis factor (TNF), interleukin-6 (IL-6) and matrix metalloproteinases (MMPs), responsible for the cartilage and bone destruction. According to this model, the immune system is first activated in a different tissue by a local inflammation and then this immune response target the joints, developing an inflammation cascade leading to an established RA.

**Figure 2: Pathogenetic model of RA.**

This figure shows four phases of the disease development. Phase 1 “triggering”: environmental factors and genetic factors enhance the autoimmune response at the mucosal surface. Phase 2 “maturation”: in the lymphoid organs, the immune response matures and increases the concentration of autoantibodies such as ACPA and RF. Phase 3 “targeting”: autoantibodies reach into the synovial tissue where they activate osteoclasts which in turn produce CXCL8. This cytokine increases osteoclasts proliferation and through its receptors induce pain. Phase 4 “fulminant disease”: citrullinated proteins can bind TLR of synovial fibroblasts, which produce IL-6, TNF and MMPs. Moreover, ACPA can bind citrullinated histones promoting the formation of neutrophil extracellular traps (NETosis). The figure is taken from Malmstrom V. et al. Nat Rev Immunol, 2016 (Malmström et al. 2016).

1.1.6. Local inflammation

Following this model of pathogenesis, the possible first local inflammation may occur in the lung mucosa. Several findings support this model. Among these, it has been shown that patient with early ACPA-positive RA presented macroscopic and microscopic changes, such as inflammatory cells infiltration, of the lung mucosa, whereas seronegative RA patients and healthy individuals do not show any changes (Reynisdottir et al. 2014). Another work has demonstrated that bronchus-associated lymphoid tissue (BALT), described as a mucosal lymphoid organ, were mainly found in RA patients compared with healthy. Interestingly they correlate with an increased tissue damage, suggesting an important role in the pathogenesis due to the overexpression of PAD2 and the production of chemokines and cytokines (Rangel-Moreno et al. 2006). Moreover, it is known that smoke and other noxious agents increase the expression of PADs, which correlate with an increased amount of citrullinated proteins, in the bronchial tissue of patients with RA (Makrygiannakis et al. 2008). All these evidence suggest that antigen presenting cells (APCs), like dendritic cells, macrophages and B-cells, locally activated by neo-citrullinated antigens may trigger T-cell mediated immunity (Figure 3).

However, since not all seropositive patients with RA present inflammation or changes in the lung mucosa, possibly other tissues are able to trigger the first immune response. Among them, the most accredited are the gums, probably because of the peridontitis caused by *phosphomonas gingivalis*, and the intestinal tract due to changes in the gut microbiota.

It is evident that RA is a clinical condition characterized by a complex crosstalk between the adaptive and the innate parts of the immune system. In particular, the complement system has an important role in this pathology (Trouw et al. 2017). Indeed, complement proteins C3 and C4 have been shown to decrease in joints of RA patients because of consumption (Swaak et al. 1987), while complement activation fragments, such as the membrane attack complex sC5b-9 and the cleavage fragments Bb, were increased several times (Brodeur et al. 1991). ACPA and RF may interact with antigens present in the joints forming immune complexes able to activate the local complement (Suwannalai et al. 2014). Other molecules, released from the extracellular matrix of cartilage or materials from dead cells, can trigger the complement activation thus suggesting that the complement system has a role in both early phase and late phase of the disease (Sjöberg et al. 2005). It was demonstrated that both classical and alternative pathways are involved in the complement activation, but only the alternative was

found to be essential and sufficient for the onset and progression of the disease (Banda et al. 2006). Instead, is not yet clear the role of the lectin pathway. Indeed it was demonstrated in animal models that the mannose-binding lectin (MBL) was not required for the disease development (Banda et al. 2007) however bypassing the MBL through the MBL-associated protein of 44kDa (MAP44) an improvement of the disease was observed (Banda et al. 2014).

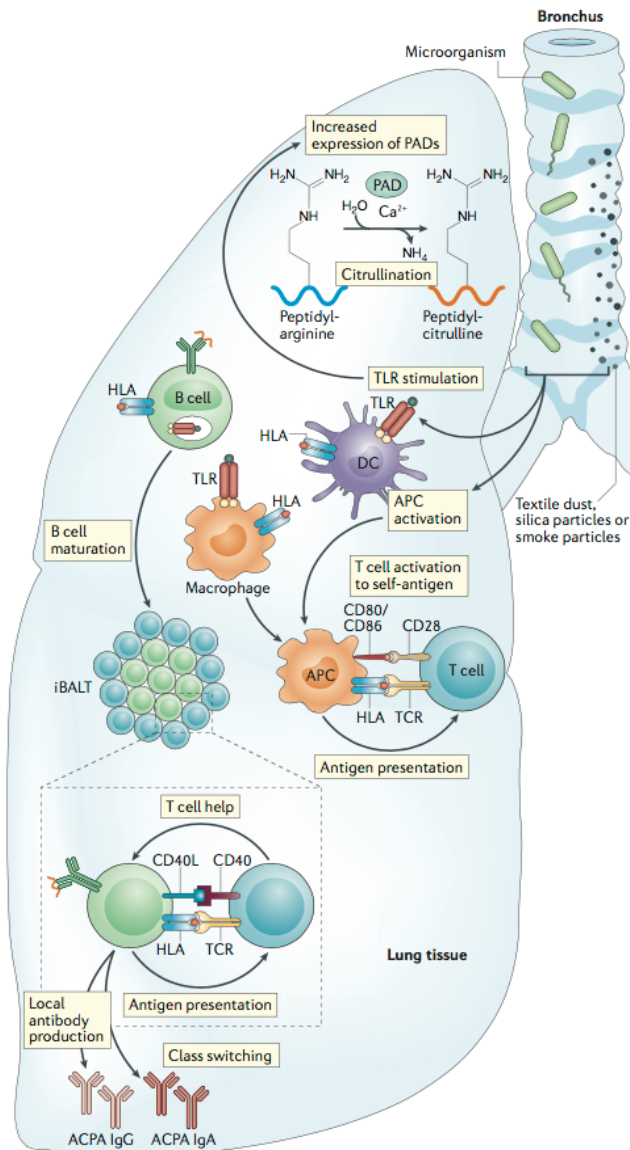


Figure 3: Early immune response.

According to the last knowledge, the first immune response occurs in the lung, gum or intestinal mucosa. The figure represents the immune activation in the lung mucosa, where environmental factors, such as noxious agents, due to specific susceptibility genes (e.g. HLA-DR) can activate dendritic cells, macrophages and B-cells through TLR. These processes can trigger the activation of PADs, with consequent RA-associated neo antigens. Later, B-cells present post-translationally modified autoantigens to T-cells with a local production of autoantibodies against citrullinated peptides. The T-cell-dependent B-cell activation usually occurs in the induced bronchus-associated lymphoid tissue (iBALT). The figure is taken from Malmstrom V. et al. Nat Rev Immunol, 2016 (Malmström et al. 2016).

1.1.7. From local to systemic inflammation

Although ACPAs have been considered pathogenic (Kuhn et al. 2006), these are present in serum years before the onset of the disease. For this reason, the presence of the ACPAs is not sufficient for the onset of the disease and an additional “hit” is needed. Indeed, it has been demonstrated that Fc of ACPA antibodies from RA patients show different glycosylation pattern, which may increase the affinity for their FCyRI enhancing the inflammation (Rombouts et al. 2015). As previously discussed, several studies indicate that specific T cell-mediated immune response against autoantigens take place outside the joints. At a certain point, the local inflammation, which probably starts in the lung mucosa (see paragraph 1.1.6), acquires a systemic feature. Therefore, B-cells react to post-translationally modified autoantigens and, helped by an HLA class II-dependent T-cell response, migrate and proliferate into the joint cavity, promoting the inflammation of the synovium. In physiological conditions (Figure 4a), the synovial membrane provides nutrients to the cartilages and lubricates the joints preventing rubbing. Anatomically is divided into two compartments: the intimal lining layer and the sublining layer. The intima layer is made of a thin layer of cells, mainly fibroblast like synoviocytes (FLS) and macrophages like synoviocytes (MLS). FLS express collagen IV and V, vimentin and secrete a protein responsible for the joints' lubrication, the so called lubricin. Instead, MLS express macrophage surface markers, such as CD68, Fc receptors, CD14, and abundant HLA-DR (Bartok & Firestein 2011)(Firestein 2013).

The inflamed synovial membrane is characterized by innate and adaptive immune cells infiltration (Figure 4b). This is possible due to the increased cytokines concentration and because of a hypoxic environment which triggers the expression of adhesion molecules on synovial microvessels (Szekanecz et al. 2009). These molecules allow leukocytes adhesion, extravasation and synovial tissue infiltration. The inflamed synovium became thicker due to the increased number of FLS, MLS and because of the leukocytes infiltration. MLS during the inflammation produce high amount of pro-inflammatory cytokines,

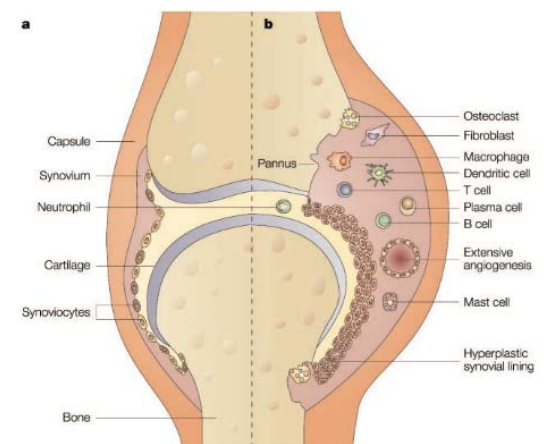


Figure 4: Joint and synovial tissue.

Comparison between healthy joint (a) and RA joint (b). The latter is characterized by a hyperplastic synovial tissue and a huge leukocytes infiltration. In addition, the inflammatory process is associated with an extensive angiogenetic process. The figure is taken from McInnes IB et al. N Engl J Med 2011 (McInnes & Schett 2011a).

chemokines and growth factors. All these factors are able to activate FLS and B-cell, which in turn produce IL-6 and matrix metalloproteinases (MMPs). Thus, the positive feedback loop, generated by the paracrine/autocrine effects of these factors, leads to a perpetual inflammation. Indeed, the inflamed hyperplastic synovial tissue at the cartilage-bone interface, called pannus, behaves like a locally invasive tumor, where activated FLS, macrophages, osteoclasts and lymphocytes are able to destroy and infiltrate the lining layer and the cartilage (Bartok & Firestein 2011). The FLS proliferation is stimulated by growth factors like basic fibroblast growth factor (bFGF) (Melnyk et al. 1990), platelet-derived growth factor (PDGF) (Mor et al. 2005) and transforming growth factor-beta (TGF-beta) (Allen et al. 1990), released by leukocytes. Moreover, the FLS apoptosis rate is decreased, probably because of p53 mutation (Firestein et al. 1997), B-cell lymphoma 2 (Bcl-2) overexpression (Perlman et al. 2000) or Fas ligand (FasL) dysregulation (Perlman et al. 2001). The FLS have a primary role in cartilage invasion and degradation, indeed they secrete a broad set of MMPs responsible for this process. In particular, during the disease, FLS stimulated with IL-1, TNF-beta and growth factors overexpress MMP1, MMP3, MMP10 (Tolboom et al. 2002), MMP8, MMP9, MMP11 and MMP13 (Mor et al. 2005). These enzymes are responsible for the collagen I and II degradation, leading to the cartilage destruction, increasing the space between joints. It was demonstrated that FLS produce IL-6, promoting Th17 differentiation and proliferation (Lin et al. 2012). FLS feed the inflammatory process contributing to the formation of new vessels, indeed numerous pro-angiogenetic factors are produced. Among these, vascular endothelial growth factor (VEGF) (Cho et al. 2002), fibroblast growth factor-2 (FGF-2) (Yamashita et al. 2002) and interleukin-18 (IL-18) (Morel et al. 2002) contribute to the inflammatory process and pannus formation due to the new vessels growth. However, the formation of new vessels and the production of MMP are not solely responsible for the progression of cartilage inflammation and destruction, since fibroblasts can directly interact with T-cells, B-cells, and osteoclasts. The latter is the primary responsible for the destruction and deformation of the bones due to their acid enzymatic machinery (able to destroy mineralized cartilage and bones). Lesions of bones and cartilage are progressively invaded by leukocytes, which in the end reach the bone marrow increasing the inflammatory process (Jimenez-Boj et al. 2005). It is known that macrophages colony-stimulating factor (M-CSF) and the receptor activator of NF- κ B ligand (RANKL) are principally responsible for the osteoclasts survival, activation and differentiation (Glantschnig et al. 2003). However, TNF- α , IL-1, IL-6 and IL-17 play a central role in the activation and

differentiation of osteoclasts (Schett & Teitelbaum 2009). Indeed, treatments able to target these cytokines were effective for the prevention of bone destruction (McInnes & Schett 2011).

1.1.8. Adaptive immunity

It is known that adaptive immunity has a pivotal role in the pathogenesis of rheumatoid arthritis. In particular, T-cells (CD4+) are activated through the interaction with antigenic peptide fragment presented by HLA class II expressed by professionals APC. Recently, enormous attention has been focused on type 17 helper T-cell (Th17). This particular subset of T helper cells has pro-inflammatory phenotype that produces TNF- α and interleukin 17A, 17F, IL-21 and IL-22 (Miossec et al. 2009). The synovial fluid of RA patients contains many cytokines that promote the differentiation of Th17 and simultaneously suppress the differentiation of regulatory helper T-cell (Treg). This process breaks homeostasis in favor of a pro-inflammatory process by creating an imbalance between pro-inflammatory cytokines, chemokines, adhesion proteins and growth factors. Indeed, it was demonstrated that this equilibrium can be restored by TNF- α inhibitors proving the key role of TNF- α in the inflammatory process (Nadkarni et al. 2007). Moreover, TNF- α and IL-17A are able to activate fibroblasts and chondrocytes, fueling the inflammatory process (Zupan et al. 2013)(Mundy 2007). B-cells, together with T-cells, have a central role in the pathogenesis, mainly producing IgG ACPA. In the synovial tissue, B-cells are often aggregated to T-cells, forming the so called ectopic (or tertiary) lymphoid follicles (Jing & Choi 2016)(Timmer et al. 2007). This structure promotes B-cell survival and proliferation through the expression of a proliferation-inducing ligand (APRIL), B-lymphocyte stimulator (BLyS) and several different chemokines (Seyler et al. 2005).

1.1.9. Innate immunity

As already described in the paragraph “local inflammation”, the complement system, which is part of the innate immune system, has an important role in the development of RA. Moreover, cells of the innate immune system contribute to the synovial membrane inflammation because of the mast cells, macrophages and natural killer cells infiltration. Neutrophils also participate in the synovitis but are mainly located in the synovial liquid. Among these cells, Macrophages are considered the main actors because of their cytokines production. Indeed, they secrete a great cytokine portfolio such as TNF-alpha, IL-1, IL-6, IL-12. Moreover, they release

chemokines, leukotrienes, prostaglandins, and complement proteins. All these molecules have the possibility to increase the vascular permeability, which in turn increase cell extravasation (Duque & Descoteaux 2014). Usually, Macrophages are activated by toll like receptors (TLR) and nucleotide-binding oligomerization domain (NOD) like receptors (NLRs). In addition, macrophages can be activated by cytokines, immune complexes and lipoproteins (McInnes & Schett 2011b). Macrophages maturation and synovial infiltration are promoted by M-CSF, G-CSF and granulocytes-macrophages colony-stimulating factor (MG-CSF) which enhance their migration from the bone marrow to the inflamed tissue (Cornish et al. 2009). Mast cells, activated by TLR, Fc receptors γ or Fc receptors ϵ produce cytokines, chemokines, proteases and vasoactive amines while Neutrophils produce prostaglandins, reactive oxygen intermediates and proteases (Cascão et al. 2010).

1.2. Neoangiogenesis

The formation of new capillaries from pre-existing vessels is a process called neoangiogenesis. This is a complex and well-orchestrated process which involves many cell types and mediators. It occurs in physiological conditions during organ development, growth and tissue remodeling due to the reorganization of the blood vessels (Konisti et al. 2013). The vessels have an inner layer formed by endothelial cells with a surrounding basal lamina, pericytes and smooth muscles cells (Bergers 2005). It has been demonstrated that precursors of endothelial cells are CD34 $^{+}$ cells, which express the vascular endothelium growth factor (VEGF) receptor 2. These cells express also the CXCR4 and migrate in response to stromal-derived factor (SDF)-1 or VEGF. (Peichev et al. 2000)(Asahara 1997). Several factors such as cytokines, chemokines, molecules for cell adhesion and growth factors stimulate the migration and activation of these cells. Once these cells are activated, they start to disrupt the underlying basal membrane invading the extracellular matrix. These proliferating cells follow the VEGF gradient to reach the tissue of interest where they organized the lumen and the final shape of the vessel with the help of pericytes attracted due to the secretion of the endothelial cell PDGF β (Bergers 2005).

Neoangiogenesis, as already mentioned, is a physiological process, however it plays an important role in several pathological processes. Usually, damaged tissues face hypoxic conditions which, in turn, promotes the formation of new vessels in order to restore the regular blood supply and therefore a suitable amount of oxygen. The hypoxia is a shared condition of many different pathologies like autoimmune and cancer diseases. In RA, during

the chronic inflammation of the synovial tissue, synovial fibroblasts acquire a high proliferative phenotype, moreover, due to the huge leukocytes infiltration, there is an increased oxygen consumption. Different studies have demonstrated that VEGF, pro-inflammatory cytokines like IL-6 and matrix metalloproteinases expression (MMP1 and MMP3) are associated to the hypoxia inducible factors (HIF) activation (Lu & Kang 2010)(Ahn et al. 2008). Therefore, hypoxia not only plays a fundamental role in the formation of new vessels but contributes to the degradation of cartilage by the expression of metalloproteases. The RA synovial membrane, infiltrated by leukocytes, expresses pro-inflammatory cytokines such as IL-1, IL-6, TNF-alpha and transforming growth factor beta (TGF β) which are able to increase the expression of VEGF (Marrelli et al. 2011). Chemokines e chemokines receptors contribute to the formation of new vessels which promotes inflammation of the synovial membrane. One of the most potent chemokines is the CXCL12, also called stromal cell-derived, which is overexpressed in inflammatory disease. Its receptor CXCR4 is expressed by hemopoietic stem cells, monocytes and lymphocytes and exerts a homing function. CXCL12-CXCR4 system is strongly implicated in the neoangiogenesis. It was demonstrated that CXCL12 induces autocrine expression of VEGF promoting the neoangiogenesis; in addition, CXCR4 knockout mice exhibit a decreased vascularization (Pablos et al. 2003). Although chemokines are responsible for the leukocyte homing in the inflamed synovial tissue, the expression of cellular adhesion molecules (CAMs) expressed by endothelial cells play a crucial role in leukocyte adhesion and transendothelial migration. At the beginning, leukocyte tethering and rolling are mediated by E-selectins and P-selectins while the firm adhesion is mediated by intercellular adhesion molecule-1 (ICAM-1) and vascular cell adhesion molecule-1 (VCAM-1) able to bind β_2 integrin and $\alpha_4\beta_2$ integrin respectively (Szekanecz & Koch 2008). Of extreme interest is the integrin $\alpha_v\beta_3$ which is involved in neoangiogenesis and have been found to be overexpressed in damaged tissue (Szekanecz et al. 2009). Its relevance was also demonstrated in animal models of RA, where the blocking of the $\alpha_v\beta_3$ reduced neoangiogenesis, cell infiltration, pannus formation and cartilage degradation (Storgard et al. 1999). For these reasons, in order to reduce neoangiogenesis, drugs able to block this integrin were developed but they were ineffective in human clinical trials (Lainer-Carr & Brahn 2007). Although, due to its overexpression in blood vessels of tumor endothelial cells or in inflamed kidney tissue, peptides containing aminoacids Arg-Gly-Asp (RGD), able to bind the $\alpha_v\beta_3$, have been used to deliver anticancer or anti-inflammatory drugs directly in the tissue of interest (Danhier, Breton, et al. 2012)(Durigutto et al. 2017).

1.3. Animal models of rheumatoid arthritis

Several experimental animal models of rheumatoid arthritis have been developed in order to understand etiology and pathogenic mechanisms of this autoimmune disease. Today, these models are important to test new therapeutics, study their pharmacokinetics, effectiveness and side effects (Asquith et al. 2009). Despite the progress made to develop animal models of arthritis, each model shows peculiar features. Indeed, the model to use should be chosen according to the aim of the research taking into account its pros and cons. Moreover, the results obtained with animal models should be assessed carefully because of the intrinsic differences between human and other animals (Hu et al. 2013).

1.3.1. Collagen induced arthritis (CIA)

The discovery of anti-collagen antibodies, that have been found in the serum of patients affected by rheumatoid arthritis, was the motivation to develop an experimental model based on type II collagen. It became the best model to test new therapeutics, such as biologicals DMARDs, and to understand pathogenic mechanisms of the disease. The reason of the success lies in the fact that it shares several aspects of the human disease. Indeed, the onset of CIA is mainly dependent on T-cells and B-cells with a huge immune response against collagen type II, which is one of the main components of the cartilage (Brand et al. 2007). This experimental method based on the intradermal injection of type II collagen was described for the first time in 1977 by Trentham et al. (Trentham et al. 1977). Thanks to this animal model, the role of T lymphocytes, in particular helper T-cells, has been clarified, indeed has been shown that they are essential for the onset and progression of RA (Klareskog et al. 1983). The model develops a polyarthritis, where each mouse can show a different number of joints involved and different degree of inflammation for each joint. It is characterized by a synovial hyperplasia, cartilage and bone degradation associated to a synovial membrane leukocyte infiltration (Trentham et al. 1977). DBA/1 (H-2^a) is the mouse strain associated with the highest percentage of disease incidence (80-90%), although several transgenic HLA-DR mouse strain has been generated in order to study specific HLA susceptibility and involvement in the pathogenesis. For example, humanized HLA-DR4-transgenic mice were generated to understand the higher RA incidence in female (Taneja et al. 2007). Moreover, it has been demonstrated that arthritic synovium of CIA mouse is characterized by an active angiogenesis suggesting that VEGF/VEGF receptor

pathway could be a potential therapeutic target (Raatz et al. 2012). Furthermore, it has been found that complement system inhibition plays a role in CIA model, reducing the progression and the onset of the disease (Linton & Morgan 1999).

1.3.2. Antigen-induced arthritis (AIA)

The antigen induced arthritis model is an experimental procedure to develop monoarthritis. First, animals are immunized with two intra-dermal injections of methylated bovine serum albumin (mBSA) or another antigen, inducing an immune response against the protein with a production of anti-antigen antibodies. Then, the same antigen is injected into a knee joint cavity inducing the formation of immune complexes and consequently the inflammation (Griffiths 1992). Three days after, the inflammation is evident due to the swollen knee joint. The inflammatory process reaches the highest degree after one week, when synovial hyperplasia, erosion of cartilage and bone are evident by histological analysis. The tissue damage is caused by both innate and adaptive immunity. It was demonstrated that purified helper T cells, previously sensitized for mBSA and injected directly into the joint together with the antigen were able to induce the inflammation into not immunized animals (Klasen et al. 1986). In addition, the complement system has a leading role in this model, indeed have been studied that animal with AIA, if treated with anti-C5 antibodies or C5a antagonist showed a decreased joint swelling and a lower histopathological score (Woodruff et al. 2002). Moreover, inflamed synovial tissues of the animal with AIA have been associated with a higher vessel density proving the fundamental role of the neoangiogenesis in this model. Indeed, the knockout of the gene VEGFB, a growth factor that belongs to the vascular endothelial growth factor family, reduced the synovial inflammation and the vascular density (Mould et al. 2003). This model was extensively used to study pathogenic mechanisms, but it has been overcome by the CIA model because of the reason described in the previous paragraph. Although AIA is considered obsolete to investigate pathogenic mechanism, this model is still excellent, at least in the first step, to study the biodistribution of new classes of therapeutics which aims to specifically target the inflamed synovial tissue (Macor et al. 2012)(Durigutto et al. 2017).

1.3.3. Other models of RA

Other rheumatoid arthritis models have been developed over the years. Among these, one of the first models of rheumatoid arthritis is based on Freund's adjuvant and for this reason it is

called “adjuvant induced arthritis”. Freund’s adjuvant is a mix of mineral oil and antigens, which acts as a booster of the immune response. This model has been used to investigate the role of T-cells, which are stimulated by the adjuvant injection to start the inflammatory process. The rat strain is important for the development of inflammation, indeed Lewis or Sprague-Dawley strains are considered susceptible strains showing 35% of incidence, while Buffalo and other strains are considered resistant strains showing 10% of incidence. After 10-15 days, the induced arthritis becomes stable for 2-3 weeks. After a month the symptoms are reduced. The adjuvant-induced arthritis by Freund’s complete adjuvant is characterized by the ankyloses, which causes the partial or complete stiffness of the joint in 50% of the affected animals. Moreover, cartilage and bone erosions are usually observed in animals developing the inflammation (Pearson 1956). Although this model is simple to develop and it requires a short time, on the other side it is important to note that this model does not fully reflect the complexity of the disease and it is not suitable for long-term studies. Another model to mention is the collagen antibody-induced arthritis (CAIA). This model is similar to CIA, and is often used to test new therapeutics. It is induced by the administration of a cocktail of antibodies against collagen. The advantage of this model lies in its speed of action and it can be used for several strains of mice, even in genetically modified mice. However, the model is expensive and very fast and aggressive compared to CIA, therefore it is less suitable to study chronic aspect of the disease (Khachigian 2006).

1.4. Treatment of rheumatoid arthritis

The comprehension of new molecular mechanisms underlies rheumatoid arthritis has improved the diagnosis and therapy of the disease. Surely, an early diagnosis is essential for a successful therapy. Indeed, treat the disease as early as possible allows avoiding cartilage degradation and bone remodelling which lead to a disability condition (Isaacs 2010). As discussed in paragraph 1.1, new classification criteria for rheumatoid arthritis were presented in 2010. These reduced the shortcoming of the previous criteria by increasing the sensitivity of 21% (Radner et al. 2014). Then, in order to understand whether the treatment is effective or not, two different systems to evaluate the disease-activity have been developed. The American College of Rheumatology (ACR) improvement criteria assesses, in percentage, the relative efficacy of the treatment compared to another therapy or placebo. The ACR20, which reflect the 20% of improvement, compared to the baseline, is considered as minimal response, while

the ACR50 (50%) is a moderate response and the ACR70 (70%) is the major response. The ACR criteria are widely used in clinical trials. By contrast, the disease activity score (DAS), using 28 joints (DAS28), is useful for daily practice. Indeed, it takes into account different parameters like tender and/or swollen joint count, global health, erythrocyte sedimentation rate or the C-reactive protein concentration. With a special equation, the DAS28 is calculated as a number which reflects the activity disease: high, moderate, low and remission (Smolen et al. 2016). However, these systems, able to evaluate the disease activity, are useful for the follow-up of patients with RA, but it is important to evaluate the structural damage of cartilage and bone. For this reason, radiographic images, MRI scans and ultrasound analysis are often performed to highlight joint narrowing space, cartilage and bone erosion (Bugatti et al. 2012).

The treatment of RA has changed over the last thirty years improving quality of life of affected patients. This was possible because of the introduction of a new class of drugs called disease-modifying antirheumatic drugs (DMARDs). Indeed, drugs belonging to this class are able to reduce structural damage while non-steroidal anti-inflammatory drugs (NSAIDs) do not interfere with the joint damage. However, these are used to reduce joint pain and stiffness. By contrast, glucocorticoids act like DMARDs, reducing disease progression in a rapid manner, however several important side effects were associated with their long term use. DMARDs are divided into two categories: synthetic DMARDs and biological DMARDs (bDMARDs), also called biological response modifier (BRM) (van Vollenhoven 2009).

1.4.1. Synthetic DMARDs and glucocorticoids

Among synthetic DMARDs, leflunomide, sulfasalazine, hydroxychloroquine and methotrexate are extensively used to treat RA and according to EULAR recommendation the treatment should start with one of these drugs in combination with low dose of glucocorticoids. However, methotrexate is considered the anchor drug because it shows a superior outcome compared with other DMARDs and because it has been demonstrated that methotrexate has a safer profile than other synthetic DMARDs, probably because of its low dose of administration.

1.4.2. Methotrexate

Methotrexate (MTX) is a chemical compound analog to folic acid capable to inhibit the dihydrofolate reductase (DHFR), an enzyme essential for the synthesis of tetrahydrofolate (THF). THF is a cofactor involved in nucleic acids synthesis, highly required during cell

proliferation. It has been widely used as a chemotherapeutic agent to treat neoplastic disease and in the mid-1980s it was introduced at low doses for the treatment of rheumatoid arthritis. Initially, the therapeutic effect of MTX on rheumatoid arthritis was attributed solely to its ability to reduce the number of high proliferative cells, such as lymphocytes and other inflammatory cells responsible for the inflammation. Other mechanisms of action have been recently demonstrated. Among them, the most accredited is that MTX inhibits 5-aminoimidazole-4-carboxamide ribonucleotide (AICAR) transformylase increasing the AICAR levels, thus leading to the release of intracellular adenine and adenosine into the extracellular space. Subsequently, extracellular adenosine that binds adenosine receptor 2 (A2) increases cyclic adenosine monophosphate (cAMP) with consequent immunosuppression due to the reduced production of pro-inflammatory cytokines such as TNF- α and IL-1 β . Moreover, the activation of A2 receptors induces the production of anti-inflammatory cytokines like IL-10 (Johnston-Cox et al. 2012). Although MTX is the most effective drug compared with other DMARDs and bDMARDs, some patients do not respond, others develop resistance or have important side effects after prolonged use. Most severe side effects associated with a long term use of MTX are: hepatic fibrosis, pulmonary fibrosis, fatigue and renal insufficiency (Tian & Cronstein 2007).

1.4.3. Biological DMARDs

In the mid 1970's a new technology allows producing monoclonal antibodies (Kohler & Milstein 1975). This technological progress opens the road to a new treatment opportunity called the antibody therapy. The potential of this treatment was immediately obvious, indeed new molecules could be designed and produced for a specific target expressed on specific cells, tissues or organs. This opportunity allowed to increase drug specificity decreasing toxic effects relative to traditional chemical compounds, which usually act with unclear mechanisms. At the moment, four different targets can be struck with bDMARDs for RA treatment: TNF- α , IL-6 receptor, CD20 and CD80/CD86 (Smolen et al. 2016). In particular, TNF- α inhibitors were the first biologicals developed to treat RA. The first monoclonal antibody approved blocking TNF- α was Infliximab (Reviewed in Campbell et al. 2011), a chimeric human-mouse monoclonal IgG. Whereas, Adalimumab was the first full human IgG approved to neutralize TNF- α (Rau 2002). Both became very popular because of the central role of TNF- α in the pathogenesis and progression of RA. TNF- α is produced mainly by T-cells and macrophages infiltrated into the

synovial membrane and its inhibition was associated to a decreased level of pro-inflammatory cytokines such as IL-1, IL-6, IL-8 and the growth factor GM-CSF (Butler et al. 1995). The effectiveness has been demonstrated in animal models of RA where the anti-TNF- α treatment reduces paw swelling and histological severity (Williams et al. 1992). These improvements were then confirmed in humans by several studies showing that anti-TNF- α inhibition prevents bone structural damage, improves physical function while slowing radiographic changes in joints (Ma & Xu 2013)(Chen et al. 2006).

1.4.4. Targeted synthetic DMARDs

The latest drug approved to treat RA is Tofacitinib, a Janus kinase (JAK) inhibitor. Drugs able to target one specific molecule, like JAK inhibitors, are included in a new class of drugs called “targeted” synthetic DMARDs. It interferes with the JAK-STAT signaling pathway, which is activated by several pro-inflammatory cytokines and growth factors such as IL-6, interferon- γ and GM-CSF. Once this pathway is active, it promotes the expression of inflammatory genes or genes involved in cell survival and proliferation (Ivashkiv & Hu 2003). Over a period of 2 years, Tofacitinib was superior if compared with Methotrexate, both as monotherapy (Lee et al. 2014).

1.4.5. Side effects of RA therapies

As previously mentioned, according to the EULAR recommendation the first line treatment is based on DMARDs. In particular, the gold standard to treat RA is still MTX due to its acceptable safety profile, low cost and great efficacy to prevent cartilage and bone destruction (Shinde et al. 2014). Indeed, biologicals drugs show similar improvement than MTX (Favalli et al. 2012) but are associated with more severe side effects. Among these, rare demyelinating syndromes, lupus-like reactions, bacterial infections and the reactivation of tuberculosis (TB) are associated with the inhibition of anti-TNF- α (Botsios 2005); common but tolerable side effects like injection-site reaction and infusion are also related to the TNF- α blocking (Scott & Kingsley 2006). Safety concerns were reported about Tofacitinib treatment, where respiratory tract infection, headache, and diarrhea were the most common side effects (Fleischmann et al. 2012)(van Vollenhoven et al. 2012). Despite MTX is still the anchor drug to treat RA, some issues are reported such as mouth ulcers, gastrointestinal intolerance, bone marrow and liver toxicity. Some of these side effects could be overcome with folate supplementation (Whittle

& Hughes 2004). However, one third of the patients treated with MTX had to discontinue the treatment after 2 years, while more than 50% discontinued the treatment after 5 years (Lee et al. 2014). Some patients discontinued this therapy because of inefficacy while other due to side effects. Pharmacogenetics' studies have been performed in order to find genes which can help to predict MTX toxicity but inconsistent data have been produced (Romao et al. 2014).

1.5. Nanotechnology and Nanomedicine

The term nanotechnology is defined in literature with different shades to explain its broad meaning and the wide range of methods, tools and possible application. For the purpose of this work the suitable definition is that accepted by the European Medicines Agency (EMA) based on the definitions provided by the UK Royal Society and Royal Academy of Engineering report (Dowling et al. 2004), the European Science Foundation foresight study on nanotechnology (Moran 2005) and the Vision paper and Basis for strategic research agenda for Nanomedicine by the European Technology Platform on Nanomedicine (Boisseau et al. 2005). Therefore, according to those documents, Nanotechnology is defined as "*the production and application of structures, devices and systems by controlling the shape and size of materials at nanometre scale. The nanometre scale ranges from the atomic level at around 0.2 nm (2 Å) up to around 1000 nm*" while Nanomedicine is defined as "*the application of nanotechnology in view of making a medical diagnosis or treating or preventing diseases. It exploits the improved and often novel physical, chemical and biological properties of materials at nanometre scale*". Despite the term nanotechnology became popular in 1986, thanks to Professor Kim Erik Drexler who used it in the title of his book "Engines of Creation: The Coming Era of Nanotechnology" (Drexler 1986), the term was coined by Professor Norio Taniguchi in 1974 to describe the precision manufacture of materials with nanometre tolerances (Taniguchi & Others 1974). However, it is important to mention the great contribution given by Richard Feynman during his provocative talk under the title "There's plenty of room at the bottom" to the California Institute of Technology. He foresees the potential to control single atoms and molecules improving the performance of instruments such as the electron microscopes. In conclusion, he foresees "Nanotechnology". That talk influenced the scientific community to challenge this research field and leading to the development of the scanning tunnelling microscope and the atomic force microscope (Toumey 2009), breakthroughs which were predicted by Feynman's talk years before. The potential offered by nanotechnology is still

underestimated, but the field of medicine is going to be revolutionised. Indeed, the opportunity to build structures in the same scale size of the biomolecules enhance a broad set of drugs features.

1.5.1. Nanocarriers

The success of nanotechnology is due to the excellent and unique properties offered by a material in its nanometre scale. Nanomaterials find application in many different fields: electronics, green technology and alternative energy, coatings, industrial chemistry, nanorobotics, cosmetics and biomedical. For examples, silver nanoparticles are widely used in disinfectants (Le Ouay & Stellacci 2015) while titanium dioxide and zinc oxide are used in sunscreen and cosmetics (Smits & Pavel 2011). The field of medicine is going to change fast due to the influence of nanotechnology leading to the new field called nanomedicine. In particular, nanoparticles are the main application of nanotechnology in the medical field (Kim et al. 2010). The success of nanoparticles lies in the advantages offered in comparison with the free drugs. Indeed, drugs encapsulated in nanoparticles are protected from the biological environment, where enzymes could degrade rapidly drugs. Nanocarriers improve the concentration of the drugs into the selected tissue and change the pharmacokinetics of a drug. Moreover, nanocarriers increase the intracellular penetration allowing different entrance mechanisms, different from those used by the free drugs. The same nanoparticles' features are now exploited to improve diagnosis, increasing the contrast and the sensitivity of currently used diagnostic probes (Peer et al. 2007). In addition, nanoparticles allow to carry at the same time diagnostic tracers and therapeutic compounds opening the way to the so called theranostics, or allow to deliver two drugs simultaneously, an option called combination therapy (Farokhzad & Langer 2009). Several different kinds of nanocarriers have been produced, characterized and finally used for many different purposes: polymer-drug conjugates, lipid-based nanocarriers such as liposomes and micelles, carbon nanotubes, dendrimers, gold nanoparticles, nanoshells and polymeric nanoparticles (Figure 5). Nanoparticles can be divided into two classes: organic and inorganic nanoparticles. Inorganics nanoparticles are made of metal atoms (metallic), non-metal atoms (organic) or a mixture of metal and non-metal (semi-conducting). Each of these types of nanoparticles shows peculiar features and are used for different application. Metallic nanoparticles usually find medical application as diagnostic probes for magnetic resonance imaging (MRI), positron emission

tomography (PET), X-ray and optical imaging. Organic nanoparticles can be made of different polymers or lipids and due to their biodegradability are widely used for drug delivery (Murthy 2007).

In 1995 the first formulation of liposomes has been approved by Food and Drug Administration (FDA) under the trade name Doxil (liposomes loaded with doxorubicin) for the treatment of the Kaposi sarcoma. This formulation demonstrated an improved circulation half-life of doxorubicin and an increased accumulation in the tumour tissue (Barenholz 2012)(Gabizon et al. 2003). To this day, 11 different formulations of liposomes have been approved for the treatment of different diseases. They are spherical vesicles essentially made of phospholipids, which, due to their amphiphilic nature, are able to self-assemble in aqueous solution. The polar shell is made of a lipid bilayer, which is able to hold lipophilic molecules between the two phospholipids bilayer. By contrast, the aqueous core can be loaded with hydrophilic molecules (Pattni et al. 2015). The surface of these structures can be functionalized with different molecules in order to target specific kind of cells or tissues. Despite the success of liposomes based nanocarriers as drug delivery systems, their use is still limited by some technical reasons. Indeed, liposomes are characterized by low stability for long term storage and the limited amount of drug that can be loaded (Sanna et al. 2014).

Polymeric micelles are self-assembled core-shell nanostructures made by amphiphilic block copolymers. In aqueous solution, the hydrophobic regions of the block copolymers aggregate in order to reduce contact with water molecules producing core-shell vesicles. These structures usually found application in the delivery of hydrophobic drugs which can be loaded into the core of these structures (Xu et al. 2013).

Polymer drug conjugates were first described in 1977 when researchers reported no immunogenicity of bovine serum albumin (BSA) when conjugated to polyethylene glycol (PEG) (Abuchowski et al. 1977). Indeed, because of its low immunogenicity, PEG is the most used polymer to make nanocarriers stealth to the immune system (Salmaso & Caliceti 2013). In addition, PEG increases the solubility of the attached proteins and increases proteins' half-life in the bloodstream because of their higher molecular weight (Pasut & Veronese 2012). The prolonged half-life associate to the use of PEG-conjugated protein was demonstrated with a commercial antibody called certolizumab pegol, a Fab fragment (described in the paragraph 1.7.1) able to block TNF- α and conjugated to PEG of 40kDa. This antibody, now used to treat RA, shows higher time of circulation and a lower rate of kidney elimination if compared to

other commercially available anti-TNF- α . Moreover, a higher tissue penetration was reported for PEG conjugated antibody fragment. In fact, PEG increases the molecular weight, enhances the retention time in the inflamed tissue, where the vessels are usually characterized by their high permeability (Palframan et al. 2009). Another successful polymer used as a conjugate agent is hyaluronic acid (HA). This is a natural polysaccharide able to bind its receptor CD44, which has been found to be overexpressed in inflamed synovial tissue. For this reason, HA is a molecule suitable for target drug delivery in inflamed joints of RA patients. Indeed, HA has been used in conjugation with MTX demonstrating that HA-MTX is able to reach the inflamed joint in a higher concentration thus showing a superior therapeutic efficacy if compared with the free drug (Shin et al. 2014). Dendrimers are tree-like branched macromolecules made of natural or synthetic elements. They have a central inner core with radially attached repeated units which possess several chemical functional groups nearby the surface (Pandita et al. 2014). Due to different functional end groups, they are multivalent nanocarriers able to carry several kinds of molecules. Dendrimers have been used to treat animal model of rheumatoid arthritis showing great ability to reduce osteoclastogenesis and to decrease the secretion of pro-inflammatory cytokines (Bosch 2011).

Carbon nanotubes are cylindrical nanostructure made of benzene rings. They can have different structures such as single-walled nanotubes (SWNTs) and multi-walled nanotubes (MWNTs). The latter is made of multiple rolled layers of graphene (Eatemadi et al. 2014). These nanostructures have been exploited mainly for diagnostic purpose. Indeed, issues regarding their toxicity are still under debate and limit their prolonged therapeutic use. Although, different approaches have been used to increase carbon nanotubes biocompatibility and biodegradability. To this aim, chemically functionalised carbon nanotubes show reduced toxicity and better degradability due to the oxidative enzymes (Bianco et al. 2011).

Polymeric nanoparticles (NPs) represent another class of successful nanocarriers, which has been used in medical application both for diagnostic and therapeutic purposes. They are composed of block copolymers with different hydrophilicity, length and molecular weight, which spontaneously assembles into a core-shell structure in an aqueous environment. High amounts of therapeutics can be loaded into the core of these structures and, due to the hydrophilic shell, encapsulated drugs are protected from the external environment (Hu & Zhang 2012). Initially, polymeric nanoparticles were mainly produced by non-biodegradable polymers, such as polystyrene, polyacrylates, poly (methyl methacrylate) (PMMA) or

polyacrylamide. Because of their non-biodegradability, these particles usually have been optimized in order to obtain a fast clearance avoiding accumulation at a toxic level. However, non-biodegradable polymers have been associated with inflammatory reactions and chronic toxicity. Indeed, recently an important work has compared the *in vivo* effects of biodegradable and non-biodegradable polymeric nanoparticles administrated through the airways into the lungs showing an increased expression of pro-inflammatory cytokines such as IL-6 and TNF- α in mice receiving polystyrene NPs (Aragao-Santiago et al. 2016). Thus, in the last years, an increased interest has been focused on the use of biodegradable polymers.

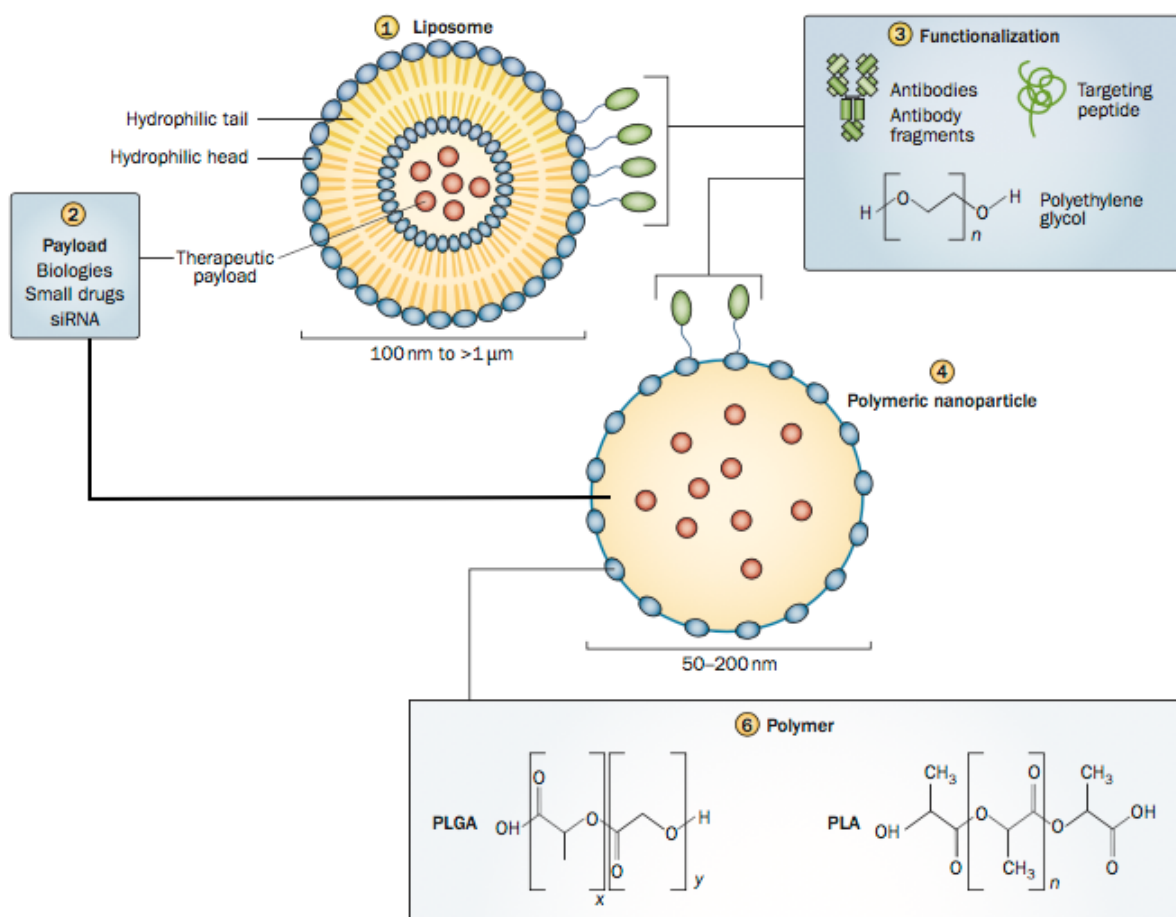


Figure 5: Basic structure of organic nanocarriers.

Liposomes (1) are made of a double layer of lipids which can be loaded with different kinds of therapeutics such as biologicals, small drugs, nucleic acids (2). Polymeric nanoparticles (4) are made of biodegradable polymers like poly (lactide-co-glycolide) copolymers (PLGA) and poly (lactide) (PLA) and other types of polymers (6). Both liposomes and polymeric nanoparticles can be functionalized (3) with antibodies, their fragments or targeting peptides. PEG is usually used to reduce the interaction with the mononuclear phagocyte system (MPS). The figure is adapted from Ferrari M et al. Nat Rev Rheumatol 2015 (Ferrari et al. 2015).

1.5.2. Biodegradable polymers

Biodegradable polymeric nanoparticles are the most popular and successful nanocarriers because they provide a controlled release, subcellular size and biocompatibility. BNPs'

polymers can be synthetic such as poly (ϵ -caprolactone)(PCL), poly (lactide)(PLA), poly (lactide-co-glycolide) copolymers (PLGA) and poly (amino acids) or can be natural like chitosan, alginate and gelatine (Banik et al. 2016). PLGA is one of the most used polymer due to its biodegradability. It is hydrolysed in two monomers, one of lactic acid and one of glycolic acid which are both non-toxic molecules for the human body. In the same way PLA is a biocompatible and a biodegradable polymer and it is metabolized in monomeric units of lactic acid, which is a natural intermediate of anaerobic respiration, showing very poor toxicity. No toxicity was reported also for PCL which is degraded by hydrolysis of its ester linkages (Mahapatro & Singh 2011)(Kumari et al. 2010). PCL is characterized by very low *in vivo* degradation time and high drug permeability and for these reasons is widely used for tissue engineering scaffolds (Ulery et al. 2011). PLGA, PLA and PCL were approved by FDA for several applications in human body.

1.5.3. Properties and rational design of nanoparticles

In order to design successful nanocarriers with a higher therapeutic efficacy or diagnostic sensitiveness it is fundamental to rationally design nanocarriers with tissue specificity in order to avoid unspecific distribution and low accumulation of the molecules in the target cell/tissue. To reach this aim, a rational design should take into account several physicochemical features of the polymers and the final structure. Likewise, the design should consider the environment in which nanocarriers will be injected and the biological barrier to cross and reach the final target (Blanco et al. 2015). The route of administration influences the biodistribution and the adsorption. Indeed, orally administrated nanoparticles have to cross the gut mucosa to reach the bloodstream. This route showed a slow rate of adsorption and only low amount of nanoparticles reach the target tissue. By contrast, intravenously administrated nanoparticles showed 100% of bioavailability and a fast biodistribution (Simon & Sabliov 2014). Biodegradability and biocompatibility are indispensable traits to satisfy in order to design nanocarriers, which can be used for medical purposes. Indeed, FDA biodegradable polymers are usually used to develop new nanotechnological therapeutics and diagnostics. Degradation time of biodegradable polymers depend on the length of the polymers while the nanoparticles' shape is mainly a result of the molecular weight and the polymer concentration as well as the encapsulation efficiency (Danhier, Ansorena, et al. 2012). Size, shape and features of the shell surface, such as the charge, define their biodistribution and stability in the bloodstream. Once

in the circulation, nanoparticles must avoid opsonisation and then cross the blood vessels to arrive in the target tissue. The process of opsonisation includes the adsorption of plasma proteins, serum albumin, immunoglobulins and complement proteins on the surface of nanoparticles. These proteins form the so called “protein corona”, which is responsible of a rapid clearance, hindrance of targeting capacity, and induction of toxicity (Nguyen & Lee 2017). Due to these proteins adsorbed on the surface, nanoparticles are often recognized by the mononuclear phagocyte system (MPS). The MPS is mainly composed by macrophages of the spleen, lymph nodes and liver, which contribute to the phagocytosis and elimination of the nanoparticles (Moghimi & Patel 1998). The formation of the protein corona is influenced by different factors such as surface charge, hydrophobicity, nanoparticles size and functional groups on the shell. The best strategy to design “stealth” nanoparticles is to cover the surface with non-immunogenic and hydrophilic molecules able to mask the hydrophobicity of the nanoparticles. The most widely used molecule is PEG, already used in conjugation with antibodies to increase their lifetime (see paragraph 1.5.1). In the same way, when PEG is used on the surface of nanoparticles, it increases the circulation time in the blood (Hamilton et al. 2002). Moreover, it reduces nanoparticles aggregation and protein corona formation (Fang et al. 2009). The conformation, the length and the density of PEG are features that affect the circulation time of nanoparticles. In general, long chain of PEG (20-50 kDa) are used in conjugation with small protein thus preventing renal excretion, while short PEG chains (3-10 kDa) are usually bound on larger nanoparticles (50-100nm) because an increased diameter could increase the interaction with the MPS. For what concerns the density, it is known that low density of PEG on the surface of nanoparticles assumes a “mushroom” conformation, by contrast, high density of PEG assumes a “brush” conformation. The latter increases the lifetime due to the fact that high density of PEG masks the nanoparticles from the MPS (Jokerst et al. 2011). Although, PEG is not the only stealth material and other hydrophilic polymers with stealth properties can be used such as poloxamer, polyvinyl alcohol, poly(amino acids) and polysaccharides (Huang & Guo 2011). Advanced strategies to produce stealth nanoparticles have been developed using cell membranes isolated from leukocytes (Parodi et al. 2012) or red blood cells (Hu et al. 2011) showing an increased circulation time. Another important characteristic is the dimension of the nanoparticles. Indeed, nanoparticles, in order to be accumulated in the target tissue, must cross the blood vessel wall. Usually healthy blood vessels have pore size about 5 nm. Thus, nanoparticles with a diameter less than 5 nm quickly

reach the extravascular extracellular space (EES), while bigger nanoparticles remain in the bloodstream for a longer time. Similarly, nanoparticles smaller than 6 nm can easily reach lymphatic vessel due to their permeability. Small particles with a hydrodynamic diameter < 5nm are usually filtered by kidney while particles bigger than 8 nm are not filtered. In this process, the surface charge effects the flow of elimination, in fact molecules with similar diameter have different filtration time due to the charge. Cationic molecules are filtrated first, followed by neutral and negative molecules. Renal filtration is the most important process associated to the clearance, although spleen and liver also play a central role in the elimination of nanoparticles. Nanoparticles, too big to be eliminated by the kidney, reach the liver and the spleen where resident macrophages internalize particles through endocytosis and destroy opsonized material. Moreover, both liver and spleen eliminate particles with a diameter of 10-20 nm because of their physiological function (Figure 6) (Longmire et al. 2008).

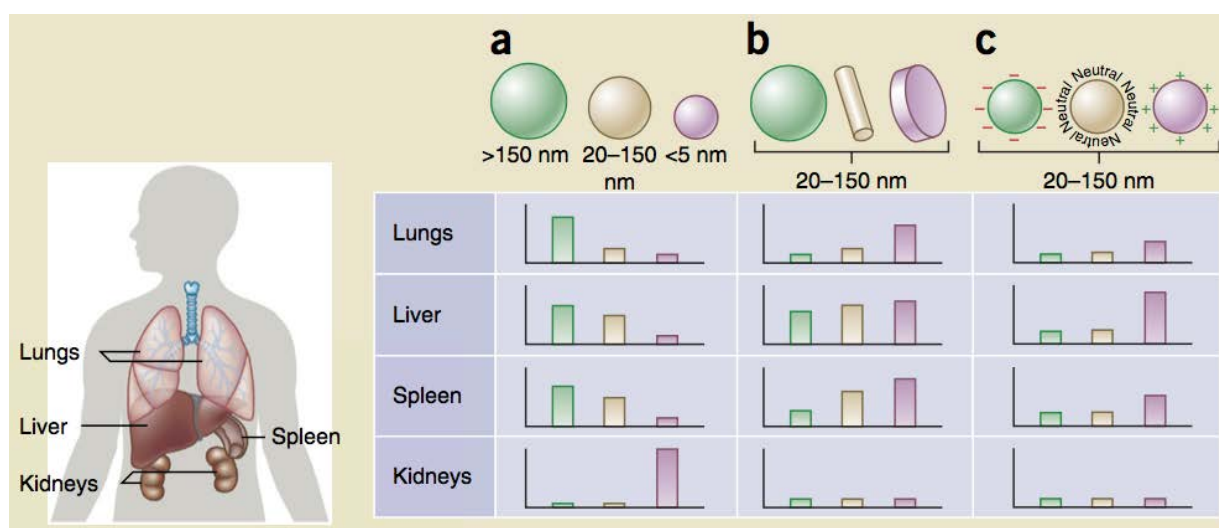


Figure 6: Biodistribution of nanoparticles.

(a) Size, shape and surface charge of the nanoparticles characterize their bio-distribution among various organs such as lungs, liver, spleen and kidneys. Medium sized nanoparticles (20-150 nm) mainly accumulate in the liver, less in spleen and especially in lungs. The same trend has been reported for the big particles (>150 nm) with a higher accumulation in the lungs. Instead, small particles (<5 nm) accumulate in the kidneys. (b) Cylindrical and discoidal particles have shown different pharmacokinetic and biodistribution compared to spherical particles. In particular, discoidal particles increase their accumulation in the lungs and spleen. (c) Positively charged nanoparticles efficiently accumulate in different organs while neutral and negative particles are characterized by a long last circulation. The figure is taken from Blanco E. Nat Biotechnol 2015 (Blanco et al. 2015).

Finally, if nanoparticles avoid all the biological barriers mentioned, they reach into the target tissue where they can enter into the cells by several internalization pathways. In general, the endocytic route depends on the nanoparticles' diameter. Phagocytosis usually occurs in many cell types such as endothelial cells, fibroblasts and immune cells. Phagocytosis is characterized by large vesicles of >250 nm, which are able to internalize materials of considerable dimension. It has been demonstrated that spheres with a radius of 12.5 μm can be internalized using this

mechanism (Champion & Mitragotri 2006). Another endocytic pathway able to internalize particles with a big diameter is called macropinocytosis. Through this pathway, it is possible to internalized particles with a diameter between 0.5 and 10 μm . Instead, smaller particles with a diameter of \sim 120 nm are internalized through the clathrin-mediated endocytosis (CME). Many proteins participate in the formation of CME vesicles, in particular clathrin, which coats the vesicles inducing the curvature of the membrane. It has been proved that cationic nanoparticles made of PLA-PEG with a diameter of \sim 100 nm are exclusively internalized by CME endocytosis (Harush-Frenkel et al. 2007). The charge effects the internalization, indeed positively charged nanoparticles are attracted by negatively charged cell surface leading to an enhanced internalization via CME (Yameen et al. 2014). Caveolae-mediated endocytosis is another route of internalization which uses a specific protein (Caveolin) to form the vesicles with a flask-shaped structure of 60-80 nm (Doherty & McMahon 2009). This is the preferential route used by viruses and other pathogens to enter into host cells because of bypass the lysosomes (Carver & Schnitzer 2003). For the same reason, this pathway should be convenient to delivery DNA or proteins. Moreover, this pathway received great attention because it is involved in the trans-endothelial pathway thus could be exploited to design particles able to deliver its content across the endothelial tissue (Oh et al. 2007). However, are known two alternative mechanisms of internalization, which do not require the presence of coat proteins: clathrin and caveolin-independent endocytosis. Usually, vesicles of these pathways can internalize particles with a diameter smaller than 90 nm (Yameen et al. 2014).

Taking into account all these knowledge, it is reasonable that nanoparticles with a diameter between 100 and 200 nm should be the best choice to obtain a long-lasting circulation.

1.6. Passive and active targeting

The process by which the nanoparticles bind their target tissue can be passive or active. The passive targeting does not require a specific surface functionalization of the nanoparticles and the movement and interaction are based only on the morphology and chemicophysical features. On the contrary, in the active targeting, particular molecules conjugated on the nanoparticles' surface are able to drive them into a specific tissue.

1.6.1. Passive targeting

The passive targeting coincides with the Enhanced Permeability Retention (EPR) effect. This effect was discovered in 1986 by Matsumura Y. & Maeda H, who described the higher accumulation of a drug polymer conjugated, compared to the free drug, into the tumor of tumor bearing mice. This effect is the result of the pathophysiologic features of the tumor hypervasculature coupled with poor lymphatic drainage (Figure 7) (Matsumura & Maeda 1986). Indeed, it is known that tumor sites, as well as inflamed tissue, are characterized by a prominent neoangiogenetic process in which blood vessel showed high pressure and enhanced permeability due to the fact that fenestration of blood vessel in this pathological tissues can reach diameters of several μm (Hashizume et al. 2000). In the inflamed tissue, several molecules such as histamine, bradykinin, leukotrienes, and serotonin contribute to the increased permeability. In addition, lack of tight junction between endothelial cells and lack of functional smooth muscle layer around the blood vessels increase the process of extravasation (Nehoff et al. 2014). Instead, the “retention” is the result of the lymphatic vessels impairment reported in tumor mass and in the hyperplastic synovial tissue of RA patients and other inflamed tissue. Indeed, the poor drainage of the lymphatic vessels has been demonstrated in several studies, although its mechanism is not yet clear (Bouta et al. 2015). Since healthy tissue does not have large fenestration in the blood vessels and shows regular pressure and lymphatic vessels functions, nanocarriers preferentially reach pathological tissue due to the EPR effect. This mechanism of nanocarriers’ distribution allows to passively delivery drugs with higher concentration into the affected tissue, increasing the effectiveness and often avoiding side effects in healthy tissue (Maeda et al. 2013). It is known that small particles are able to quickly reach and diffuse in the target tissue, but their retention would be low and clearance would be fast. By contrast, particles with a bigger diameter reach their target slowly but their retention and clearance would be enhanced. Thus, in order to exploit the potential of the EPR effect, it is important to find the right compromise during the particles’ design (Blanco et al. 2015).

1.6.2. Active targeting

Despite advantages of the passive targeting, some limitations are known. Indeed, due to the variability present among tumors or inflamed tissues, an insufficient amount of nanocarriers

reach the desired target. Moreover, the passive targeting, despite the EPR effect, is not sufficient to distinguish healthy tissue from pathological tissue (Steichen et al. 2013). For this reason, the research focuses its attention on the active targeting. In addition to the passive EPR effect, the active targeting exploits molecules able to recognize a tissue-specific marker, which is expressed or overexpressed by the target tissue (Figure 7). Several studies have demonstrated that targeting nanocarriers have a superior therapeutic efficacy and diagnostic sensitivity compared to untargeted nanocarriers (Phillips et al. 2010). In addition, nanocarriers with tissue specificity avoid delivering drugs or diagnostics in healthy tissue reducing side effects (Steichen et al. 2013).

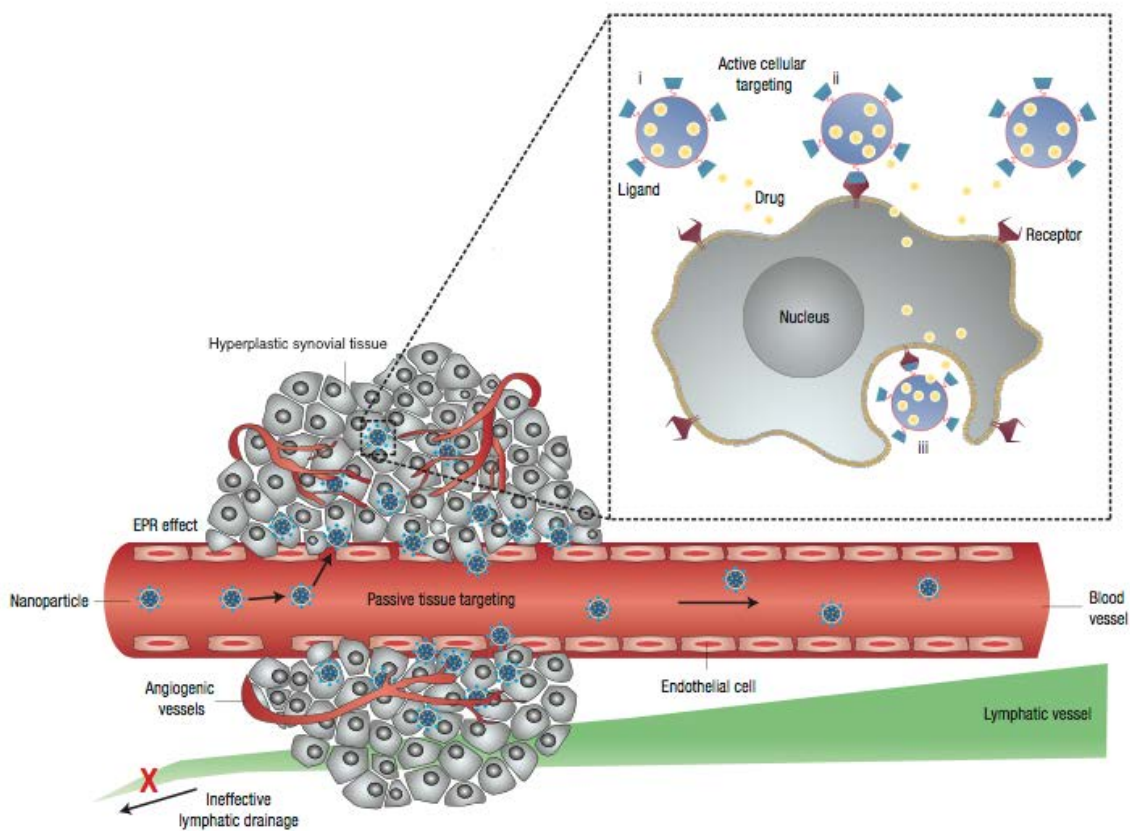


Figure 7: Passive and active targeting.

The figure represents nanoparticles that can deliver their payload into the inflamed synovial tissue. Because of the increased permeability of the blood vessels, nanoparticles can easily reach the hyperplastic synovial tissue (EPR effect). The active targeting can be achieved thanks to targeting molecules conjugated on the surface of the nanoparticles able to bind specific ligands on the target cells. With this targeting systems, drugs can be released in close proximity of the target cells/tissue and/or inside these cells. The figure is adapted from Peer D. Nat Nanotechnol, 2007 (Peer et al. 2007).

1.7. Targeting agents for rheumatoid arthritis

Different classes of targeting agents can be used to deliver nanocarriers in a specific tissue: proteins, like antibodies or their fragments, aptamers (nucleic acids) or other small molecules

such as peptides, vitamins and carbohydrates (Peer et al. 2007). This approach potentially increases the therapeutic efficacy, avoiding off-target side effects. Moreover, a reduction in costs of disease management is expected because the doses required to achieve same efficacy to untargeted drugs might be lower (Ferrari et al. 2015).

1.7.1. Recombinant antibodies and their fragments

The antibodies are heterodimeric proteins composed of two structural elements defined as Heavy (H) and Light (L) chains because of their aminoacidic composition and molecular weight. The heavy chain is made of 440aa with a molecular weight of 50kDa whereas the light counterpart consists of 220aa with a molecular weight of 25kDa (Wang et al. 2000). Each chain can be divided into two basic building blocks: the variable (V) domain (NH₂-terminal), able to interact with the antigen, and the constant (C) domain (COOH-terminal), responsible for the effector functions such as the macrophages binding or the complement system activation. The heavy chain differs from the light chain for the number and composition of these functional domains: the light chain contains one constant domain (CL) whereas the heavy chain could be composed by either three or four constant domains (CH) (Figure 8). A spacer hinge region is located between CH1 and CH2 and confers particular flexibility to the final structure (Schroeder Jr. & Cavacini 2010). Depending on the constant composition, the human heavy chains could be classified into 5 isotypes: IgM, IgG, IgA, IgD and IgE. The subclasses IgM and IgE have four CH in contrast to the others, which have only three constant domains and the hinge region. In the variable domain three hypervariable loops are responsible for the antigen identification, called complementarity determining region (CDR) (Kim et al. 2005). Three functional domains can be identified by papain digestion: two identical Fab, “fragment antigen-binding”, which consist of the whole L-chain linked with the VH and the CH1 portion of the heavy chain; one Fc, “fragment crystallisable”, made of two covalently linked CH2-CH3 (or CH2-CH3-CH4). Instead, the immunoglobulin can be cleaved in two part by pepsin: F(ab')² fragment and a Fc fragment. The Fab can be separated into a variable fragment (Fv), made of VH and VL responsible for the antigen binding and another fragment composed of the CL and CH1. Taking advantage of this functional domains, different fragments have been designed and produced by recombinant technology. Indeed, fundamental were the studies conducted by Kohler and Milstein in 1975 (Kohler & Milstein 1975). They find a way to immortalize B cell precursors through the fusion with mouse myeloma cells to generate stable monoclonal

antibody production. Although this technique provides a useful method for the production of monoclonal antibodies, the murine origin of the antibodies causes immunogenicity in humans (Schroff et al. 1985)(LoBuglio et al. 1989). However, improvement of molecular biology technique allows researchers to reduce the murine component in favor of the human component, generating different kinds of antibodies such as chimeric, humanized or fully human. Most successful engineered antibodies used are: the scFv (single chain fragment variable) or Fab. However, some issues are associated with the small molecular size: fast clearance, poor stability and monovalent binding to the antigen. Although, in order to solve this problem two different engineered antibodies have been designed: the scFv-Fc made of the scFv fused to the CH3-CH2 portion; the so called “minibody” made of the scFv fused to the CH3. These formats showed an improved pharmacokinetics with a prolonged circulation time, increased tissue penetration and enhanced epitope selectivity (Olafsen & Wu 2010). However, many types of these antibodies have been used as therapeutic agents (immunotherapy) or as targeting agents for nanocarriers.

1.7.2. Peptides

Although the antibodies are used as targeting agents able to delivery nanocarriers in a specific tissue, recently peptides have been used with great success. Due to their small size, high stability, low immunogenicity and easy production, peptides have huge potential as targeting agents (Sanna et al. 2014)(Ferrari et al. 2015). Peptides containing the aminoacidic sequence Arg-Gly-Asp (RGD) are able to bind integrins $\alpha_v\beta_3$, which are expressed on endothelial cells of the inflamed synovial tissue and tumours. Indeed, in a mice model of the syngeneic transplantable liver tumor (TLT) have been demonstrated the retarded tumor growth and a prolonged survival time of mice treated by paclitaxel (PTX)-loaded RGD-nanoparticles when compared to non-targeted nanoparticles (Danhier, Pourcelle, et al. 2012). In the same way, it has been proved that RGD-MTX-PLGA-Au (gold) nanoparticles injected in a model of collagen-induced arthritis had a superior therapeutic efficacy, compared with untargeted nanoparticles, with a much smaller dosage of MTX in the nanoparticles (Lee et al. 2013).

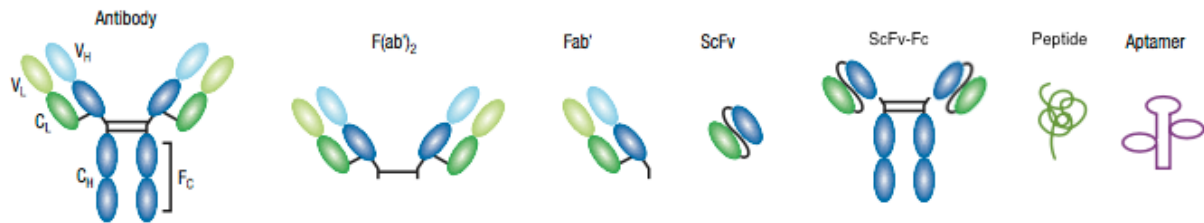


Figure 8: Antibodies and their fragments used as targeting molecules.

The figure represents the structure of a full immunoglobulin (starting from the left) with the VL, VH, CL and CH. Then, fragments such as $F(ab')_2$, Fab' and another format like the ScFv and ScFv-Fc are reported. Finally, are represented small targeting molecules such as peptides and aptamers. Figure adapted from Peer D. Nat Nanotechnol, 2007 (Peer et al. 2007).

1.7.3. Targeting the vasculature

As already discussed in paragraph 1.2, the neoangiogenesis has an important role in the pathogenesis of rheumatoid arthritis. For this reason, the microvasculature of the synovial tissue is becoming an interesting target for the diagnosis and treatment of this chronic disease. Indeed, the endothelial tissue is the first barrier that leukocytes have to cross to infiltrate the synovium (Ferrari et al. 2015). Lee et al. have isolated a peptide with specificity for the human arthritic synovium, in particular for the inflamed microvasculature, by injecting a phage display library in a human synovium–SCID mouse transplantation model. The isolated peptide is made of 7 aminoacids (CKSTHDRLC) flanked by two cysteines, which constrain the circularization of the peptide (Lee et al. 2002)(Onuoha et al. 2015). This peptide was already used in fusion to IL-4 in order to delivery cytokines into the human RA synovium in the SCID mouse xenograft model, proving the great potential of the peptide-targeting approach. Using the same strategy, this peptide has been fused to the Fc portion of the anti-complement C5 antibody increasing its accumulation into the inflamed joints compared with the parent anti-C5 antibody. The targeting antibody, as consequence, showed an improved efficacy allowing a threefold lower administration dose (Macor et al. 2012).

2. Aim and rationale of the thesis

The use of immunotherapy has now become part of common clinical practice for the treatment of several diseases. Indeed, immunotherapy is widely used to treat cancer and it has been used to successfully treat RA patients, improving their quality of life. Although, their administration recognizes and blocks their targets systemically enhancing the risk of developing side effects, such as bacterial and viral infections. Moreover, high costs of biological drugs are holding back their widespread usage. For these reasons, synthetic DMARDs, such as MTX, are still the anchor drugs to treat RA. Despite the improvements, patients are treated lifetime, true remission is achieved by minority and most of them have to face relapses.

In this scenario, there is the need to develop smart drugs with tissue specificity able to act avoiding systemic complications, increasing the effectiveness and reducing doses and costs. Another important aspect to improve is the diagnosis of RA. According to the classification criteria for rheumatoid arthritis 2010 ACR/EULAR, the diagnosis is based on clinical objective evaluations, laboratory tests and imaging analysis. Today, radiography is the mainstay for the diagnosis and follow-up of RA, however, radiations limit its usage. Moreover, the diagnosis of the disease is still challenging due to the lack of tissue specific contrast agents.

For this reason, it would be of great interest to develop new therapeutics able to increase imaging sensitivity highlighting synovial inflammation, cartilage and bone erosions maintaining low toxicity and invasiveness, possibly developing an approach that allows the diagnosis with biocompatible materials, suitable for different imaging techniques such as radiography, ultrasounds and magnetic resonance imaging.

Nanotechnologies, particularly nanoparticles, have peculiar characteristics able to satisfy needs described above. In fact, nanoparticles can be functionalized with antibodies and peptides that specifically target tissues or cells, allowing the delivery of a considerable amount of their payloads (diagnostic tracer or drugs). This strategy should increase the concentration of drugs or diagnostics into the desired tissue, allowing the reduction of the dose with a consequent reduction of costs and side effects.

Our group in 2012 developed an anti-complement C5 antibody (ScFv-Fc) able to specifically target inflamed synovial tissues due to the synovial homing peptide fused with the Fc portion of this antibody (Macor et al. 2012). This strategy demonstrated that the targeted peptide increases the accumulation of therapeutic or diagnostic molecules onto the microvascular endothelial tissue of the inflamed RA tissue.

As a matter of fact, neoangiogenesis is a key process in the development of RA with the involvement of adhesion molecules, cytokines and chemokines, regulating the inflammatory process and in particular allowing inflammatory cells infiltration in the synovial microenvironment.

The aim of this work is to design, produce and characterize a diagnostic or drug delivery system specific for the inflamed synovial tissue combining a targeting strategy based on the synovial peptide already used by us with the potential features of the biodegradable nanoparticles. In particular, the synovial peptide, specific for the inflamed synovia, has been conjugated on the surface of biodegradable polymeric nanoparticles, which in turn can be loaded with drugs (in this case MTX) or conjugated with diagnostic tracers (Cy5.5, a near infrared dye). This plan aims to demonstrate *in vivo*, using animal models of rheumatoid arthritis, that targeted nanoparticles (tBNPs), compared to untargeted nanoparticles (BNPs), are able to specifically target the inflamed synovial tissues.

Labelled tBNPs will have the possibility to concentrate into inflamed synovial microenvironment providing information about the stage of the pathology.

The local drug delivery through tBNPs-MTX should provide greater therapeutic efficacy than free MTX, using lower doses of MTX encapsulated in tBNPs; this will retain its effectiveness reducing side effects.

3. Materials and methods

3.1. Production of the targeting molecule

The sequence of the synovial peptide, which is a peptide of 9 aminoacids (CKSTHDRLC), used to drive nanoparticles into the inflamed synovial tissue, has been previously cloned in fusion with a ScFv-Fc in order to generate the targeting molecule (Macor et al. 2012).

The monoclonal cell line transfected with the vector pcDNA3.1/Hygro+ coding for the targeting molecule (ScFv-Fc-synovial peptide) has been cultured in the CELLlineTM Device (BD Biosciences). This device is a small bioreactor, which allows reaching a high amount of proteins compared with traditional culture flasks. First, the cells have been expanded in a T75 tissue culture flask in ProCHO5 (Lonza), penicillin 10U/mL (Sigma), streptomycin 1 μ g/mL (Sigma), L-glutamine 2mM (Sigma), FBS 10% (fetal bovine serum) and Hygromycin B 200 μ g/mL (Sigma). Once the confluence has been reached, the cells have been detached by Trypsin 0.25mM-EDTA (Ethylene diamine tetra acetic acid) (Sigma) and resuspended with 15mL ProCHO5 (Lonza), penicillin 10U/mL (Sigma), streptomycin 1 μ g/mL (Sigma), L-glutamine 2mM (Sigma), FBS 10% (fetal bovine serum), Hygromycin B 200 μ g/mL (Sigma) to a final concentration of 1x10⁶ cells/mL. Thus, cells have been added to the cultivation chamber while 300mL of ProCHO5 (Lonza) have been added to the nutrient supply chamber. The cells have been cultivated at 37°C with 5% of CO₂. Twice a week the supernatant containing the targeting molecule has been collected from the cultivation chamber and replaced with 15x10⁶ fresh cells. The collected supernatant has been centrifuged at 1500 g for 20 minutes to remove debrides and cells.

3.2. Purification of the targeting molecule

The targeting molecule has been purified by affinity chromatography using the HiTrap rProtein A FF 1 mL (Amersham Biosciences). The column has been equilibrated with 20mM sodium phosphate buffer pH 7 (equilibrating buffer) and the supernatant passed through the column with a flow of 1mL/minute with the help of a peristaltic pump. Afterwards, the column has been washed with the same equilibrating buffer and finally, the target molecule has been eluted using 0.1 M sodium citrate buffer pH 3.0 (elution buffer). Fractions of 1.5mL have been collected and quickly equilibrated with 300 μ L 1 M Tris-HCl pH 9.0 (neutralizing buffer) to restore the pH to a physiological value. Finally, these fractions containing the purified antibodies have been dialyzed with DPBS O/N at 4° quantified by absorbance assay at A280nm using a spectrophotometer (Eppendorf BioPhotometer Plus).

3.3. SDS page and Western blot of the target molecule

Fractions containing the purified targeting molecules have been subjected to an SDS page. The gels were characterized by stacking 4% and resolving 10% acrylamide concentration. In particular, the stacking was made with Acrylamide/Bis-acrylamide 30% solution (Sigma), Tris-HCl 130mM pH 6.8, SDS 0,1%, Ammonium persulfate 0,1% and TEMED (N,N,N',N'tetrametiletilendiamina) 0,01% (Sigma). The resolving was made with Acrylamide/Bis-acrylamide 30% solution (Acrylamide 29.2g/ Bis-acrylamide 0.8g in 100mL of H₂O) (Sigma), Tris-HCl 400mM pH 8.8, SDS 0,1%, Ammonium persulfate (APS) 0,1%, TEMED 0,01% (Sigma). The gels have been prepared by Mini-PROTEAN, Tetra Vertical Electrophoresis Cell, Biorad with a thickness of 0.75mm. For reduced conditions, samples have been diluted in sample buffer (Tris-HCl 61.5mM pH 6.8, SDS 2.5%, Glycerol 10%, bromophenol blue 0,0025%, β-mercaptoethanol) and then boiled for 5'. The run has been performed in running buffer (Tris-HCl 50mM, Glycine 384mM, SDS 0,1%) at 15mA until proteins reached the running gel, then the current has been increased to 20mA. Proteins separated by SDS page have been transferred to nitrocellulose membrane (GE Healthcare, Amersham UK) by Western blot using a Mini Trans-Blot® Module, Bio-rad. The transfer has been performed at 3.5mA cm² for 45' in transfer buffer (Tris-HCl 25mM, Glycine 192mM, Methanol 20%, pH 8.3). Afterwards, the membrane has been blocked with 2% of skim milk (S.M.) in PBS at 4°C overnight. Then, the membrane has been washed three times with wash buffer (0,1% of Tween 20 (Polyoxyethylene Sorbitan monolaurate)(Sigma) in PBS) and incubated 1h RT (room temperature) in agitation with the primary antibody mouse anti-SV5-biotinylated (homemade produced) diluted 1:2000 in the diluent buffer (0,1% S.M. and 0,05% Tween 20 in PBS). Then the membrane has been washed three times with wash buffer and incubated 30' RT in agitation with Streptavidin-alkaline phosphatase (Sigma) diluted 1:2000 in diluent buffer. Finally, the membrane has been washed three times and developed with 0,3 mg/ml of BCIP (5-Bromo-4-Chloro-3-Indolyl-phosphate, Sigma) and 0,6mg/ml of NBT (Nitro Blue Tetrazolium, Sigma) in alkaline phosphatase buffer (Tris-HCl 100mM, NaCl 0,1M, MgCl₂ 5mM, pH 9.6).

3.4. Nanoparticles production

In collaboration with Prof. Luis Nunez founder of BioTarget, company based in Chicago, nanoparticles have been produced under class 100 clean room condition using a patented

technology and methodology described in the patent number US20080187487 A1. Polymers used are: COOH-poly(ethylene glycol)-b-polylactide (PEG-b-PLA) and Poly(caprolactone)-COOH (PCL). Methotrexate has been purchased from TEVA. The targeting molecule, provided by us, have been conjugated on the surface of the nanoparticles exploiting its primary amines, which can react with polymers functionalized with NHS groups. Nanoparticles produced have been resuspended in PBS pH 7.4 with 10% of bovine serum albumin (BSA).

3.5. Characterization of nanoparticles by DLS, Nanoparticles tracking, TEM and STEM.

Nanoparticles produced have been characterized by Dynamic light scattering (DLS). The hydrodynamic diameter distribution has been measured using a Malvern Nano ZS instrument (Malvern Instruments, Ltd, Malvern, UK). Then, nanoparticles diluted 1:100 in ultrapure H₂O have been analyzed by Malvern NanoSight LM10. Through this technique diameter and number of nanoparticles have been determined. For transmission electron microscopy (TEM) analysis, nanoparticles have been diluted 1:50 in ultrapure H₂O and then a drop of nanoparticles' solution have been deposited on a carbon foil supported on copper microgrids. Images have been acquired by Philips CM100 TE microscope (Philips Research, Eindhoven, The Netherlands) operating at 80kV. For scanning transmission electron microscopy (STEM) analysis, nanoparticles have been diluted 1:50 in ultrapure H₂O and images acquired with a GAIA 3 Tescan microscopy (Tescan, Czech Republic) with a STEM detector operating at 30kV.

3.6. MTT viability assay

In order to test the ability of BNPs-MTX to affect endothelial cells and to demonstrate that empty BNPs do not show toxic effects, 5x10³ EA.hy926 cells have been seeded in wells of a 96 well cell culture plate (Sarstedt). Cells have been cultured at 37°C with 5% of CO₂ in Dulbecco's Modified Eagle's Medium (DMEM) supplemented with penicillin 10U/mL (Sigma), streptomycin 1µg/mL (Sigma), L-glutamine 2mM (Sigma) and FBS 10%. After cells adhered to the wells, different amounts of nanoparticles have been incubated for 48h. Then, 20µL of [5mg/mL] MTT formazan (1-(4,5-Dimethylthiazol-2-yl)-3,5-diphenylformazan) have been added to each well for 4h. Afterwards, the plate has been centrifuged at 2250 g in order to precipitate all the formazan crystals and the supernatant have been discarded. Finally, each well has been resuspended with 200µL of dimethyl sulfoxide (DMSO) and the absorbance have

been measured at 570nm by Infinite M200 Pro plate reader (Tecan). The % of viable cells have been calculated using not treated cells as the reference of 100% viable.

3.7. Release of MTX from nanoparticles

The release of MTX from nanoparticles has been quantified by dialysis. In particular, 200 μ L [2mg/mL] of nanoparticles have been placed in a dialysis device for small volumes with a dialysis membrane characterized by a molecular weight cut-off (MWCO) of 3,5 kDa and immersed in 10mL of PBS pH 7.4 at 37°C in slight agitation for 24h. During the first hour, 200 μ L of PBS of the dialysis has been collected every 15', while in the second hour only two samples have been collected (every 30'). Then, only one sample has been collected at 3, 4 and 5h. The last samples have been collected at 24h. As a control, the same procedure has been used to quantify the dialysis release of 200 μ L of non-encapsulated MTX [2mg/mL]. 150 μ L of each sample collected has been placed in a 96 well plate (Corning 96 well flat clear polystyrene plate) and quantified by spectrophotometric readings at 310nm by Infinite M200 Pro plate reader (Tecan). The optical density of 150 μ L of MTX [2mg/mL] diluted in 10mL of PBS have been used as the reference of 100% of MTX released. The amount of released MTX have been calculated as follow: (OD samples x 100)/ OD 100% MTX in solution.

3.8. Labelling of the targeted molecule and nanoparticles

The targeting molecule and the nanoparticles have been labelled with fluorescent probes in order to be detectable with several techniques. In particular, Fluorescein Isothiocyanate Isomer I (FITC) (Sigma) have been used for green fluorescence at 488nm, while FluoroLink Cy5.5 Monofunctional Dye (GE Healthcare) have been used for near-infrared fluorescence at 695nm. For FITC labeling, 1mg of nanoparticles have been centrifuged at 5900g for 1'30" and resuspended in 500 μ L of sodium carbonate buffer pH 9.3 (repeat this step three times). Then, 50 μ L of FITC [1mg/mL] in DMSO has been added drop by drop in slight agitation and finally placed in a rotating mixer overnight (O/N) at 4°C. Afterwards, add NH₄Cl to a final concentration of 50mM and incubate 2h at 4°C. Finally, nanoparticles have been centrifuged at 5900g for 1'30" and resuspended in 500 μ L of PBS (repeat this step three times). The same procedure has been used to label 1mg of targeting molecule by replacing the centrifugation step with a dialysis performed O/N at 4°C using dialysis tubes with a MWCO of 12.4 kDa (Spectra/Por). Instead, for the Cy5.5 labeling a commercial kit has been used to label both

nanoparticles and the targeted molecule. First, 1mg of nanoparticles or targeting molecule have been resuspended in 1mL of sodium carbonate buffer pH 9.3, respectively by centrifugation and by dialysis as described for FITC labeling. Then, the solutions with nanoparticles or the targeting molecule have been incubated into the commercial vials containing the powder of Cy5.5 for 30' RT. To eliminate the excess of dye, nanoparticles have been centrifuged at 5900g for 1'30" and resuspended in PBS pH 7.4 (repeat this step three times), while the targeting molecule has been dialyzed using dialysis tubes with a MWCO of 12.4 kDa. The amount of Cy5.5 associated with the nanoparticles or with the targeting molecule has been quantified by spectrophotometric methods. A molar extinction coefficient of $250,000 \text{ M}^{-1}\text{cm}^{-1}$ at 678nm has been used for Cy5.5, while a molar extinction coefficient of $68,000 \text{ M}^{-1}\text{cm}^{-1}$ at 494nm has been used for FITC.

3.9. Staining of tissue sections

3.9.1. Preparation of paraffin embedded sections of human synovial tissues

Paraffin embedded synovial tissues, obtained from patients with RA, have been kindly provided by Prof. Jessica Bertrand. First, sections of $7\mu\text{m}$ thick have been cut by microtome hyrax m55 (Carl Zeiss), dried for 2h at RT and baked at 55°C for 2h. Slices have been de-waxed by immersion in Xylene twice for 5' followed by one wash in 100% Ethanol (2'), one in 96% Ethanol (2'), one in 80% Ethanol (2')and one in 70% Ethanol (2'). Then, slides have been rehydrated in distilled H_2O for 2' and then soaked in TBS for 2'. Antigen retrieval has been performed enzymatically with a solution of 0.05% Trypsin, 0.5% CaCl_2 in distilled H_2O . Few drops of this solution have been placed on the slices and incubated at 37°C for 20'. Afterward, slices have been washed with distilled H_2O and blocked for 30' at RT in a humid chamber with blocking buffer (2% serum of the animal in which has been developed the secondary antibody in PBS) in order to prevent unspecific antibody binding. The excess of blocking buffer has been removed and the primary antibody (concentration depends on the primary antibody, see below) has been incubated at 4°C O/N in the diluent buffer (0,2% BSA and 0,05% Tween20 in PBS). Then, one wash of 5'with gentle rocking has been performed in PBS and two washes of 5' have been done with 1 %o of Triton x100 in PBS. A secondary antibody conjugated with a fluorescent probe and diluted (concentration depend on the secondary antibody) in the

diluent buffer has been incubated at RT for 1h. Three washes have been performed as before and nuclei have been stained with DAPI diluted in PBS 1:1000 incubated for 5' at RT. Finally, usual washes have been done and slices have been mounted with Mowiol anti-fade medium (Polysciences, Inc.). Sometimes, a secondary antibody conjugated to streptavidin has been used, in this case, an additional step of washes and incubation with biotin conjugated probe was required.

Staining with ScFv-Fc-synovial peptide (target molecule)

This molecule has been used with a final concentration of 10 μ g/mL and incubated at 4°C O/N. Co-staining have been performed with the target molecule already conjugated to Cy5.5 or FITC. Otherwise, in order to detect the target molecule, a mouse anti-SV5 (homemade antibody used 1:200 in the diluent buffer) able to bind the tag sequence SV5 present into the target molecule have been used. Finally, a goat anti-mouse Alexa Fluor 488 (Thermo Fisher) or a goat anti-mouse Alexa Fluor 594 (Thermo Fisher) have been used 1:200 in diluent solution.

Staining of vWF.

A rabbit anti-vWF (Dako) has been used 1:400 in the diluent buffer, in turn, recognized with goat anti-rabbit-Cy3 (Jackson) 1:200 in diluent buffer.

Staining of CD34+.

A rabbit anti-CD34 (Bioss) has been used 1:200 in the diluent buffer, in turn, detected with a goat anti-rabbit-Cy3 (Jackson) 1:200 in the diluent buffer

Staining of nuclei

Nuclei have been stained with DAPI (4',6-diamidin-2-phenylindole) (Sigma) diluted 1:1000 in PBS.

3.9.2. Preparation of frozen sections of AIA and CIA

Tissues collected from rats and mice have been included in a biocompatible gelatinous matrix with polyvinyl alcohol 10% and polyethylene glycol 4% (Tissue Tek OCT) and finally frozen at -80°C. Sections of 7 μ m thick have been cut by cryostat Leica CM 3050 S equipped with a microtome at -22°C. Sections are dried O/N at RT and then stored at -20°C.

3.9.3. Staining of frozen sections with antibodies

Sections stored at -20°C have been thawed for 5 minutes at RT and fixed with cold Acetone (Carlo Erba) for 15' at 4°C. Then, sections have been rehydrated with 0.9% NaCl. Samples have

been blocked with blocking buffer (2% of serum of the animal in which has been developed the secondary antibody in PBS) for 30' RT in a humid chamber. Sections have been incubated with the primary antibody (concentrations depend on the antibody, see below) diluted in diluent (0,2% BSA and 0,05% Tween20 in PBS) at 4°C O/N and then one wash of 5' with gentle rocking has been performed in PBS and two washes of 5' have been done with 1 % Triton x100 in PBS. Afterwards, the secondary antibody (concentrations depend on the antibody, see below) diluted in diluent has been incubated for 1h RT and then washed as before. Nuclei have been stained with DAPI diluted in PBS 1:1000 incubated for 5' at RT. After usual washes, slices have been mounted with Mowiol anti-fade medium. Sometimes, a secondary antibody conjugated to streptavidin has been used, in this case, an additional step of washes and incubation with biotin conjugated probes was required.

Staining with ScFv-Fc-synovial peptide (target molecule)

This molecule has been used with a final concentration of 10µg/mL and incubated at 4°C O/N. Co-staining have been performed with the targeting molecule already conjugated to Cy5.5 or FITC. Otherwise, in order to detect the targeting molecule, a mouse anti-SV5 (homemade antibody used 1:200 in the diluent buffer) able to bind the tag sequence SV5 present into the targeting molecule have been used. Finally, a goat anti-mouse Alexa Fluor 488 (Thermo Fisher) or a goat anti-mouse Alexa Fluor 594 (Thermo Fisher) have been used 1:200 in the diluent buffer.

Staining of vWF.

A rabbit anti-vWF (Dako) has been used 1:400 in the diluent buffer, in turn recognized with goat anti-rabbit-Cy3 (Jackson) 1:200 in the diluent buffer.

Staining of C3

A goat anti-C3 (Cappel) has been used 1:50 in the diluent buffer, in turn recognized with rabbit anti-goat-TRITC (Sigma) 1:100 in the diluent buffer.

Staining of nuclei

Nuclei have been stained with DAPI (4',6-diamidin-2-phenylindole) (Sigma) diluted 1:1000 in PBS.

3.9.4. Staining of frozen sections with nanoparticles

In order to study the binding of BNPs and tBNPs on the synovial tissue of rats, sections stored at -20°C have been thawed for 5 minutes at RT and fixed with 4% paraformaldehyde (PFA)

(Sigma) for 15' RT. Then, sections have been rehydrated with 0.9% NaCl and blocked with universal blocking buffer (2% of BSA, 0,25% of casein and 0,10% of gelatin in PBS) for 30' at RT in a humid chamber. Afterwards, 10 μ g of BNPs-FITC and tBNPs-FITC have been incubated 1h at 37°C. Finally, three washes have been performed to remove unspecific bound nanoparticles and slices have been mounted with Mowiol anti-fade medium.

3.9.5. Staining of viable EA.hy926 cells with nanoparticles

EA.hy 926 endothelial cells have been used to test the binding of tBNPs to endothelial cells. In particular, 3x10⁴ cells have been cultured in each well of an X-well Tissue Culture Chamber (Sarstedt) for high-resolution microscopy. Cells have been cultured at 37°C with 5% of CO₂ in DMEM supplemented with penicillin 10U/mL (Sigma), streptomycin 1 μ g/mL (Sigma), L-glutamine 2mM (Sigma) and FBS 10%. 20x10⁷ BNPs-Cy5.5 and tBNPs, normalized after Cy5.5 labeling for their number of nanoparticles by NanoTrack analysis, have been incubated for 1h at 37°C. Afterwards, three washes have been performed with PBS and then cells have been fixed 15' with 4% PFA. Other three washes have been performed to remove excess of PFA and finally nuclei have been stained with DAPI (4',6-diamidin-2-phenylindole) (Sigma) diluted 1:1000 in PBS. Two more washes have been done and then glass microscope slides have been detached from the chamber vessel in order to mount the slides with Mowiol anti-fade medium.

3.9.6. Microscopes used in this work

- Zeiss AxioPlan 2 Microscopy System (Carl Zeiss) equipped with a AxioCamHR3 camera.
- Nikon Eclipse Ti-E Live Cell Imaging System (Nikon) equipped with a Nikon DS-Qi2 camera and stage incubation system able to control temperature, humidity and percentage of CO₂.

Post processing of the images has been conducted with FIJI (ImageJ) software.

3.10. Imaging flow cytometer

5x10⁵ EA-hy926 have been cultured in a 6-well cell culture plate (Sarstedt) at 37°C with 5% of CO₂ in DMEM supplemented with penicillin 10U/mL (Sigma), streptomycin 1 μ g/mL (Sigma), L-glutamine 2mM (Sigma) and FBS 10%. The day after, cells have been washed two times with PBS and 10 μ L of BNPs-FITC and tBNPs-FITC, normalized by fluorescence intensity by spectrophotometric method, have been incubated with cells for 1h at 37°C with 30% of FBS in

PBS. Afterwards, cells have been washed two times with PBS and detached with trypsin-EDTA solution (0.5g/L porcine trypsin and 0.2g/L EDTA)(Sigma) for 5' at 37°C. Finally, cells have been centrifuged with DMEM medium at 500g for 10' and resuspended in 50µL of 2% of FBS in PBS. Data have been acquired with FlowSight (EMD Millipore, USA) with a 20x objective and analyzed using IDEAS software version 6.0. Cells of each sample have been gated in order to select images with single cells in focus. An erode mask has been used to define the inner part of the cell. This mask removes two pixels from the edges of the starting mask using bright field images of the cells. The ratio becoming from the intensity fluorescence between the inside of the cell and the fluorescence intensity of the total cell has been defined has internalization. Negative scores represent no internalization, while cells with high internalization have positive scores. Representative images from cells populations have been chosen.

3.11. ELISA on EA.hy926

3x10⁴ Ea.hy926 cells/ well have been seeded in a 96 well cell culture plate (Sarstedt) in 200µL of DMEM medium supplemented with penicillin 10U/mL (Sigma), streptomycin 1µg/mL (Sigma), L-glutamine 2mM (Sigma) and FBS 10%. After 24h, wells have been washed twice with 300µL of PBS and then fixed with 200µL of 1% PFA for 30' at RT. Afterwards, wells have been washed two times with PBS and then blocked with 200µL of 1% BSA in PBS. 2,4µL of BNPs-FITC and tBNPs-FITC, normalized by fluorescence intensity by spectrophotometric method, have been incubated with cells for 1h at 37°C with 30% of FBS in PBS. In order to remove nanoparticles which do not bind cells, wells have been washed three times with PBS. Finally, the intensity of fluorescence has been detected with a FLUOstar Omega microplate reader (BMG Labtech) at 520nm.

3.12. Antigen induced arthritis (AIA)

Antigen induced arthritis have been induced in male rats Wistar Hannover strain with a weight of 120-150g. Animals have been purchased from Harlan Laboratories (San Pietro al Natisone, Italy) and maintained in Cluster in BioMedicine (CBM, Basovizza, Trieste) facilities during the study of biodistribution, while animals have been maintained in the animal house of Trieste (University of Trieste) for the study of therapeutic efficacy. Experiments have been conducted following the European (86/609/EEC) and Italian guidelines (D.L 116/92) for the *in vivo* animal experimentation after the approval by the Ministry of Education, Universities and Research

(approval n° 220/2013-B) and by the ethics committee of the University of Trieste. All the experimental procedures have been conducted under total anesthesia by intraperitoneal injection of Zoletil (25mg/ Kg) and Xylazine (7.5mg/ Kg). The immunization has been performed with two intradermic injections (the second one after one week) of 150 µg of methylated bovine serum albumin (mBSA) in 200µL of NaCl 0.9% physiologic solution and emulsified with 200µL of Complete Freud adjuvant (CFA) (Sigma). After 14 days from the second immunization, the inflammation has been induced by injecting 100µg of mBSA (diluted in 100µL of physiologic solution) in the intraarticular right knee of the rats. The contralateral knee joint has been injected with the physiologic solution as the control.

Study of biodistribution

Explore Optix MX pre-clinical optical imaging system (GE Healthcare), equipped with a pulsed laser diode and a time-correlated single-photon detector, have been used to evaluate the biodistribution of 4.8 nmol of BNPs-Cy5.5 and tBNPs-Cy5.5 diluted in physiologic solution (final volume 100µL) injected intravenously (tail vein) 2h after the intraarticular injection of mBSA. The anatomical region to scan has been previously shaved to avoid laser scattering caused by hair. A blank image has been performed before intravenous injection of labelled nanoparticles. The animals have been monitored at multiple time points using a 670 nm pulsed laser diode with a repetition frequency of 80 MHz and a time resolution of 12 light pulses. Fluorescence emission has been collected at 700 nm and detected through a fast photomultiplier tube and a highly sensitive time-correlated single-photon counting system. Two-dimensional scanning regions of interest have been selected through specific software and laser power, integration time and scan step, which have been optimized according to the signal emitted. The data have been recorded as temporal point-spread functions, and the images have been reconstructed as fluorescence intensity and fluorescence lifetime. After 23 days the animals have been euthanized under total anesthesia. Organs have been analyzed *ex vivo* for their fluorescence and then embedded in biocompatible gelatinous matrix OCT (Tissue TEK) and stored at -80°C. Blood samples have been collected for subsequent analysis.

Therapeutic efficacy

1mg/ Kg /day of MTX and tBNPs-MTX diluted in physiologic solution (final volume of 500µL) have been administrated intra-peritoneum for three days in rats developing AIA. The swelling of the knees has been measured with a caliper. At the end of the study, animals have been euthanized under total anesthesia and the articular cavities of the right and left knees have

been washed several times with 2mL of PBS in order to collect synovial fluids. Moreover, part of the synovial membranes have been collected and embedded in biocompatible gelatinous matrix OCT (Tissue TEK) and stored at -80°C, while the whole articulation has been embedded in paraffin for histological analysis by hematoxylin eosin staining. Blood samples have been collected for subsequent analysis.

3.13. Collagen induced arthritis (CIA)

In order to develop CIA model, susceptible male mice DBA/1J strain with a weight of 13-16g have been used. Mice have been purchased from Harlan Laboratories (San Pietro al Natisone, Italy) and maintained in the Molecular & Preclinical Imaging Centers (University of Turin, Italy) during the study of biodistribution, while animals have been maintained in the animal house of Trieste (University of Trieste) for the study of therapeutic efficacy. Experiments have been conducted following the European (86/609/EEC) and Italian guidelines (D.L 116/92) for the *in vivo* animal experimentation after the approval by the Ministry of Education, Universities and Research (approval n° 220/2013-B) and by the ethics committee of the University of Trieste. The first immunization have been conducted with 50µL of a solution made of 25µL (4mg/ mL) of bovine collagen type II (Chondrex) diluted in acetic acid 10mM and 25µL of CFA (4mg/ mL of M.Tuberculosis in 15% Arlacel A (Sigma) and 85% heavy mineral oil (Sigma)). A second immunization has been performed two weeks later with the same concentration of collagen type II using Incomplete Freund Adjuvant (IFA)(without M. Tuberculosis). After 20 days mice show first signs of RA. Erythema and swelling characterized the early stage of the disease in this model affecting randomly different paws with different degree of inflammation (polyarthritis). Objective evaluations have been performed three days per week establishing a score from 0 (no arthritis) to 4 (severe swelling and ankyloses) for each paw. The weight of each animal has been recorded three times per week in order to control side effects.

Study of biodistribution

Mice showing signs of arthritis have been enrolled in two different groups; one group has been injected i.v. with 0.5nmol of BNPs-Cy5.5 and the other one has been treated with 0.5nmol of tBNPs-Cy5.5. Animals previously anesthetized with Isoflurane have been scanned by IVIS Spectrum 2000 *in vivo* imaging system (Perkin Elmer) at time 0, 1, 6, 24, 72, 96, 168 h. At the end of the study, mice have been euthanized under total anesthesia in order to collect organs such as paws, brain, liver, kidneys, spleen, lungs and heart. These organs have been embedded

in biocompatible gelatinous matrix OCT (Tissue TEK) and stored at -80°C, except paws which have been previously fixed in 10% neutral buffered formalin (BioOptica) for 24h and then decalcifying for 24h with Decalcifying Solution-Lite (Sigma).

Therapeutic efficacy

Five different groups of mice have been used to assess the therapeutic efficacy of MTX encapsulated into tBNPs. In particular, one group have been treated i.p. with 200µL of the sterile saline solution, one group with 1mg/ Kg three times per week, one group with MTX 3mg/ Kg per week, one group with tBNPs-MTX 3mg/ Kg per week and one group with 1mg/ Kg per week. All the treatments have been administrated i.p. in a total volume of 200 µL of sterile saline solution. Animals have been treated for 25 days and then euthanized under total anesthesia with Zoletil (25mg/ Kg) and Xylazine (7.5mg/ Kg). Organs such as paws, brain, liver, kidneys, spleen, lungs and heart have been embedded in biocompatible gelatinous matrix OCT (Tissue TEK) and stored at -80°C, except paws which have been previously fixed in 10% neutral buffered formalin (BioOptica) for 24h and then decalcifying for 24h with Decalcifying Solution-Lite (Sigma). Blood samples have been collected for subsequent analysis.

3.14. Hematoxylin Eosin staining

In order to evaluate the histological scores of the paws collected in CIA mice, Hematoxylin Eosin staining have been performed in these samples. The specimens have been fixed in 10% buffered formalin solution and embedded in paraffin. Four micrometer-thick sections have been dewaxed by immersion in xylene twice for 5' followed by one wash in 100% ethanol (2'), one in 96% ethanol (2'), one in 80% ethanol (2')and one in 70% ethanol (2'). Afterward, slides have been rehydrated in distilled H₂O for 2' and then stained with Hematoxylin for 40''. Sections have been washed with running tap water for 1' and then stained with Eosin for 20''. Thus, sections have been washed with running tap water for 1' then they have been soaked in 95% ethanol for 30'' and twice in 100% of ethanol for 1'. Finally, sections have been washed twice in xylene for 1' and mounted with Eukitt mounting medium (BioOptica). The histopathological analysis has been made in collaboration with Prof. Claudio Tripodo and Dr. Beatrice Belmonte at University of Palermo (Palermo, Italy).

3.15. Blood analysis

Blood samples collected from rats and mice have been analyzed in order to assess the number of red blood cells, white blood cells and platelets. 10 μ L of each blood samples have been analyzed by ABX Micros ES60 (Horiba ABX Diagnostics, France). Analysis has been conducted in collaboration with Prof. Gabriele Pozzato at Ospedale Maggiore (Trieste, Italy).

3.16. ELISA mouse anti-collagen antibodies

An ELISA test has been performed in order to verify that all mice enrolled in the study develop an immune response against bovine collagen type II. A solution of 5 μ g/ mL (100 μ L/ well) of bovine collagen type II (Chondrex) in carbonate buffer 0,1 M pH 9 have been used O/N at 4°C as the coating. The day after, wells have been washed three times with washing buffer (0,1% Tween 20 in PBS) and blocked 1h at RT with 200 μ L of 2% skim milk in PBS. Then, wells have been washed three times with washing buffer and serum samples, previously diluted 1:2000 in diluent buffer (0,05% Tween 20 and 0,1% skim milk in PBS), have been placed in each well in a final volume of 100 μ L. Other three washes have been done with washing buffer and then the secondary antibody goat anti-mouse AP (Sigma) has been diluted 1:2000 in the diluent buffer and incubated for 1h at RT. Finally, three washes have been done with washing buffer and the alkaline phosphatase substrate p-nitrophenylphosphate (pNPP) (Sigma) has been used 1mg/ mL in glycine buffer (0,1M Glycine, 0,1mM MgCl₂ and 0,1mM ZnCl₂, pH 9.6) in order to develop the reaction. The plate has been measured at 405 nm by Infinite M200 Pro plate reader (Tecan).

3.17. ELISA rat anti-mBSA antibodies

In order to verify that rats enrolled in the study developed an immune response against methylated bovine serum albumin (mBSA) an ELISA test has been used. A solution of 5 μ g/ mL (100 μ L/ well) of mBSA (Sigma) in carbonate buffer 0,1 M pH 9 have been used O/N at 4°C as the coating. The day after, wells have been washed three times with washing buffer (0,1% Tween 20 in PBS) and blocked 1h at RT with 200 μ L of 2% skim milk in PBS. Then, wells have been washed three times with washing buffer and serum samples, previously diluted 1:2000 in the diluent buffer (0,05% Tween 20 and 0,1% skim milk in PBS), have been placed in each well in a final volume of 100 μ L. Three washes have been done with washing buffer and then

the secondary antibody rabbit anti-rat biotin (Sigma) has been diluted 1:4000 in the diluent buffer and incubated for 1h at RT. After three more washes with wash buffer, streptavidin conjugated to horseradish peroxidase (HRP)(Sigma) diluted 1:2000 in the diluent has been incubated for 30' at RT. Finally, three washes have been done with washing buffer and the peroxidase substrate 3,3',5,5'-Tetramethylbenzidine (TMB)(Sigma) has been used (100µL) to develop the reaction, which has stopped with 100µL of H₂SO₄ 1M (Sigma). The plate has been measured at 450 nm by Infinite M200 Pro plate reader (Tecan).

3.18. Number of polymorphonuclear (PMN) leukocytes.

In order to measure the number of PMN leukocytes in synovial fluids of AIA rats, the myeloperoxidase activity has been measured. For this purpose, a standard curve with rat's PMN with known concentration (500000cells/mL) has been prepared. Hundred µL of each sample has been loaded in well of a 96 well plate polystyrene flat bottom (Costar) and then, 100 µL of peroxidase substrate TMB (Sigma) has been added to each well. The colorimetric reaction has been stopped with 100µL of H₂SO₄ 1M (Sigma). Finally, the plate has been measured by the spectrophotometric reader (ELISA reader, Anthos 2020) at 450nm.

3.19. Multiplex ELISA

Cytokines and chemokines have been quantified using the Bio-Plex Pro Mouse Cytokines 23-plex Assay (BioRad), according to the manufacturer's instructions. Serum samples of each mice group have been pooled and then 12,5µL has been analysed in triplicate. In particular, IL-1α, IL-1β, IL-2, IL-3, IL-4, IL-5, IL-6, IL-9, IL-10, IL-12 (p40), IL-13, IL-17A, KC, MCP-1, MIP-1α, MIP-1β, Eotaxin, G-CSF, GM-CSF, INF-γ, RANTES and TNF-α have been analysed by this method. Data have been acquired with Bio-Plex 200 reader (BioRad) and analysed with the software Bio-Plex Manager to calculate results as concentration in pg/ mL.

4. Results and discussion

4.1. Design and characterization of biodegradable nanoparticles

4.1.1. Design and characterization of the targeting molecule

The targeting synovial peptide, used in this study, is made of 9 aminoacids (CKSTHDRLC) containing two flanking cysteines (Figure 9b), which constrain the peptide in a circular shape improving the binding of the consensus motif (aminoacids DRL) to its counterpart (Lee et al. 2002). Due to the small size of the synovial peptide, we avoided to directly link the peptide on the nanoparticles because polymers, in particular, PEG exposed on particles' surface, could mask the exposure of the peptide. For this reason, the synovial peptide has been fused to the Fc of a ScFv-Fc (Figure 9 A), which acts as a spacer able to display the peptide far from the nanoparticles' surface. The sequence coding for the targeting molecule has been cloned in the vector pcDNA3.1/Hygro+; it contains the sequence of a non-correlated ScFv, the sequence coding for the hinge-CH2-CH3 of the rat IgG2b, the sequence for the SV5 tag (used for detection) and the sequence for the synovial peptide. In order to obtain a stable clone able to produce high amount of the targeting molecule, the vector coding for its sequence, previously checked by DNA sequencing, has been transfected in mammalian cells of Chinese Hamster Ovary (CHO). The 3D structure of the targeting molecule has been predicted through the web server Phyre2 (Kelley et al. 2015), aiming to understand the peptide's orientation in the 3D space and whether the peptide could be masked during the folding of the final structure (Figure 9 C). The prediction is performed through a combination of multiple template modelling and *ab-initio* folding simulation. The 94% of residues of the final 3D structure reported in the figure 9 C have been modelled with a confidence higher than 90% and the peptide (Figure 9 C red box) appears available to interact with its counterpart.

The targeting molecules have been produced and purified by affinity chromatography exploiting the binding between the Fc and the protein A. The molecular weight and the quality of the protein produced and purified have been assessed by western blot; as expected in reducing conditions, the molecular weight of the monomers have been determined as 62kDa and low amount of aggregated or degraded proteins have been detected (Figure 9 D).

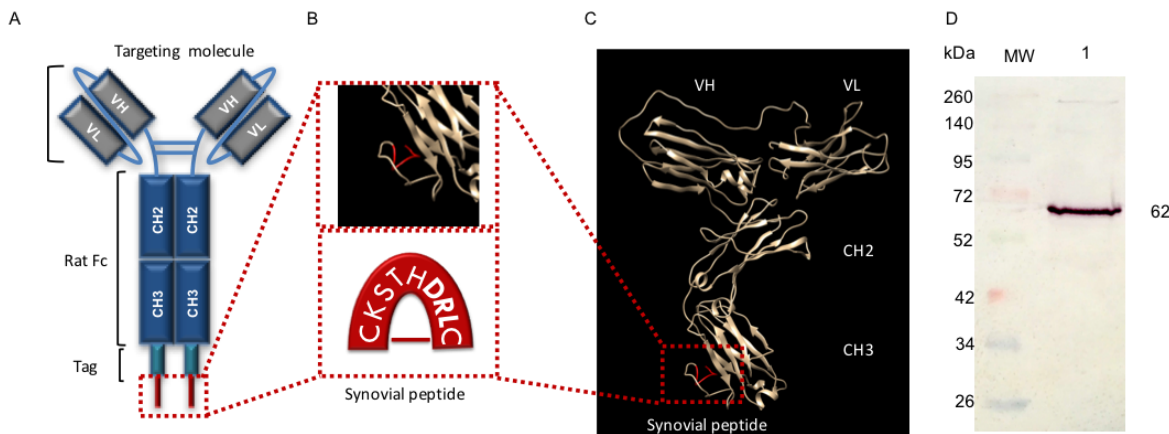


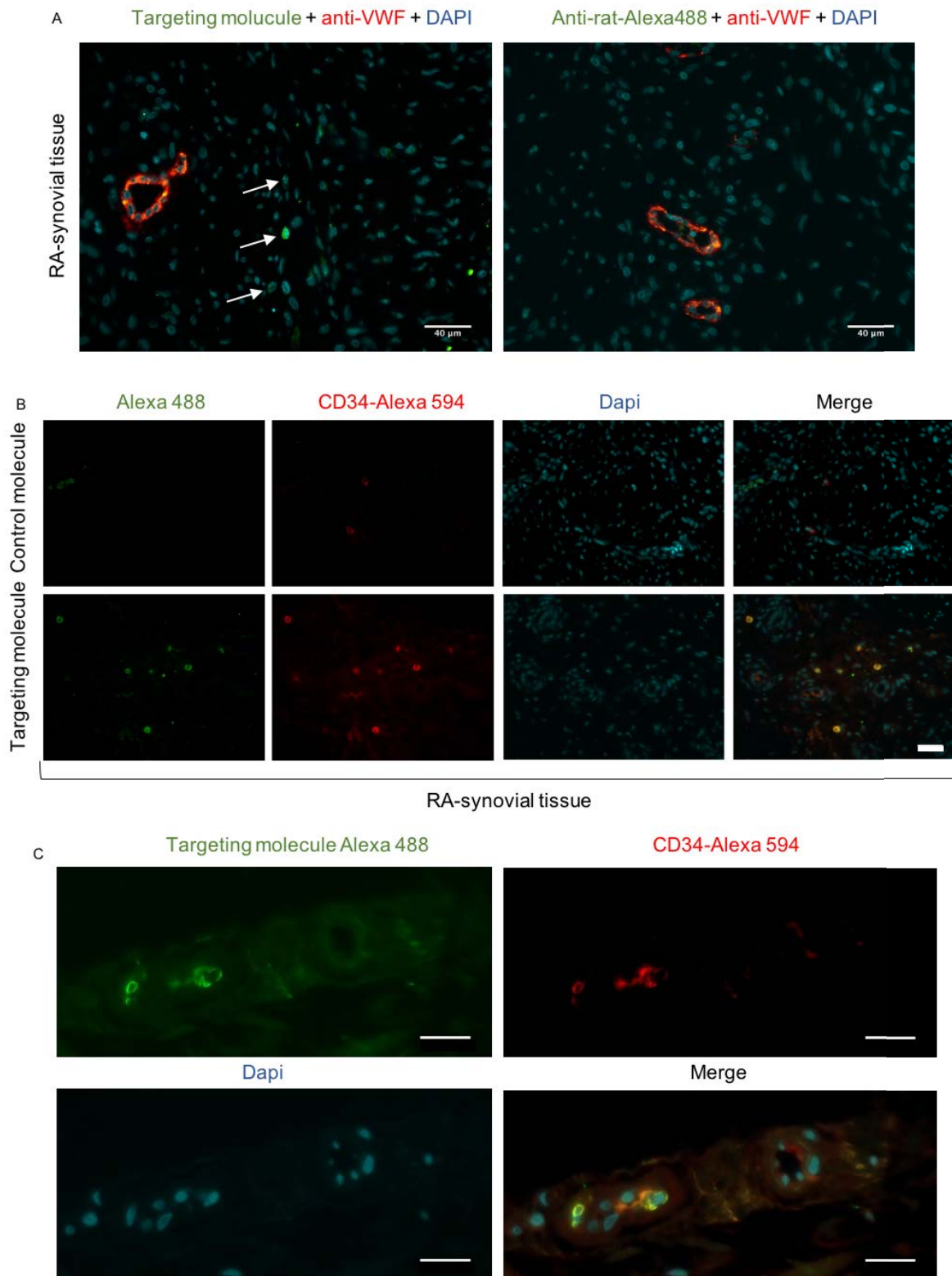
Figure 9: Targeting molecule.

(A) Schematic representation of the targeting molecule made of a non-correlated ScFv (grey VL-VH) linked through a hinge to the rat Fc (blue CH2-CH3). In turn, the Fc is fused with an SV5 tag (cyan), which ends with the synovial peptide (red). (B) Schematic representation of the synovial peptide, which assumes the circular shape due to the presence of the flanking cysteines. (C) 3D structure of one monomer of the targeting molecule predicted with Phyre2 prediction tool. In the red boxes the synovial peptide. (D) Western blot conducted in reducing condition of 100ng of the targeting molecule (lane 1), which shows the correct molecular weight of 62 kDa.

As previously discussed, the synovial peptide is specific for the microvascular endothelial tissue of the inflamed synovia, but it is not yet known which is the protein expressed or overexpressed responsible for the selective targeting. Knowing the identity of this protein would be of great importance, indeed this could be involved in pathogenesis. In order to identify the counterpart of the synovial peptide, synovial tissue from RA patients have been double stained with the targeting molecule and with markers expressed on endothelial cells. A generic endothelial marker expressed by all endothelial cells, such as the von Willebrand Factor (vWF), have been used first (Gragnano et al. 2017). However, there was no co-localization between the targeting molecule and the vWF (Figure 10 A). For this reason, RA synovial tissues have been stained for the CD34. This is a marker for hematopoietic stem cells and is highly expressed on vascular endothelial progenitors (Krause et al. 1996)(Sidney et al. 2014). In this case, we found a co-localization between the CD34 and the targeting molecule, demonstrating that endothelial cells CD34+ could be the target of the synovial peptide (Figure 10 B and C). The staining of the targeting molecule was peculiar, indeed many isolated cells, in close proximity to the blood vessels, have been recognized by the targeting molecule. However, this unusual staining pattern has been supported by Pusztaszeri and co-workers, who described the great variability in the expression and distribution of endothelial cell markers among many types of vascular tissues and different anatomic compartments (Pusztaszeri et al. 2006). The co-localization between the CD34+ cells and the targeting peptide means that targeted nanoparticles could transport their payload on CD34+ endothelial cells of

the inflamed synovia. Our finding is also supported by Lee et al. who have isolated the peptide proving its ability to bind the microvasculature of the RA synovial tissue (Lee et al. 2002). For these reasons, subsequent in vitro tests to study and characterize targeted-nanoparticles will be conducted on a endothelial cell line EA.hy926.

In order to better identify the protein bound by the targeting molecule, an immunoprecipitation followed by mass spectrometry analysis has been conducted; in particular, the targeting molecules have been coupled to Sepharose beads and a lysate of EA.hy 926 endothelial cell line has been used as loading material. A ScFv-Fc fused with a RGD peptide coupled to Sepharose has been used as the control. Several proteins differentially bound by the synovial peptide have been identified, however, any of them could be reasonably associated with a surface protein of endothelial cells. Indeed, most of the proteins identified comes from the inner part of the cells, so are in contrast with our immunofluorescence findings and literature. Probably, the method should be improved for the enrichment of surface proteins.

**Figure 10: Study of colocalization.**

(A) The picture on the left is a RA human synovial tissue co-incubated with the targeting molecule (green fluorescence) and anti-vWF (red fluorescence). The arrows highlight the cells stained by the targeting peptide, which do not colocalize with the blood vessels stained due to the vWF. The picture on the right is the control, thus only the secondary antibody anti-rat-Alexa488 has been incubated. Nuclei have been stained with Dapi in both pictures. Scale bar 40 µm. (B) RA human synovial tissues incubated with both targeting molecule and its control (untargeting molecule) in co-staining for the CD34. Both targeting and untargeting molecules are associated with green fluorescence, the CD34 with red fluorescence and nuclei are stained with DAPI. The merge highlights the colocalization between the targeting molecule and the CD34. Scale bar 40 µm. (C) Enlargement of blood vessels in a RA synovial tissue, where it is clear the binding of the targeting molecule (green

fluorescence) in colocalization with the CD34 (red fluorescence). Nuclei are stained with Dapi. Scale bar 20 μm .

4.1.2. Design and characterization of targeted nanoparticles for rheumatoid arthritis

According to the recent literature, already discussed in the introduction of this work, nanoparticles can be designed in order to increase specificity for a target tissue reducing doses of drugs and their consequent toxicity. Following the rationale of the project, core-shell biodegradable polymeric nanoparticles made of COOH-poly(ethylene glycol)-b-polylactide (PEG-b-PLA) and Poly(caprolactone)-COOH (PCL) were produced in collaboration with Prof. Luis Núñez founder of BioTarget, a company based in Chicago. Due to their patented technology and methodology (number US20080187487 A1) based on a electrohydrodynamic coaxial two-capillary system, polymeric nanoparticles can be customized; the shell can be produced with different polymers and later functionalized with targeting molecules using N-Hydroxysuccinimide (NHS) as coupling agent; the core can be loaded with different drugs and diagnostic tracers. Moreover, the dimension of the nanoparticles can be controlled by varying the flow speed inside the capillaries. Four different kinds of biodegradable nanoparticles (BNPs) were produced to develop this project (Figure 11). In particular: BNPs with empty core and the shell made of PEG-b-PLA and PCL, targeted BNPs (tBNPs) which are BNPs conjugated with the targeting molecule, BNPs loaded with MTX (BNPs-MTX) and tBNPs loaded with MTX (tBNPs-MTX).

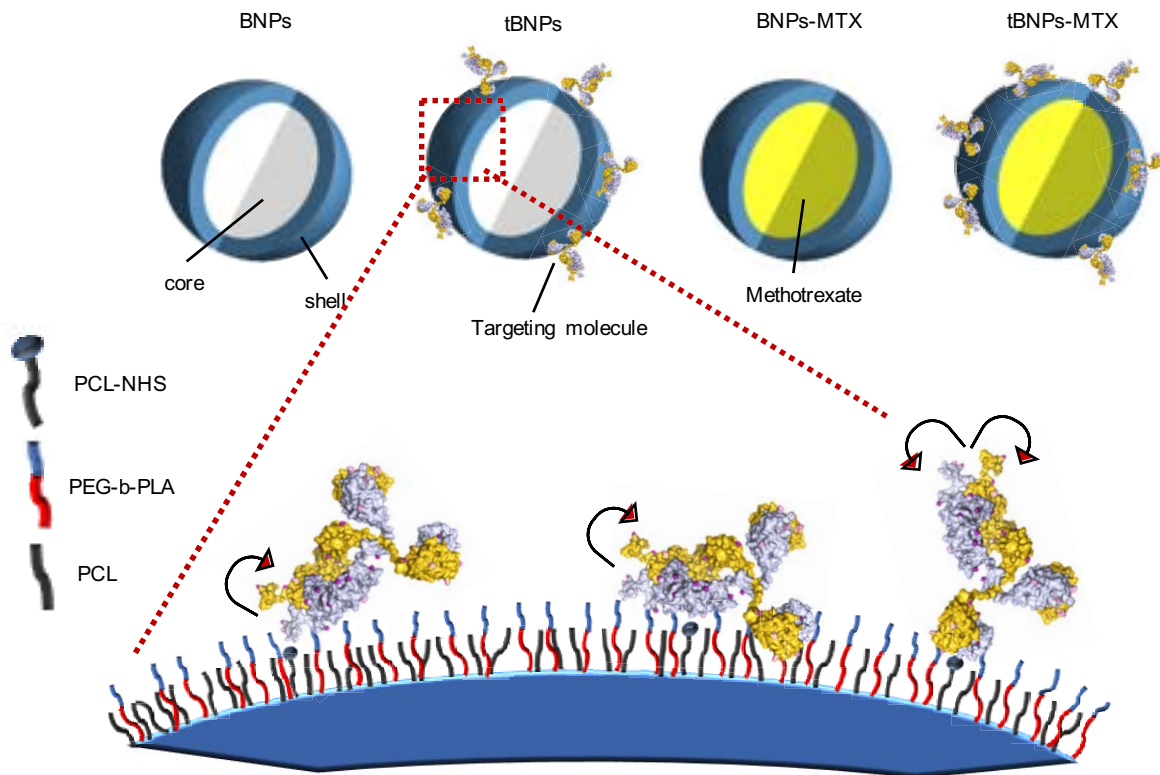
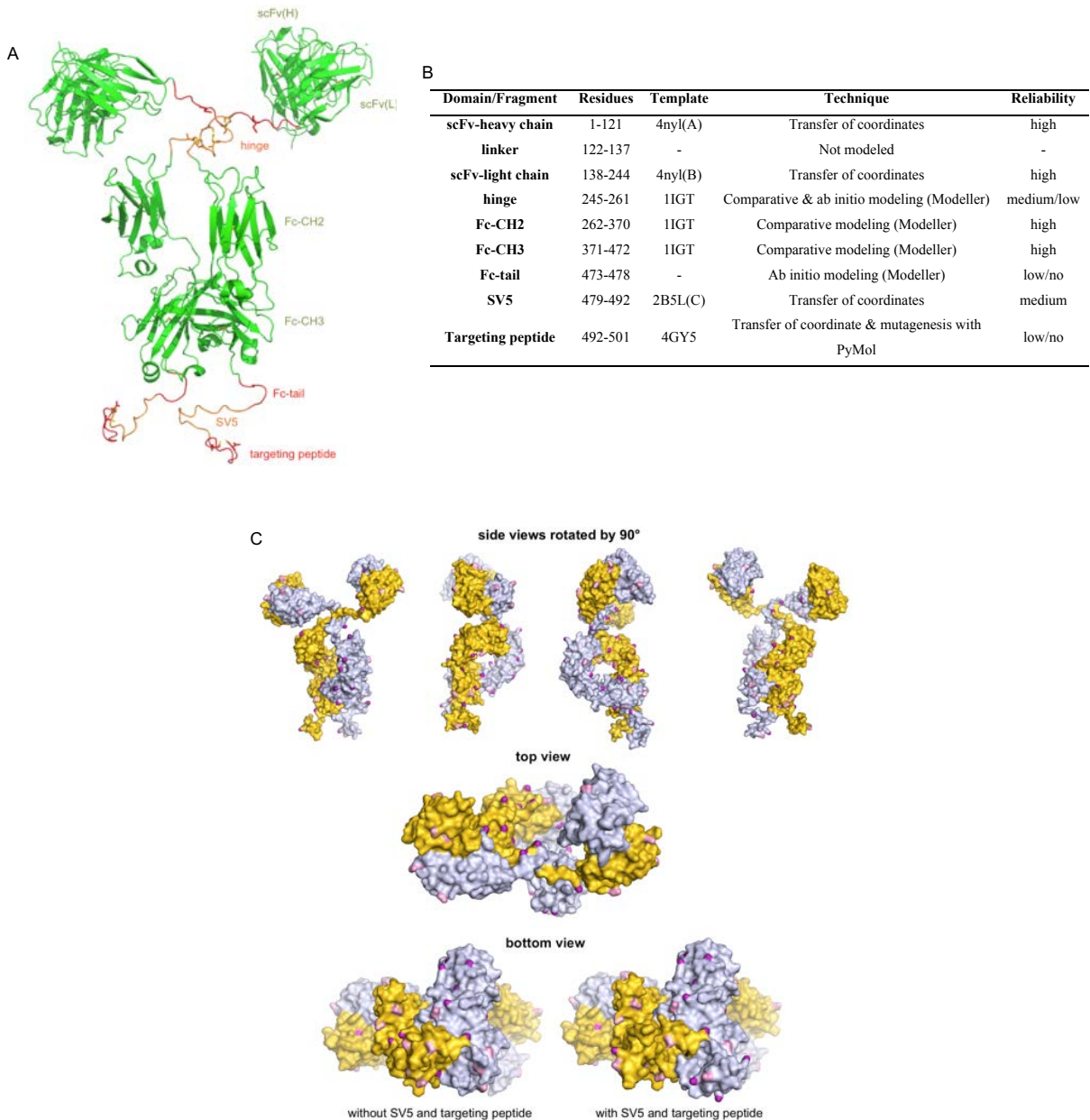


Figure 11: Schematic representation of polymeric nanoparticles.

Starting from the right: BNPs with polymeric shell (blue) made of PEG-b-PLA, PCL and empty core (white); tBNPs are identical to the BNPs except for the target molecule linked on the surface; BNPs-MTX are identical to the BNPs with MTX loaded into the core; tBNPs-MTX represent the complete format of the nanoparticles, loaded with MTX and provided of the targeting molecule on the surface. Below, the schematic representation of nanoparticles' surface with three possible orientations of the targeting molecule. The arrows highlight the flexibility of the targeting molecule.

Recently, several works have been published on the use of targeted nanoparticles in biomedicine (Sanna et al. 2014)(Ferrari et al. 2015). Most of these works focus on the physicochemical properties of the nanoparticles' structure and on the targeting molecules. Many different molecules have been used for a tissue specific targeting. Among these, aptamers, proteins, fatty acids, sugars, peptides, antibodies and their fragment have been widely employed (Richards et al. 2017). However, antibodies, due to their excellent features, are becoming very popular. Despite the large number of publications focused on targeted nanoparticles, very few works are focused on the conjugation of these molecules on their surface. Indeed, there is the need to improve methods by which targeting molecules are linked on the surface of the nanoparticles. In our study, the targeting molecules have been coupled to the surface subsequently the nanoparticles' production exploiting its available amino groups. Because this kind of functionalization is not oriented but random, in order to understand possible coupling orientation, an *in-silico* study have been performed in collaboration with Romina Oliva (Parthenope University of Naples) to predict the number and

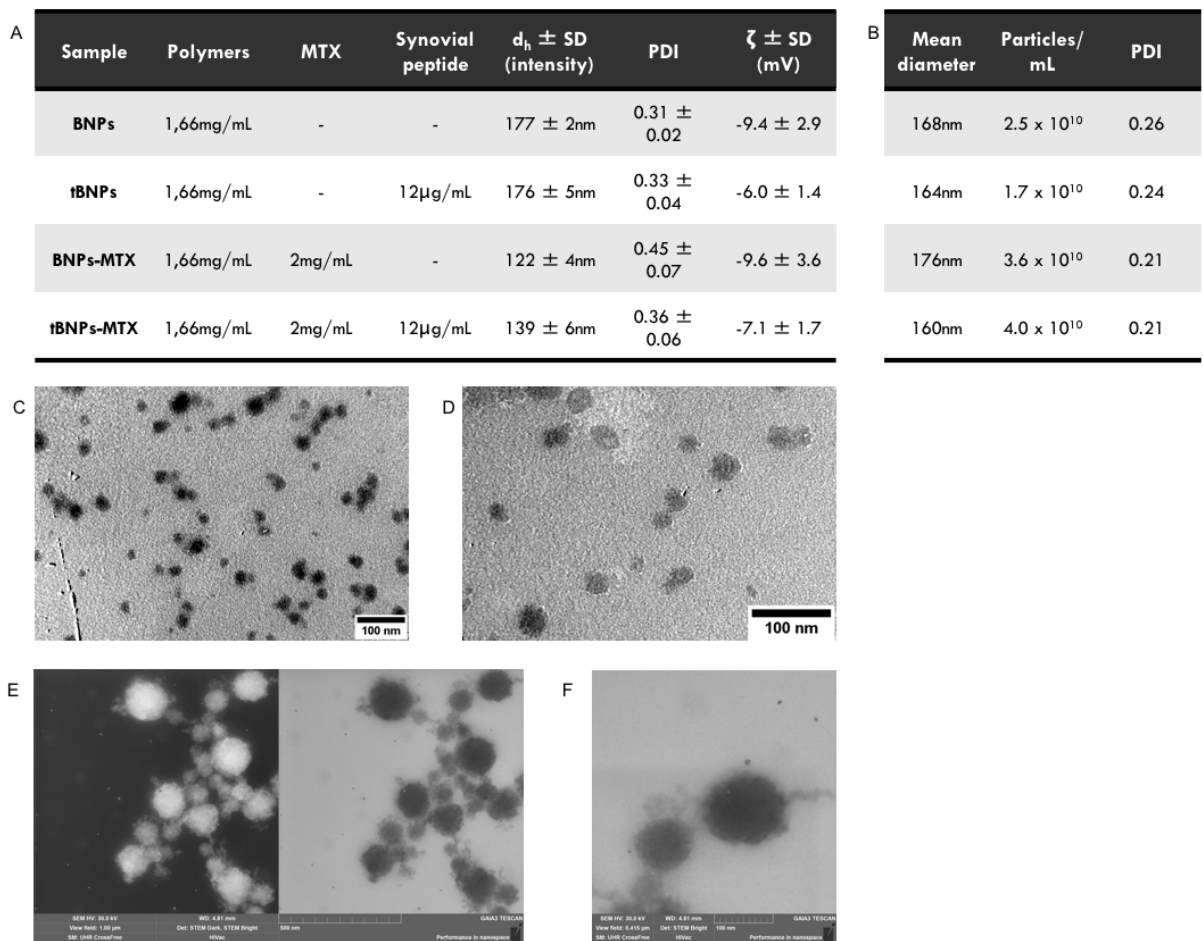
position of free amino groups available for the conjugation. To this aim a detailed 3D structure have been performed showing the ScFv-Fc-targeting molecule folding in its dimeric form (Figure 12 A). The ScFv fragment and the Fc have been modelled with high reliability, while the linker between the VL and VH has not been modelled because no similar crystal structures were present in literature. The hinge region has been modelled with medium reliability and due to the presence of four cysteines, same disulphide bridges may be formed. Moreover, by definition, the hinge region is extremely flexible and the orientation of the Fc and the ScFv could be different from this prediction. However, the tag SV5 has been modelled with medium reliability due to the presence of a similar crystal structure. This information gives confidence regarding the orientation of targeting peptide, which is fused to the tag. Indeed, it is possible to speculate that the targeting peptide protrudes in the space avoiding unwanted interaction with parts of the own molecule. However, the synovial peptide has been modelled with low reliability based on a crystal structure fragment of the E3 ubiquitin-protein ligase. Despite the low reliability, 5 residues out of 9 are identical to those of E3 ubiquitin-protein ligase, in particular the identical residues are located in both extremities of the sequence, which contains the two flanking cysteines responsible for the circularization of the peptide. Thus, it is highly truthful that the targeting peptide assumes a circular shape excluding other possible folds. To conclude, free amino groups available on the surface of the target molecule have been highlighted (Figure 12 C). In particular, amine groups of Lys residues are presented in purple, while the guanidinium group of Arg residues are shown in pink. In the 3D models, reported from different viewpoints, is possible to appreciate many free amino groups spreads all over the surface of the targeting molecule. Thus, is not possible to predict the correct orientation, but the higher number of free amino groups are located in the Fc of the molecule with a higher availability for the binding. Considering this assumption correct, it is reasonable that only one monomer of the molecule is involved in the binding with the polymers of the nanoparticles, therefore the other monomer is available to display the targeting peptide (Figure 11).

**Figure 12: 3D model of the targeting molecule.**

(A) 3D structure of the ScFv-Fc fused to the synovial target peptide predicted in-silico. In green regions of the molecule predicted with high reliability; in orange are reported regions predicted with medium reliability; regions modelled with low/no reliability are shown in red. (B) The table reports main features of the modelling process such as the reliability, the technique used for the modelling and the template used for each region. (C) Steric hindrance of the target molecule. The two monomers are colored in white and gold respectively. Purple spots represent Lys residues, while pink dots represent Arg residues. Both Lys and Arg amino groups can be available to bind the polymers of the nanoparticles' shell. On the top of the figure are shown the side views rotated by 90° around the Y axis, in the middle the top view and finally the bottom view with/out the targeting peptide.

In general, these nanoparticles have been designed in order to develop nanocarriers for drug delivery or diagnostic purpose, which may find application in the management of RA. For this reason, these nanostructures should have the following features: a biocompatible and biodegradable structure, a negative charge, a hydrodynamic diameter < 200nm and a good polydispersity index (PDI). As discussed, the biocompatible and biodegradable structure is

fundamental to transfer this technology in a clinical context. The negative charge prevents undesired interaction with the MPS and shows low toxicity than positively charged nanoparticles. Usually, the charge is expressed as Zeta potential (ζ), which reflex the charge on the nanoparticles' surface. The diameter plays an important role in the clearance, circulation time and internalization mechanisms. To this aim, nanoparticles with a diameter < 200nm should guarantee a good circulation time. Finally, the PDI is an important parameter, which describes the heterogeneity of the size distribution of molecules or particles in a solution. The dispersity index value ranges from 0 to 1, where values close to 0 are considered monodisperse while values close to 1 are considered polydisperse. After the production, the nanoparticles have been characterized by dynamic light scattering (DLS), which measures the PDI, the Zeta potential, and the hydrodynamic diameter. The DLS data confirm an average hydrodynamic diameter of 150nm, an average PDI of 0.3 and a slight negative charge between -6mV and -9.6mV (Figure 13 A). Data obtained by DLS have been confirmed by nanoparticle tracking analysis (NTA), a technique similar to the DLS, which give us additional information regarding the number of nanoparticles in solution (Figure 13 B). Indeed, through this technique, the average diameter has been 170nm while the PDI about 0.2. Concerning the number of nanoparticles in solution, the average concentration has been 3×10^{10} particles/ mL. Moreover, information regarding the morphology and the state of aggregation has been collected by transmission electron microscopy (TEM) (Figure 13, C and D) and scanning transmission electron microscopy (STEM) (Figure 13, E and F).

**Figure 13: Nanoparticles characterization.**

(A) The table summarizes main features of the nanoparticles. All kinds of nanoparticles have a polymer concentration of 1,66mg/ mL, while BNPs-MTX and tBNPs-MTX are loaded with 2mg /mL of MTX. Instead, the targeting molecule is concentrated 12 μ g /mL in the tBNPs and tBNPs-MTX. The last three columns show results obtained by DLS: hydrodynamic diameter, PDI and Zeta potential. (B) The table summarizes data obtained by NTA such as the mean diameter, the number of particles per mL and the PDI. (C) TEM image of BNPs, scale bar 100nm. (D) TEM image of tBNPs, scale bar 100nm. (E) STEM image of tBNPs in dark field (left) and bright field (right), scale bar 500nm. (F) Enlargement of the bright field STEM image of the tBNPs, scale bar 100nm.

4.1.3. Biocompatibility of nanoparticles and MTX release kinetics.

In literature, the biocompatibility of the polymers used for the production of the nanoparticles used in this work has been extensively demonstrated. However, it is essential to test their biocompatibility once the nanoparticles are formed. Indeed, the shape and the charge could induce toxicity to the cells, so it is of primary importance to assess their safe profile. For this reason, two different concentrations of nanoparticles, targeted and non-targeted, with and without MTX have been incubated with endothelial cells EA.hy 926 and compared with the same concentration of free MTX. Endothelial cells have been chosen as the first cells that could enter in contact with the particles after their in vivo injection. From the graph in the figure 14 A, obtained from data collected at 48h, it is possible to notice that empty nanoparticles, both

BNPs and tBNPs, minimally influence the viability of the cells, showing an average viability of 78% compared to not treated cells. Despite the statistical difference reported between not treated cells and cells treated with empty BNPs and tBNPs, a viability of 80% should not be considered an index of toxicity, since this result depends on the cell line and the conditions used for *in vitro* tests. Indeed, a 98% of living cells have been reported using same empty BNPs and tBNPs and same experimental condition, but using a different cell line such as MDA231 or other cell lines (data not shown). Instead, same volumes of BNPs-MTX and tBNPs-MTX showed a decreased percentage of living cells compared to cells treated with free MTX (yellow bars). As expected, MTX encapsulated into nanoparticles had a superior cytotoxicity against endothelial cells, proving that nanoparticles are able to enter into cells delivering a higher amount of MTX.

Once nanoparticles have been characterized by their physicochemical properties and for their biocompatibility it is important to study the pharmacokinetic release of the encapsulated drug. To this aim, BNPs-MTX have been dialyzed in PBS pH 7.4 at 37° in slight agitation and the released MTX have been measured by UV-Vis spectrophotometer at 310nm. The drug has been measured for 24 hours and compared with the release of MTX non-encapsulated (Figure 14 B). As shown in the graph, more than 60% of non-encapsulated MTX comes out from the dialysis tube in five hours, while 40% of MTX have been released from tBNPs. However, after the initial release, a plateau is reached after 5 hours demonstrating that 50% of MTX is still stable encapsulated in the core of the nanoparticles for at least 24h. This result suggests that nanoparticles, once injected and reached the target, may release 50% of the drug over a period longer than 24h. The initial fast release is known as “burst release”, a phenomenon characterizing drug delivery systems. Indeed, numbers of papers have been published to explain and overcome negative effects of this initial release (Huang & Brazel 2001). Main reasons concerning the burst have been associated with the shape and pore sizes of polymeric nanoparticles as well as to the drug low molecular weight. Moreover, during the process of the drug encapsulation, part of the drug entrapped in the shell could be quickly released causing the burst effect.

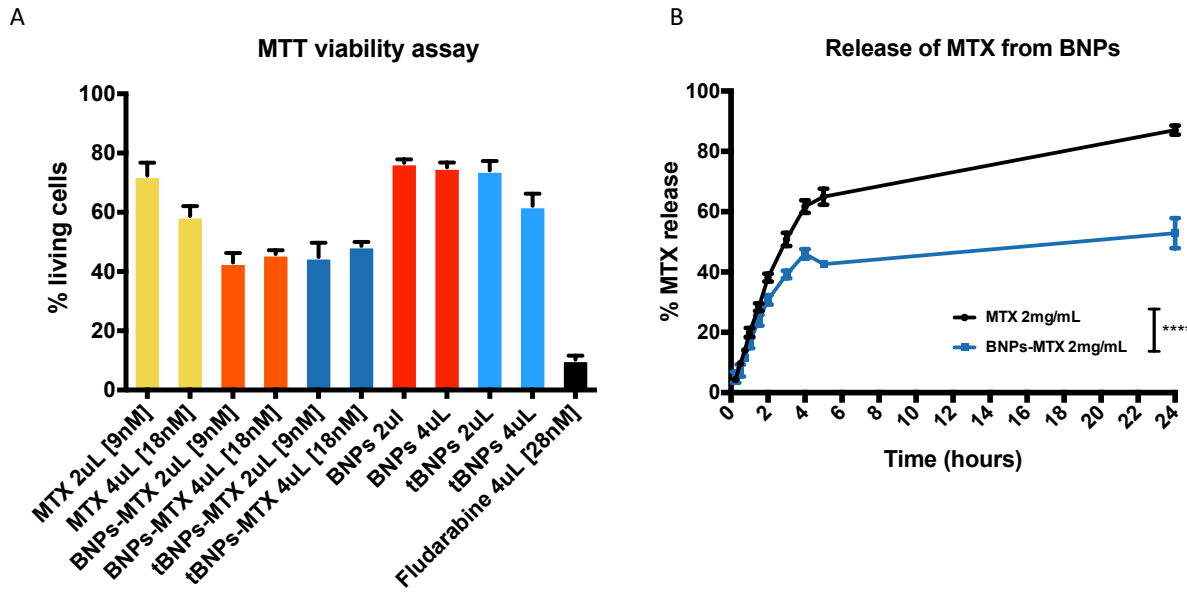


Figure 14: Evaluation of nanoparticles' toxicity in vitro.

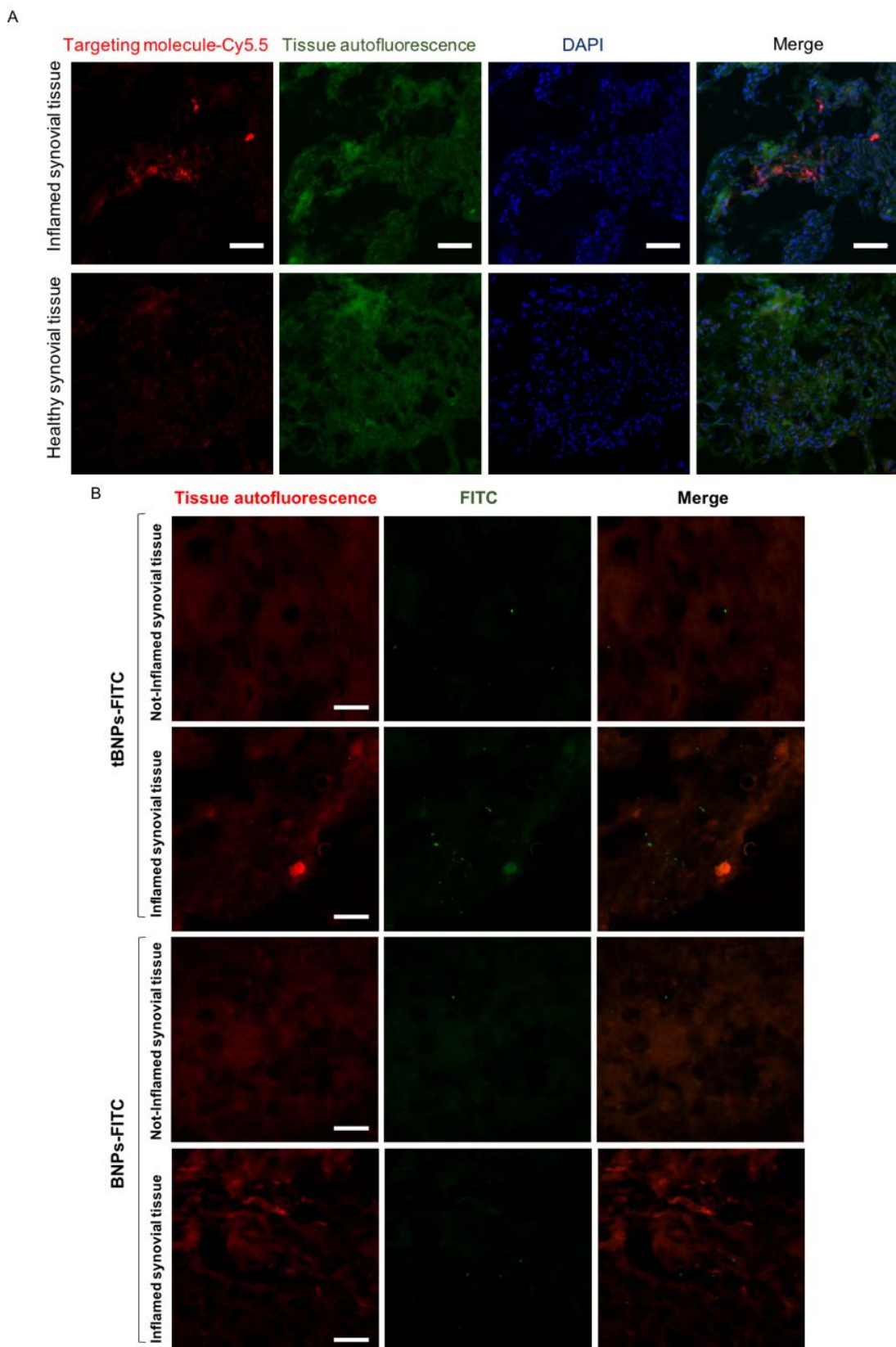
(A) MTT viability assay using EA.hy 926 cell line. Two different concentrations of MTX, BNPs-MTX and tBNPs-MTX have been used: 9nM, 18nM. Respectively are represented by yellow, orange and dark blue bars. MTX encapsulated into nanoparticles showed a superior cytotoxicity compared to the free drug. In order to investigate toxic effects of empty nanoparticles, both BNPs (red bars) and tBNPs (light blue bars) have been tested using same volumes of nanoparticles used for cells treated with MTX loaded nanoparticles. Fludarabine (black bar) have been used with a concentration of 28nM as a positive control of killing. On the Y axis the % of living cells has been calculated compared to not treated cells (100% of living cells). Results are reported as the mean of biological triplicate +/- SD. Statistical significance was calculated with One-way ANOVA multiple comparison test. Each group was analysed compared to not treated cells group. All the groups showed a significant difference compared to not treated cells with a P ≤ 0.0001 = ****. (B) The graph shows the release of MTX in dialysis with PBS pH 7.4 at 37°C in slight agitation over a period of 24h. 200µL of 2mg/mL of free MTX (black line) and BNPs-MTX (blue line) have been analysed in triplicate. During the first hour samples have been collected every 15 minutes from the dialysis and replaced with fresh PBS, then samples have been collected every 30 minutes during the second hour and finally one sample per hour until five hours. The last samples have been collected after 24h. Samples, in triplicate, have been analysed by spectrophotometer at 310nm and data have been reported as the mean ± SD. Two-way ANOVA has been used to assess statistical significance. P ≤ 0.0001 = ****.

4.2. Targeting the endothelial tissue of the inflamed synovia

4.2.1. Binding and internalization of BNPs and tBNPs with EA.hy926 cell line

The capacity of the synovial peptide to bind the inflamed synovium has been tested in the paragraph 4.1.1 Figure 10, where RA human synovial tissues have been stained with the target molecule. Macor et al. in 2012 have shown the cross-reactive of the peptide with other species, particularly rat and mouse. However, due to the fact that the synovial peptide is fused to a different ScFv-Fc, in order to demonstrate its unchanged functionality, immunofluorescence staining has been performed using inflamed synovial tissue of AIA rats. The healthy synovial tissue has been used as a control. As shown in the figure 15 A, the targeting molecule, previously labelled with Cy5.5, preferentially bound the inflamed synovial tissue (red

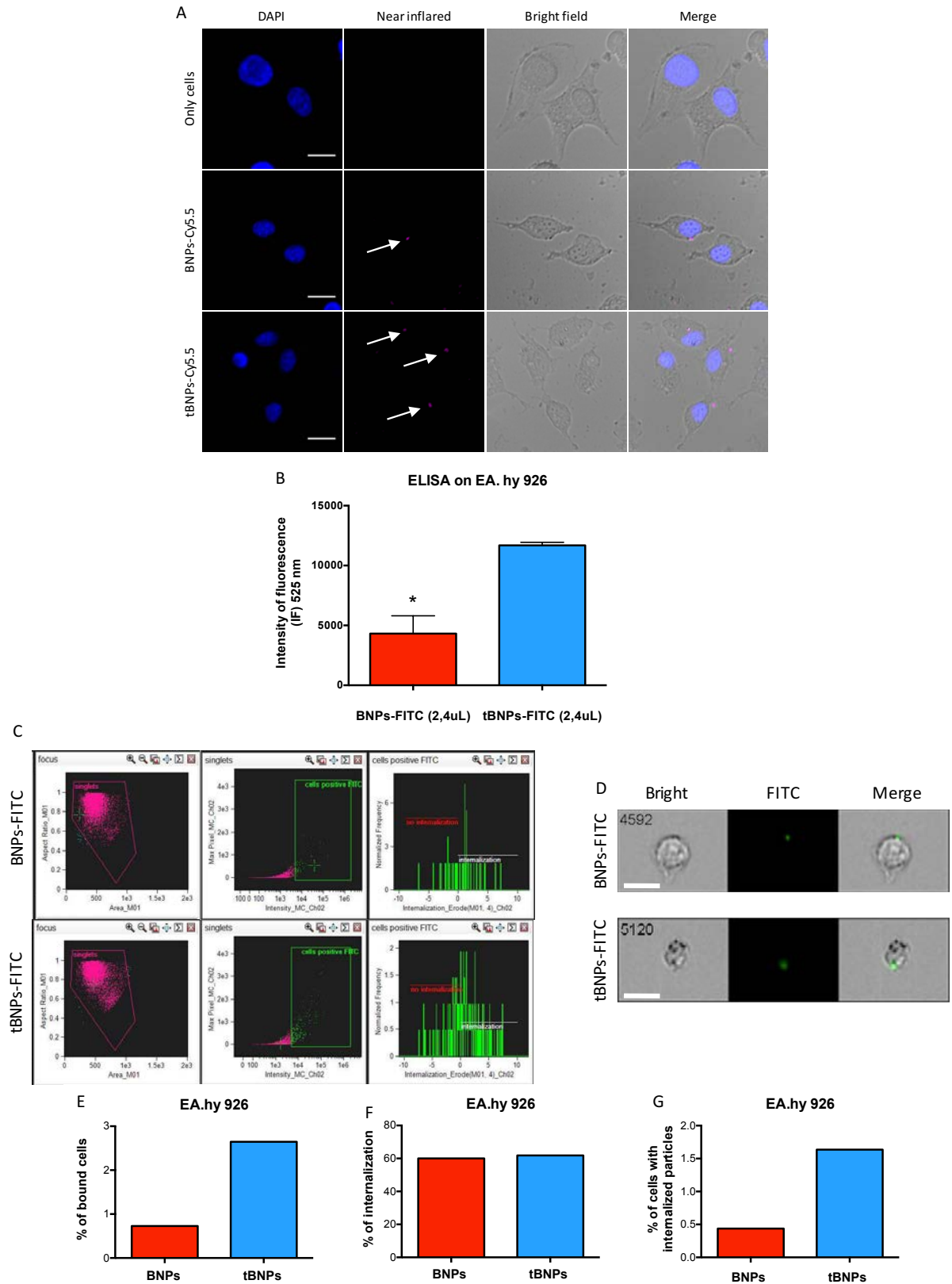
fluorescence) if compared with the healthy synovial tissue. Later, nanoparticles coupled with/out the target molecules and labelled with FITC have been incubated with inflamed and healthy synovial tissue (Figure 15 B). A higher number of green spots, in other words nanoparticles, have been detected on the inflamed synovial tissue incubated with tBNPs compared with the control tissue. In addition, very few spots have been found on the staining performed with untargeted BNPs in both inflamed and healthy synovial tissues. Most of these spots have been localized outside the tissues, probably because of a nonspecific binding of the BNPs. As predicted from the 3D molecular models, performed during the design of target molecule and the tBNPs, these experiments proved the functionality of the targeting peptide once fused to the ScFv-Fc and also when the targeting molecule is coupled with nanoparticles.

**Figure 15: Target the inflamed synovial tissue.**

(A) Inflamed and healthy synovia from AIA rats (green autofluorescence) incubated with the target molecule-Cy5.5 (red staining). Nuclei were stained with DAPI. Scale bar 50 µm. (B) Inflamed and healthy synovia from AIA rats (red autofluorescence) incubated with tBNP-FITC and BNPs-FITC both detected as green spots. Scale bar 50 µm.

As already shown, the targeting molecule is able to preferentially bind cells of the inflamed synovial tissue. Moreover, once the target molecule is coupled with the nanoparticles, these, in turn, are able to target the inflamed synovia. However, immunofluorescence staining with nanoparticles is troublesome and results are usually qualitative. Indeed, this method requires the use of fixative solution and the use of detergents, which can be incompatible with the stability of the nanoparticles. Thus, in order to improve our knowledge about the targeting and the internalization into endothelial cells, *in vitro* experiments have been conducted with EA.hy926 trying to overcome methodological problems. First, in order to investigate the binding and internalization, living EA.hy926 cells have been incubate for 1h with both BNPs-Cy5.5 and tBNPs-Cy5.5. The figure 16 A clearly shows the binding of both kinds of nanoparticles to EA.hy926, nevertheless it is not possible to understand whether the nanoparticles are inside the cells or if they are only in contact with the cellular membrane. For this reason, in order to have quantitative data, an ELISA test has been performed on living EA.hy926. Results are shown in the figure 16 B. It is evident that tBNPs-FITC are able to bind endothelial cells more than BNPs because of the targeting molecule, which is capable of a stable binding. Instead, BNPs bind cells by chance using their charge or possible hydrophobic interaction. However, by ELISA test it is not possible to discriminate between those nanoparticles that are simply bound to the cell surface and those that are internalized. Thus, a powerful instrument called AMNIS, combining speed and sample size of flow cytometry and with the resolution and sensitivity of microscopy has been used to quantify the number of cells bound by tBNPs-FITC and BNPs-FITC. Moreover, this method allows to quantify the percentage of internalised nanoparticles. EA.hy926 cells have been incubated for 2h with both BNPs-FITC and tBNPs-FITC and then analysed by AMNIS (Figure 16 C). The gate has been applied for cells positive for FITC in order to quantify cells bound by nanoparticles. About 2.7 % of cells incubate with tBNPs-FITC have been detected positive for FITC compare with 0,7% of cells incubated with BNPs-FITC. This data confirms that tBNPs, due to the target mechanism, are able to improve the binding with endothelial cells. During the analysis, cells positive for FITC, so bound by nanoparticles, have been individually photographed with a microscope both in bright field and fluorescence. Then, the images have been processed to discriminate if the nanoparticles are inside or outside the cells; a dedicated software creates a mask of the cell shape using the bright field and then, merging the fluorescence image, it defines the localization of the nanoparticles. The figure 16 D shows representative images of tBNPs-FITC inside a cell and BNPs-FITC in contact with the

cell membrane. Graphs reported in the figure 16 E, F and G summarize respectively data regarding the percentage of cells positive for FITC, the percentage of internalization, which is the same for both tBNPs and BNPs, and the final percentage of cells internalizing particles. It is possible to conclude that the percentage of internalization does not change between the BNPs and the tBNPs, however because the targeting molecule increases tBNPs binding, as consequence, percentage of tBNPs internalised is higher.

**Figure 16: Binding and internalization of BNPs and tBNPs with EA.hy926.**

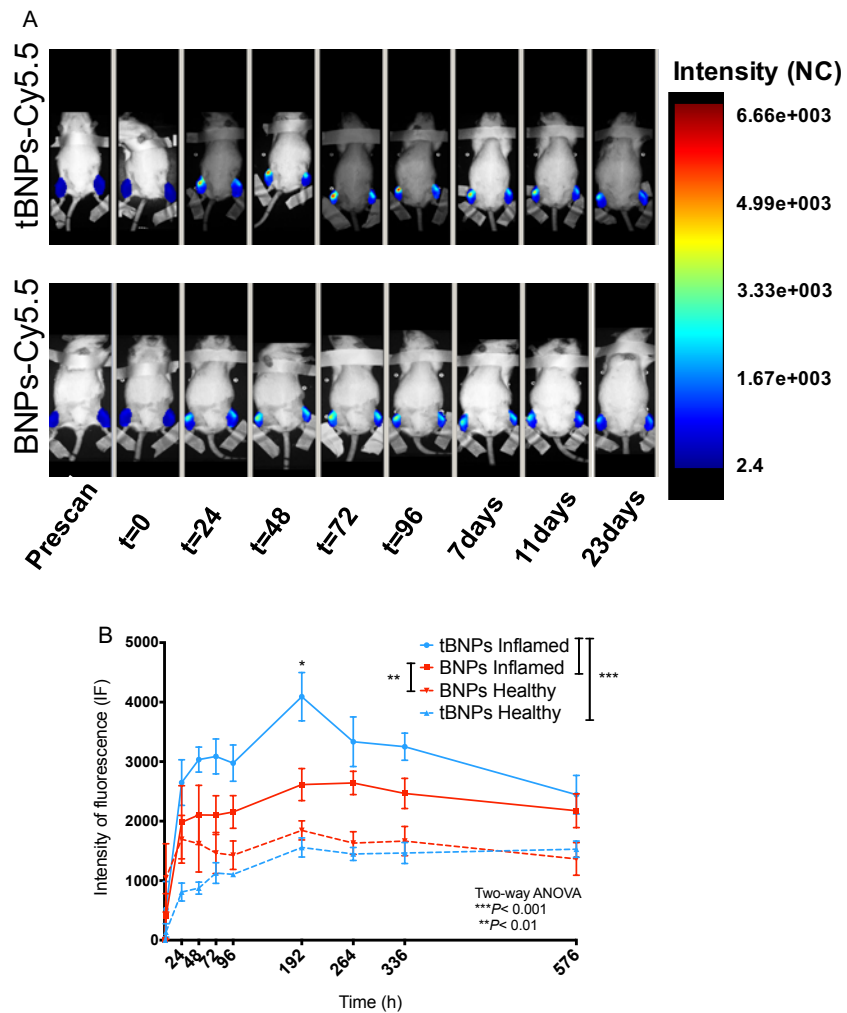
(A) EA.hy926 cells incubated with tBNPs-Cy5.5 and BNPs-Cy5.5 for 1h at 37°C with 5% of CO₂. Nuclei of cells have been stained with DAPI while nanoparticles labelled with Cy5.5 have been detected at 697nm (near infrared). Whole cells have been detected by differential interference contrast (DIC) bright field and finally merged with DAPI and near infrared channels. White arrows highlight nanoparticles. Scale bar 20μm. (B) ELISA test performed on living EA.hy926 cells. 2,4uL of tBNPs-FITC and BNPs-FITC have been incubated with EA.hy926 for 1h at 37°C with 5% of CO₂. FITC intensity of fluorescence has been detected

at 525nm by ELISA plate reader. (C) EA.hy926 cells incubated with BNPs-FITC and tBNPs-FITC have been gated for their fluorescence using as control not-treated cells. The first plot shows in focus objects described with the “aspect ratio” (Y axis) defined as the minor axis divided by the major axis and describes how round an object is, while the X axis defines the “Area” in μm^2 . In the second plot, the Y axis shows the “max pixel”, which measure the largest value of the background-subtracted pixels contained in the input mask, while the X axis shows the intensity of fluorescence. The third plot shows the “frequency” of particles internalized on the Y axis while on the X axis the “internalization” is defined as the ratio of the intensity inside the cell to the intensity of the entire cell using specific masks to define the inner part. Finally, pixels on the edge of the main mask have been removed by the “erode mask”. The higher score represents a greater concentration of intensity inside the cell. Cells with internalized nanoparticles typically have positive scores while cells with no internalization have negative scores. (D) Representative images acquired during the analysis of two cells positive for FITC, one with tBNPs-FITC and one with BNPs-FITC. Scale bar 20 μm . (E) The graph summarises percentage of cells positive for FITC when incubated with BNPs-FITC or tBNPs-FITC while (F) reports the percentage of internalization. (G) The percentage of cells with internalized particles has been obtained applying the % of internalization on the % of bound cells.

4.2.2. *In vivo* biodistribution of BNPs and tBNPs in a AIA rat model

In the paragraph 4.2.1 it has been demonstrated that the targeting molecule and the tBNPs were able to preferentially bind inflamed synovial tissue *in vitro*. In order to confirm this result *in vivo*, 4.8 nM of Cy5.5 labelled on tBNPs and BNPs were injected, through the tail vein, in rats developing inflammation in the right knees. This model of monoarthritis, called AIA, is a useful, easy and quick model to study biodistribution of new therapeutic and diagnostic compounds for the management of RA. After three days from the induction of the inflammation in the right knee, nanoparticles have been injected and then followed for 23 days (Figure 17 A). The animals, analysed following Cy5.5 by near infrared optical imaging, clearly show a higher accumulation of fluorescence in the right knee of the animals receiving tBNPs-Cy5.5 compared to the contralateral knee (not inflamed) or animals treated with BNPs-Cy5.5. Plotting the fluorescence data from figure A, it is possible to obtain the graph of the figure 17 B. The graph highlights an improved accumulation of tBNPs-Cy5.5 in the right inflamed knees, reaching the maximum after 7/8 days. In order to assess the accumulation in other tissues, at the end of the study, the fluorescence has been measured *ex vivo* in the main organs such as liver, spleen, lungs, kidneys, brain, heart and paws. Indeed, from the picture 17 C, it is possible to appreciate the higher accumulation of nanoparticles into the liver, followed by kidneys. It is interesting to notice that the target mechanisms coupled on tBNPs did not influence the accumulation in these organs. Moreover, the higher fluorescence intensity detected in the liver suggests that these nanoparticles, as already studied by our group, due to their physicochemical features are mainly eliminated through the bile in the gut and finally removed with the faeces. Fluorescence data detected on the knees have been correlated with their swelling (Figure 17 E), which is the main inflammatory parameter to evaluate AIA. It is important to notice that both tBNP-Cy5.5 and BNPs-Cy5.5 groups of animals had the same swelling for the inflamed

knees (right) and healthy knees (left), however the fluorescence intensity of tBNPs-Cy5.5 was higher than the contralateral knees and knees of animals receiving BNPs-Cy5.5. In addition, the figure 17 F shows the immune response against mBSA, the antigen used to immunize these animals and to induce the inflammation. The graph shows the same quantity of immunoglobulins anti-mBSA, confirming that the higher accumulation of the tBNPs into the inflamed knee is not a result of a different degree of inflammation but it is the outcome obtained using an active targeting. These results obtained *in vivo* are of great interest because it proves the superior accumulation of targeted nanoparticles compared with the untargeted nanoparticles, demonstrating that the targeting molecule actively guides nanoparticles in the inflamed knees. Moreover, this is another proof that targeted nanoparticles could be the key to overcome the lack of efficacy of nanocarriers based on a passive delivery. It is reasonable to conclude that tBNPs could be studied both as therapeutic and diagnostic agents for the RA management, improving the efficacy and the sensitivity respectively.



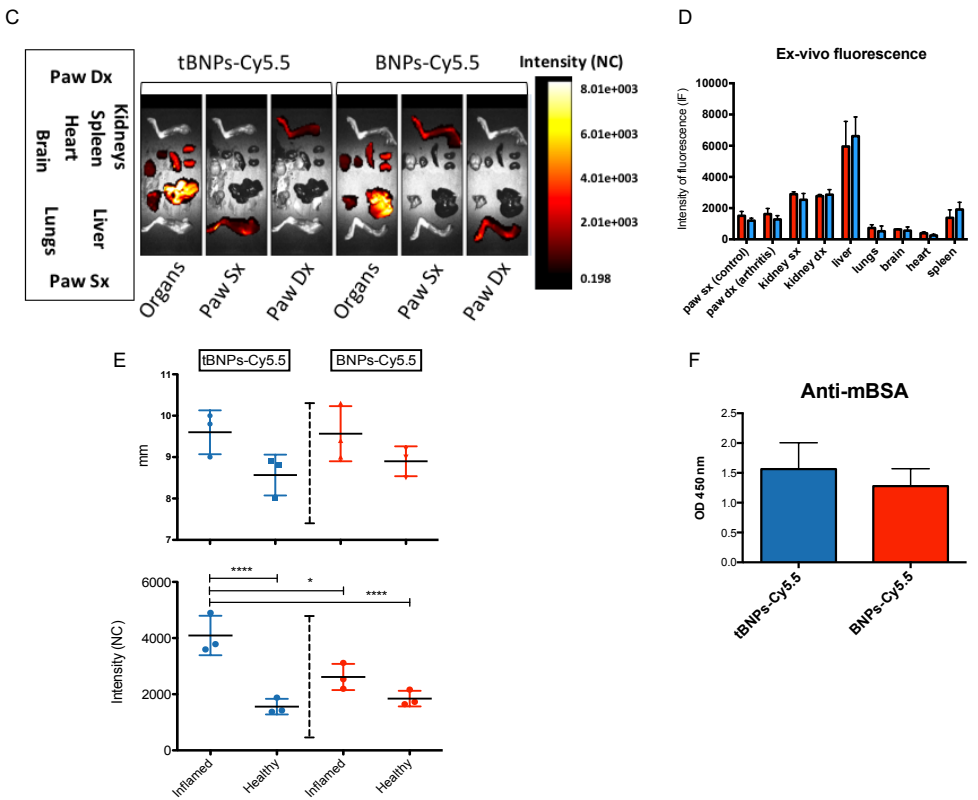


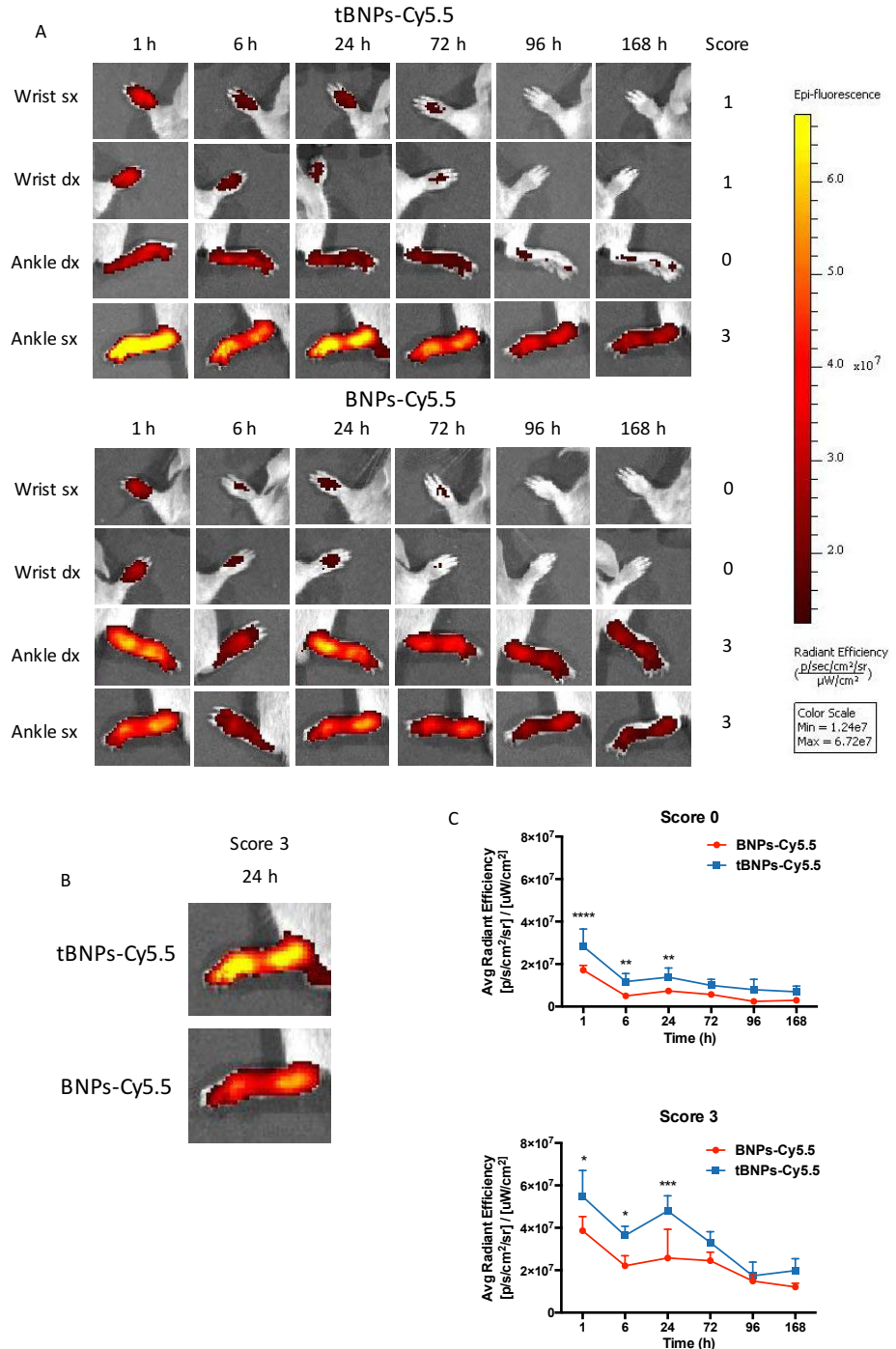
Figure 17: In vivo biodistribution of tBNPs and BNPs in a model of rat AIA.

(A) Images acquired by time domain optical imaging of two representative AIA rats treated intravenously respectively with 4.8 nM of tBNPs-Cy5.5 (first row) and BNPs-Cy5.5 (second row). The fluorescence has been followed for a total of 23 days. The highest intensity of fluorescence was detected at day 7 in the right knees of tBNPs-Cy5.5 treated rats. Fluorescence intensity has been reported as normalized counts (NC). (B) The graph shows fluorescence intensity as NC of the images acquired by time domain optical imaging. Fluorescence intensity of the right and left paws of the animal treated with tBNPs-Cy5.5 have been reported respectively as continuous blue line and dotted blue line. Instead, the fluorescence intensity of the right and left paws of the animals treated with BNPs have been reported respectively as continuous red line and dotted red line. (C) Ex-vivo images, acquired by time domain optical imaging, of the main organs of two representative AIA rats treated respectively with tBNPs-Cy5.5 and BNPs-Cy5.5. (D) The fluorescence intensity (express as NC) mean \pm SEM of all rats (three per group) has been reported. (E) This image shows the swelling in relation with the intensity of fluorescence recorded for each paw at day 7. Blue bars represent data of rats treated with tBNPs-Cy5, while red bars are data belonging to BNPs-Cy5 treated rats. (F) ELISA test for the evaluation of the rat IgG anti-mBSA in blood samples of the rats treated with tBNPs-Cy5.5 and BNPs-Cy5.5. Data are reported as the mean \pm SEM of three rats per group. Two-way ANOVA has been used to assess statistical significance between groups during the time in the graph B, while unpaired parametric t-test has been used to assess statistical significance in the graph E. P \leq 0.05 = *; P \leq 0.01 = **; P \leq 0.001 = ***; P \leq 0.0001 = ****.

4.2.3. *In vivo* biodistribution of BNPs and tBNPs in CIA mouse model

After testing the ability of tBNPs to specifically bind the inflamed joints of an AIA monoarthritis, the next step was to study biodistribution in a CIA polyarthritis model. This model is considered the gold standard to test new compounds to be used in the diagnosis and treatment of rheumatoid arthritis. Indeed, as discussed in the introduction, it is a model that share several features with the pathology in humans, involving all the animal's limbs with different degrees of inflammation. Animals immunized against bovine collagen type II, spontaneously develop an immune response against their own collagen, which is one of the most abundant proteins

in the joints. Once animals, in this case mice, developed the disease, they were enrolled in two groups, receiving tBNPs or BNPs. Mice have been scanned for 7 days and images of the limbs of two representative mice are shown in the figure 18 A. Moreover, the arthritis score, ranging from 0 (no arthritis) to 4 (worst arthritis) and reflecting the severity of the disease, have been assessed in order to associate the fluorescence with disease progression. It is important to notice from figure 18 B that paws with the same score show a different intensity of fluorescence and the highest have been detected in the paw of a mouse treated with tBNPs-Cy5.5. In fact, graphs of the figure 18 C show a higher fluorescence intensity at both score 0 and 3. Importantly, the statistical significance has been reached in the first 24h. This result, however, diverges from the biodistribution obtained in AIA, where the highest fluorescence difference has been reached after 1 week. Nevertheless, these two RA models are based on two different pathogenesis processes. Indeed, the AIA is an acute model and the inflammation increase together with the formation of new vessels, supporting the data showing a progressive accumulation during the first week. Instead, the CIA is a chronic model of RA where the inflammation and the new blood vessels are already established before the study, thus tBNPs are able to accumulate immediately after their injection. Of interest is the trend showed by the tBNPs-Cy5.5 fluorescence (figure 18 C), indeed the initial fluorescence peak, due to the nanoparticles injected in the tail vein, is followed by a decrease fluorescence intensity (6h), probably due to the clearance of the excess of nanoparticles. Finally, the fluorescence increased again after 24h in mice receiving tBNPs-Cy5.5 only, proving their accumulation compared with BNPs.

**Figure 18** In vivo biodistribution of tBNPs and BNPs in a model of mouse CIA.

(A) Images acquired by time domain optical imaging of two representative CIA mice treated intravenously respectively with 0.5 nM of Cy5.5 bound to tBNPs (first panel) or BNPs (second panel). The fluorescence has been followed for a total of 7 days. Starting from the first row: wrist sx, wrist dx, ankle dx and ankle sx. The score of each paw has been reported on the right of each row. (B) Images of two mice ankles, treated respectively with tBNPs-Cy5.5 and BNPs-Cy5.5, show same arthritic score but different fluorescence intensity. Indeed, the highest has been detected in the paw of the tBNPs-Cy5.5 treated mouse. (C) The graphs show the intensity of fluorescence detected for a total of 7 days in paws with score 0 (graph above) and paws with score 3 (graph below). The statistical significance has been reached in the first 24 h in the paw of mice treated with tBNPs-Cy5.5 (blue line) compare with mice receiving BNPs-Cy5.5 (red line). Fluorescence intensity has been reported as average radiant efficiency \pm SD. In this study have been enrolled 7 mice. Four of them treated with tBNPs-Cy5.5 and three with BNPs-Cy5.5. The graph regarding the score 0 takes into account 5 paws of tBNPs-Cy5.5 treated mice and 7 of BNPs-Cy5.5. Instead, the graph of the score 3 takes into account 4 paw of tBNPs-Cy5.5 treated mice and 4 of BNPs-Cy5.5. Two-way ANOVA multiple comparisons test has been used to assess statistical significance. $P \leq 0.05 = *$; $P \leq 0.01 = **$; $P \leq 0.001 = ***$; $P \leq 0.0001 = ****$.

Further, we investigate the higher intensity of fluorescence detected after 1h in joints of mice receiving tBNPs-Cy5.5 and scored as 0 by external objective evaluation. We wondered if this difference was the result of an initial inflammatory state, which is not perceptible with the objective examination. To this aim, we performed haematoxylin eosin staining of joints scored as 0, founding the initial infiltration of the subchondral bone by monocytes and neutrophils (Figure 19). This evidence highlights the potential of using tBNPs as a diagnostic tool, indeed they show early inflammation, which was not detectable by objective examination (swelling, erythema, ankylose). Moreover, this study of biodistribution proves a correlation between the intensity of fluorescence and the degree of inflammation, which is an essential feature to detect disease progression during the follow-up.

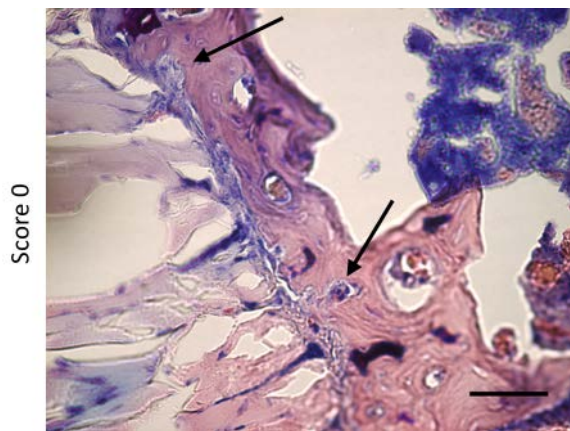


Figure 19. Haematoxylin Eosin staining.

Representative image of a joint of CIA DBA/1 mouse with score 0. Arrows highlight bone infiltration by monocytes and neutrophils. This condition demonstrates that joints usually scored by 0, meaning no arthritis, if analysed by histology reveals the initial inflammatory state due to leukocyte bone infiltration (black arrows). Scale bar 20 μ m.

4.3. Preclinical studies in a model of polyarthritis

4.3.1. Efficacy of tBNPs-MTX in CIA mouse model

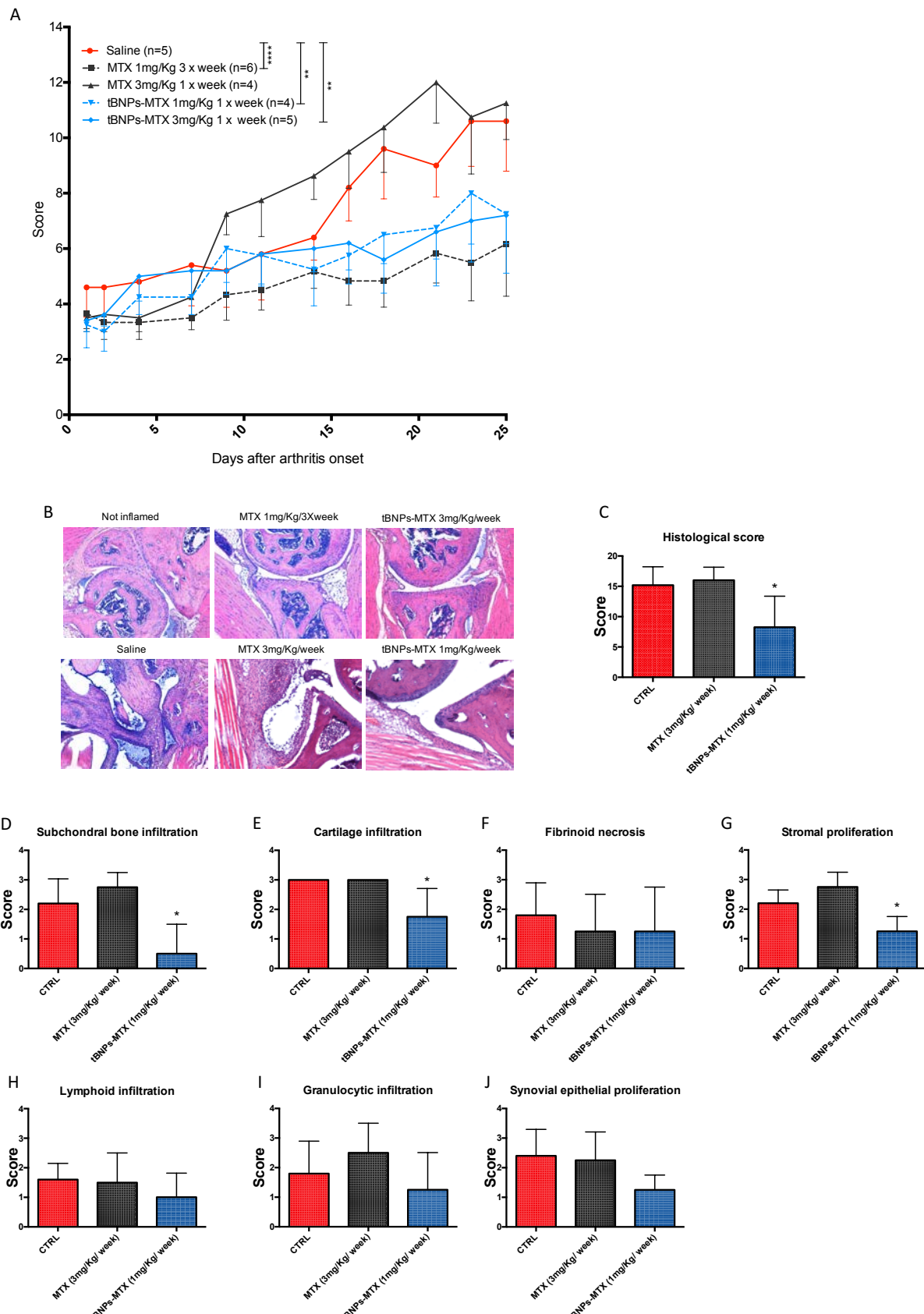
The studies of biodistribution prove the superior accumulation of the tBNPs compared with the untargeted BNPs into the inflamed knees of both arthritic models. However, in order to demonstrate that a higher accumulation means higher efficacy, the therapeutic effect of tBNPs loaded with MTX has been investigated in CIA mouse model and compared with free MTX. According to the results obtained during the biodistribution in rats and in mice, tBNPs accumulate into the inflamed synovia for a period of a week. Instead, it is known from the literature that MTX has a fast clearance. In particular, Lobo and Balthasar demonstrated that MTX half-life is 33.8±6.5 minutes when injected intraperitoneal (i.p.) in mouse (Lobo &

Balthasar 2003). Considering this information, one group of arthritic mice has been treated i.p. with saline solution (as negative control); another group has been treated with 1mg/Kg of free MTX three times per week and represents the positive control, adapting data present in literature (Lange 2005)(Jung et al. 2015). Because nanoparticles persist in the inflamed synovium for about a week, a group of mice has been treated with an equivalent dose of tBNPs-MTX, in particular not 1mg/Kg three times per week but a single dose of 3mg /Kg per week. As shown in the graph 20 A, this dose of tBNPs-MTX (continuous blue line) showed a decreased arthritic score, compared to control animals (red line), proving its efficacy. This result is in line with the therapeutic effect provided by the treatment with the free drug.

One of the primary objectives of the project is to demonstrate that the selective delivery, which increases the concentration of nanoparticles and MTX in the inflamed joints, may allow a dose reduction compared to a standard treatment. To this aim, another group of mice has been treated with a lower dose of tBNPs-MTX equivalent to 1mg/Kg per week (dotted blue line). Even with a lower dose, the targeting mechanism guarantees therapeutic efficacy over the free drug.

As expected, the group of mice treated with a single injection of 3mg/Kg of free MTX (dotted black line) did not show any efficacy compared to control group, confirming that MTX, due to its fast clearance, cannot be administrated once per week.

At the end of the study, mice have been euthanized and paws have been collected for subsequent analysis. Indeed, the therapeutic efficacy of the tBNPs-MTX compared to control and free MTX have been validated by histological analyses (Figure 20 B). These images were then analysed and histological scores (Figure 20 C) show reduction of the cartilage and subchondral bone infiltration (Figure 20 E, D), as well as a reduction in the stromal proliferation (Figure 20 G) in mice treated with the effective doses of tBNPs-MTX and free MTX.

**Figure 20: Efficacy of tBNPs-MTX in CIA model.**

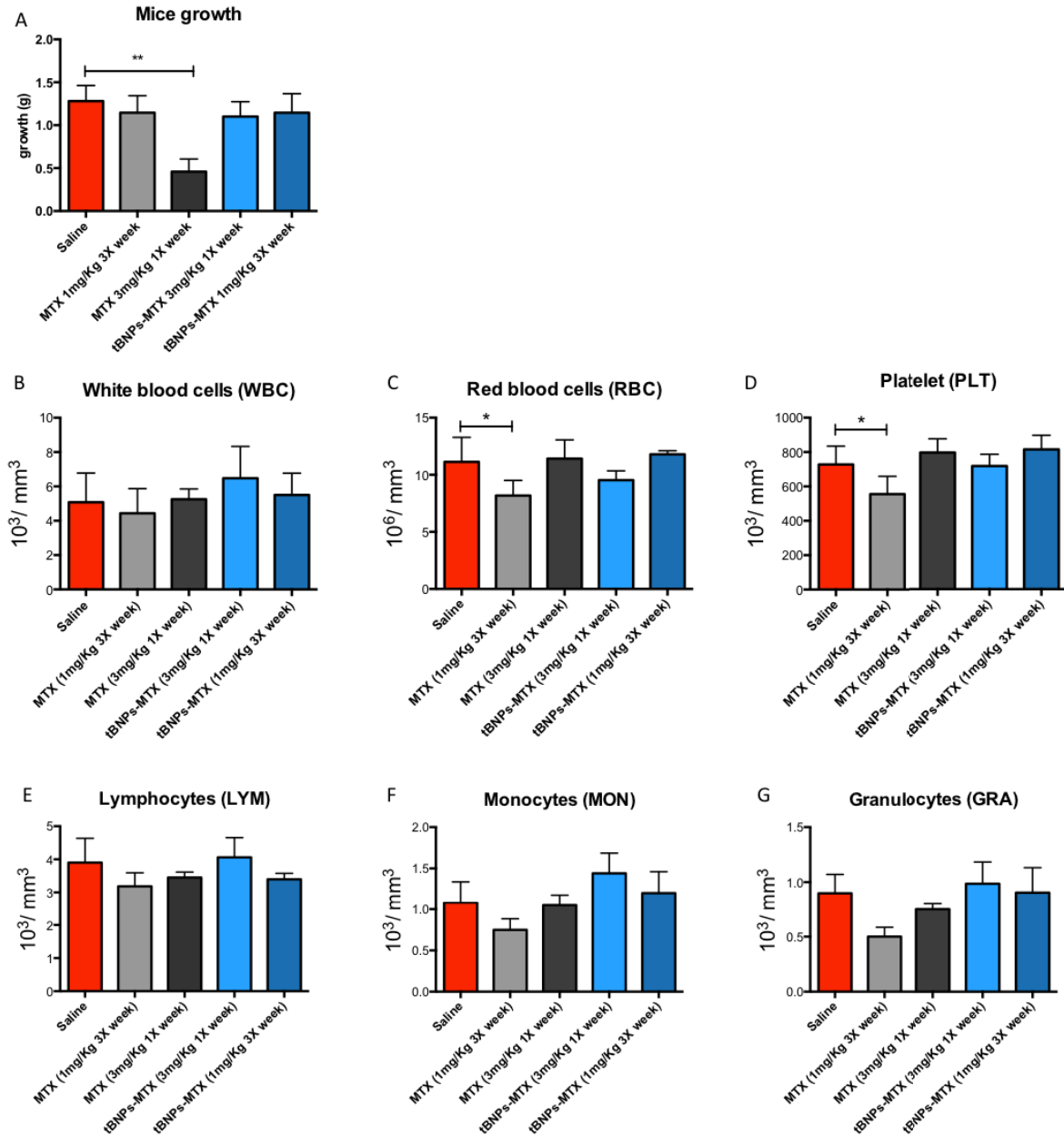
(A) The graph shows arthritic scores of CIA DBA/1 mice treated i.p. for 25days with different doses of tBNPs-MTX and free MTX. Groups of mice have been enrolled as follow: saline solution as control (red line); MTX 1mg/ Kg three times per week (continuous black line); MTX 3mg/ Kg one time per week (dotted black line); tBNPs-MTX 3mg/ Kg one time per week

(continuous blue line); tBNPs-MTX 1mg/ Kg one time per week (dotted blue line). The scores have been reported as the mean of the sum of the scores \pm SEM assessed for each paw of the mouse. The score values range from 0 (no arthritis) to 4 (highly inflamed, swollen or ankylosed paw). Statistical significance has been assessed by Two-way ANOVA test. $P \leq 0.05 = ^*$; $P \leq 0.01 = ^{**}$; $P \leq 0.001 = ^{***}$; $P \leq 0.0001 = ^{****}$. (B) Histological images representative of each group of mice treated in this study. An additional image of a healthy paw was added to the panel as the negative control. The group treated with saline solution shows the worst profile characterized by a hyperplastic synovial tissue, huge infiltration of leukocytes and loss of cartilage and bone structure. (C) Histological total score reported as the mean \pm SD of the scores assigned for each mouse of the study. The score is the result of scores assigned for 7 different parameters such as subchondral bone infiltration (D), cartilage infiltration (E), fibrinoid necrosis (F), stromal proliferation (G), lymphoid infiltration (H), granulocytic infiltration (I) and synovial epithelial proliferation (J). Statistical significance has been assessed by unpaired parametric t-test. $P \leq 0.05 = ^*$

4.3.2. Evaluation of toxic effects in CIA mice treated with tBNPs-MTX

One of the goals of this project is to demonstrate that same therapeutic effects can be obtained using a lower dose of drug by targeted approaches. As a result, a lower dose of the encapsulated drug and a different route of elimination (liver-bile-intestine) should coincide with lower side effects. One of the parameters considered to assess toxicity is the reduction of the body weight (Figure 21 A). The histogram shows the reduction of gain weight in mice treated with MTX 3mg/ Kg once per week compared to control mice and mice treated with both doses of tBNPs-MTX. Moreover, another parameter used to demonstrate less toxic effects is based on blood analysis (Figure 21 B-G). Reduction of WBC, RBC and PLT usually reflect toxic effects of the treatment. Regarding WBC, mice treated with 1mg/ Kg of MTX three times per week showed a reduction compared with control mice, although no statistical significance has been reached. On the contrary, the statistical reduction has been assessed for RBC and PLT in mice receiving this treatment. Despite the therapeutic effects of this dose of MTX some toxic effects were evident compared to control animals, while mice treated with both doses of tBNPs-MTX did not show any toxic effects. A safe toxicological profile has been also demonstrated in mice treated with a dose of 3mg/ Kg of MTX. This could be again justified by the fast elimination of the single dose.

Both gain weight and blood analysis highlight toxic effects due to the treatment with free MTX. By contrast, MTX encapsulated in tBNPs showed a really safe profile in CIA mice.

**Figure 21: Blood analysis and gain growth in CIA mouse.**

The histograms represent data regarding mice growth (A) and blood analysis such as WBC (B), RBC (C), PLT (D), LYM (E), MON (F), GRA (G). All histograms report data as the mean \pm SD. Each coloured bar represents a different group of mice: red bars stand for mice receiving saline (n=5); bars of mice treated with MTX 1mg/ Kg 3X week have been coloured with light grey (n=6); bars of mice treated with MTX 3mg/ Kg 1X week have been coloured with dark grey (n=4); light blue bars stand for mice treated with tBNPs-MTX 3mg/ Kg 1X week (n=4); dark blue bars stand for mice treated with tBNPs-MTX 1mg/ Kg 3X week (n=5). Statistical significance has been assessed by unpaired parametric t-test. P \leq 0.05 = *; P \leq 0.01 = **.

4.3.3. Cytokines multiplex analysis.

In order to have a complete picture of the inflammatory process that occurred in mice treated with tBNPs-MTX, serum samples have been analysed to quantify cytokine levels by multiplex ELISA. In this case, the interest was to understand cytokines profiles in mice treated with lower doses of tBNPs-MTX and MTX compared to the control group. Despite the great amount of

information that can be obtained, it is difficult to fully understand and contextualize their variation in the inflammatory cells network happened in this chronic model of RA. Moreover, these profiles concern the systemic cytokines and do not perfectly reflect cytokines levels in the inflamed synovia, where the local profiles could be different. Moreover, cytokines act through their receptors, which in turn can be upregulated or downregulated to compensate cytokines low expression or overexpression. However, cytokines quantification gives a reasonable idea of the inflammatory landscape and should be used as additional information to support or explain other data. Overall, from the results summarized in figure 22, mice treated with tBNPs-MTX showed an increased amount of IL-1 β , IL-2, IL-12p70, IL-17 and MIP-1a (Figure 22 B, C, I, K, X). Despite the increased levels of these cytokines, the levels of TNF- α , which is the pivotal pro-inflammatory cytokine, have been unchanged compared to control mice. In addition, IL-6, also known for its central role in rheumatoid arthritis, have been decreased as well as RANTES (regulated on activation, normal T cell expressed and secreted). The latter is a chemokine with a chemotactic role principally for leukocytes. KC (keratinocyte-derived cytokine) is another chemokine that has been found decreased compared to control group of mice. This chemokine has neutrophil chemoattractant activity and has been proved to be involved in neoangiogenesis (Vries et al. 2015).

Due to the therapeutic effects reached in the group of mice treated with tBNPs-MTX, it is possible to conclude that, probably, the decrease levels of IL-6, RANTES and KC could balance the increased levels of pro-inflammatory cytokines such as IL-1 β , IL-2, IL-12p70, IL-17 and MIP-1 α .

Concerning cytokines levels of the mice treated with MTX, cytokines profile is substantially different than tBNPs-MTX, in fact following cytokines have been increased: IL-3, IL-10, IL-13, Eotaxin, GM-CST, INF- γ , MCP-1, MIP-1 β and most importantly TNF- α . The increased levels of these cytokines demonstrate once again the ineffectiveness of the treatment with this dose of MTX.

Results and discussion

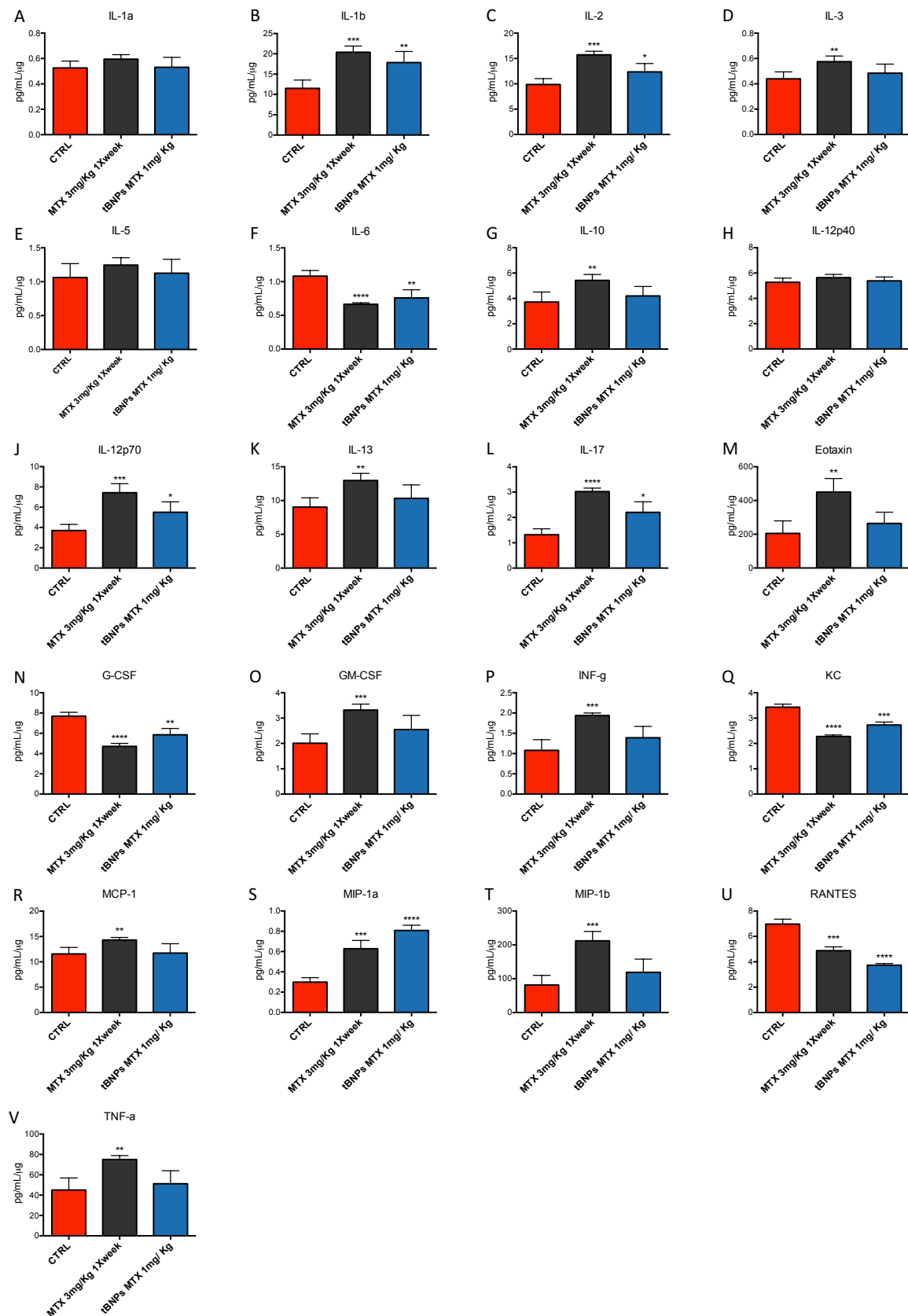


Figure 22: Multiplex cytokine profiles in CIA mice.

The histograms represent data regarding the analysis of 21 mouse cytokines. All histograms report data as the mean \pm SD of quadruplicate pooled serum samples. Results have been normalized for the total protein concentration in μg . Each colored bar represents a different group of mice: red bars stand for mice receiving saline ($n=5$); bars of mice treated with MTX 3mg/ Kg 1X week have been colored with dark grey ($n=4$); dark blue bars stand for mice treated with tBNPs-MTX 1mg/ Kg 3X week

(n=5). Statistical significance has been assessed by unpaired parametric t-test. P ≤ 0.05 = *; P ≤ 0.01 = **; P ≤ 0.001 = ***; P ≤ 0.0001 = ****.

4.4. Mechanism of action of MTX encapsulated into tBNPs.

4.4.1. Efficacy and side effects of tBNPs-MTX therapy in AIA rat model.

The studies of biodistribution prove the superior accumulation of the tBNPs into the inflamed knees of both models of AIA and CIA compared with the BNPs. Moreover, the superior efficacy of tBNPs-MTX has been proved in CIA model, with a safer profile of this treatment compared with the free drug. However, we wondered if these promising results were due only to the targeting strategy, thus a higher concentration of MTX into the synovial tissue, or whether there was a contribution of a different mechanism of action of the drug encapsulated in targeted nanoparticles.

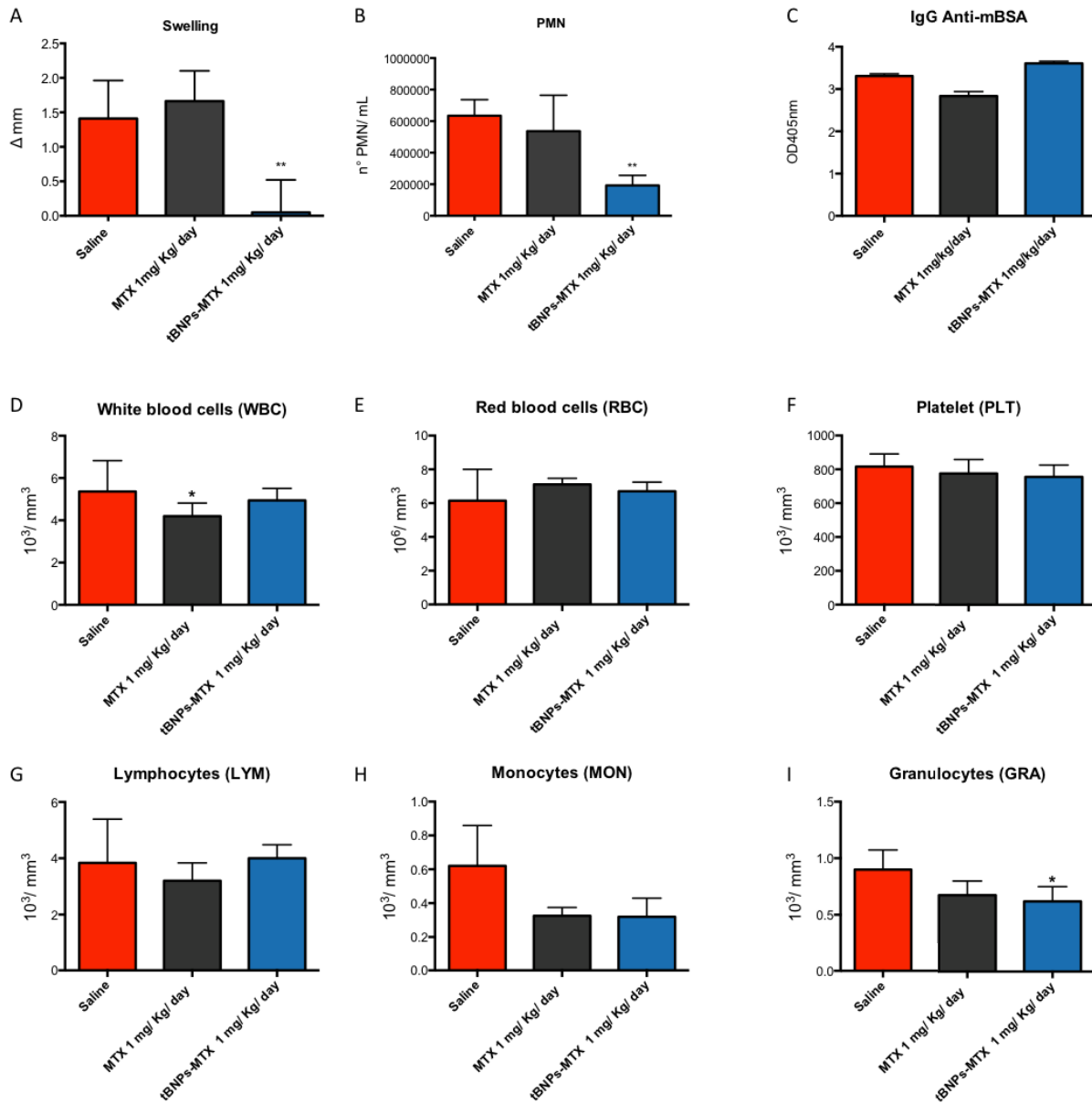
In order to dissect the mechanism of action of tBNPs loaded with MTX, the treatment of the AIA model has been taken in consideration because it is known in the literature to be not treatable with free MTX (Williams et al. 1996)(Williams 2001). In fact, in this acute model, the inflammatory damage is mainly caused by the production of immune complexes in the joint microenvironment, by the activation of the complement system and the subsequent recruitment of immune cells. In this acute situation (3-4 days), MTX has not the time to reduce the production of antibodies and its administration become obvious ineffective.

Three groups of rats have been enrolled: 5 rats received saline solution as control, 4 rats were treated with MTX 1 mg/ Kg/ day and 5 rats were treated with tBNPs-MTX 1mg/Kg. The treatments started simultaneously with the induction of the inflammation. The fourth day, animals have been euthanized and synovial liquids, blood and synovial tissue have been collected. As the main inflammatory index, the swelling has been measured the first and the last day in order to calculate the Δ reported in the graph of the figure 23 A. From this graph, it is evident that tBNPs-MTX prevents the inflammation compared with both rats treated with saline solution and MTX. Moreover, to confirm swelling data, number of PMNs in the synovial liquid has been evaluated. Thus, in the figure 23 B, rats treated with tBNP-MTX present a strong decreased number of PMN cells compared with control or MTX treated animals.

In order to demonstrate that the effects are depending on the treatment and not to a reduced immunization of the animals, anti-mBSA IgG levels have been quantified in the serum of these animals (Figure 23 C). From this graph, it is evident that all animals developed a comparable immune response.

From the data obtained so far, it is clear that tBNPs-MTX were able to prevent inflammation in rat AIA where the same dose of free MTX was ineffective, providing the indication that the mechanisms of action of the two therapeutic approaches are different.

Side effects of these treatments should be compared with data obtained in CIA model. For this purpose, blood samples of the AIA rats have been collected at the end of the treatments (3 days treatment) and analysed. RBC, WBC and PLT have been quantified (Figure 23 D, E and F). In addition, due to the fact that MTX is associated to the bone marrow suppression (Lim et al. 2005), with consequent reduction of WBC, subpopulations of lymphocytes, granulocytes and monocytes have been quantified (Figure 23 G, H and I). As expected, a significant reduction of white blood cells has been reported in the group of rats treated with free MTX, while rats treated with the same dose of tBNPs-MTX showed similar WBC than control rats. This result highlights the fact that in our approach, MTX remains mainly encapsulated into tBNPs, it performs its activity directly in the inflamed synovia, decreasing side effects associated with a non-specific delivery. Although the total number of WBCs remained unchanged in rats treated with tBNPs-MTX, a slightly reduced number of granulocytes have been found. Instead, a reduction of monocytes has been observed in both MTX and tBNPs-MTX treated groups, even though no statistical significance has been found.

**Figure 23: Efficacy and blood analysis in AIA rat treated with tBNPs.**

(A) Results of the Δ swelling in mm of the right knees obtained after three days of treatment. Swelling of rats treated with saline solution is reported in red, in grey swelling of rats receiving 1mg /Kg / day of free MTX and in blue the swelling of rats treated with 1mg /Kg / day of tBNP-MTX. (B) The graph shows the number of PMN /mL in the synovial liquid of rats treated with saline solution (red), rats receiving 1mg /Kg / day of free MTX (grey) and treated with 1mg /Kg / day tBNP-MTX (blue). In both graph, A and B data are reported as the mean \pm SD. 5 rats have been enrolled for the groups treated respectively with saline solution and tBNPs-MTX, while 4 rats have been enrolled for the group treated with free MTX. A parametric unpaired t-test has been used to assess a statistical significance. (C) Data obtained by ELISA test for the evaluation of IgG anti-mBSA in rats' serum of the groups already analysed for swelling and PMN. The bars colour follows the colours of previous graphs. Data are shown as the mean \pm SD of a technical triplicate of pooled serum for each group of rats. The graphs summarise results of the blood analysis in rats treated with: saline solution (red bars), MTX 1mg/ Kg/ day (grey bars) and tBNPs-MTX 1mg/ Kg/ day (blue bars). Data have been reported as the mean \pm SD. The number of samples for each group is as follow: saline solution (n=5), MTX 1mg/ Kg/ day (n=4); tBNPs-MTX 1mg/ Kg/ day (n=5). Statistical significance has been calculated with a parametric unpaired t-test. P \leq 0.05 = *; P \leq 0.01 = **.

4.4.2. tBNPs-MTX reduce neoangiogenesis of the inflamed synovia

Despite these positive results, we wondered about the mechanism of action of MTX encapsulated in tBNPs. Due to the fact that AIA model is primarily based on the formation of immune complexes in the articular cavity with a consequent activation of the complement system, we analysed whether the anti-inflammatory effect could reduce the activation of the complement system. To this aim, inflamed synovial tissues of the rats enrolled in the study have been stained for deposits of C3 (Figure 24 A), a complement component common to all three pathways. The C3 stain was comparable for all treated groups without any differences. Thus, the effects of the tBNPs-MTX treatments did not influence the cause of the inflammation, as observed for specific IgG production.

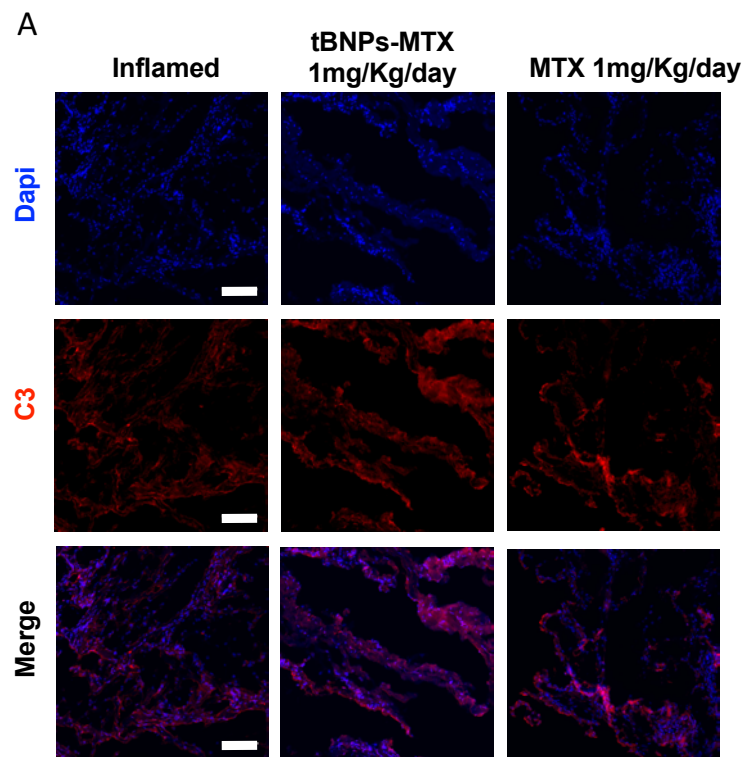
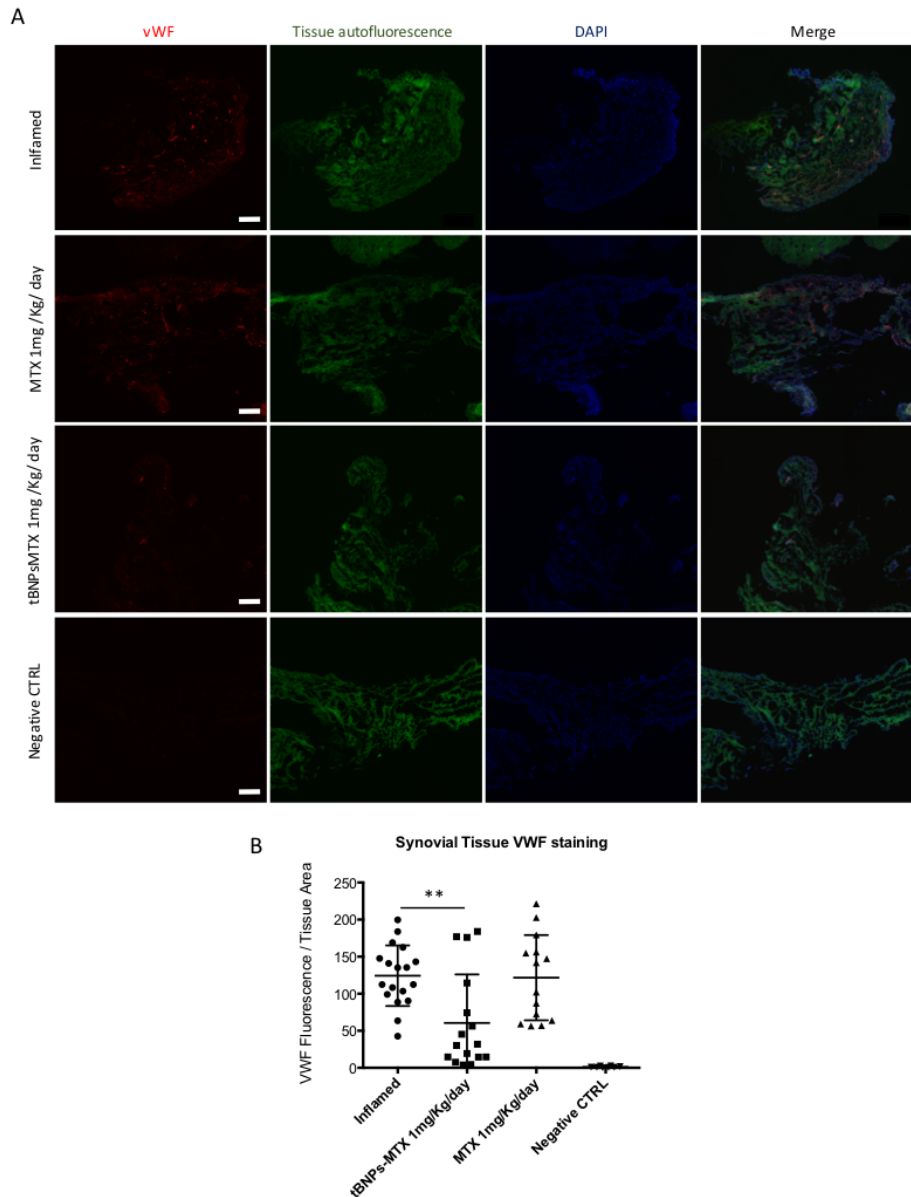


Figure 24: C3 staining of AIA rats' synovial tissues.

(A) Immunofluorescence staining for the C3 complement component on the inflamed synovial tissue (right knees) of rat treated with saline solution (first column), rats treated with tBNPs-MTX (second column) and rats treated with free MTX (third column). C3 has been stained in red and merged with nuclei stained with DAPI. Scale bar 100μm.

Going back to the target of the synovial peptide, it is known that it drives tBNPs on endothelial cells, releasing MTX inside them and interfering with the formation of new vessels. One possibility is that targeted nanoparticles allow the delivery of a sufficient amount of this cytotoxic drug and cause endothelial cell death.

Synovial tissues have been stained for the vWF in order to verify this hypothesis, analysing the number of the formed vessel (Figure 25 A). In this figure, four representative synovial tissues have been analysed: rats treated with saline solution, the synovial tissue of a healthy synovia (as a negative control), rats treated with both tBNPs-MTX and free MTX. It is evident that synovial tissue of tBNPs-MTX treated rats shows a reduced vWF staining, so a reduced number of blood vessels, compared with synovial tissues of control rats or rats treated with free MTX. Fluorescence intensity of vWF of the rats enrolled in the study have been quantified and summarized in the graph of the figure 25 B. The graph confirms a reduced vWF staining compared with control rats and rats treated with free MTX. This result strengthens our hypothesis by which MTX encapsulated into tBNPs interferes with the formation of new vessels in inflamed synovium. It is possible to speculate that the selective delivery of MTX to CD34+ cells in synovial tissue, which is expressed on precursors of endothelial cells, causes the death of these cells, reducing the possibility to develop new vessels in the inflamed synovial tissue. This process is mandatory for the leukocytes recruitment in synovial tissue and consequent progression of inflammation. The reduced number of vessels observed in the inflamed synovial tissues of rats treated with tBNPs may justify the decreased number of inflammatory cells such as PMN and, at the end, the reduction of the knee swelling observed in these animals (Figure 23 B and A).

**Figure 25: vWF staining in AIA rats' synovial tissues.**

(A) Four representative images obtained through the overlay of the vWF staining (red), tissue autofluorescence (green) and nuclei staining (DAPI). Each image is a large field obtained through the stitching of 9 images. In addition to the usual three groups of rats, as a negative control, a healthy synovial tissue has been used. Scale bar 200µm. (B) Mean fluorescence intensity of the vWF normalized for the tissue area has been determined by ImageJ software for each experimental group. For each synovial tissue 2/3 regions of interest (ROIs) of the large field images have been analysed. Number of ROIs analysed for each group: inflamed=18; 1mg/ Kg/ day of tBNPs-MTX=16; 1mg/ Kg/ day MTX= 14; negative CTRL=8. Statistical significance has been assessed through a parametric t-test. $P \leq 0.05 = *$; $P \leq 0.01 = **$.

5. Conclusion

Rheumatoid arthritis is a chronic autoimmune disease affecting joints due to the persistent inflammation of the synovial membrane, which leads to a condition of disability and pain. Despite the introduction of biological drugs, which improve patients' quality life, they are usually treated lifelong and true remission is rare. Moreover, biological drugs show several side effects for long term treatments and some patients do not respond to this kind of treatments. For these reasons MTX, belonging to the synthetic DMARDs class, is still the cornerstone of RA treatment because of its safe profile, effectiveness and low cost. However, some issues arise with MTX treatment due to the fact that 50% of patients, after 5 years have to discontinue the treatment because of inefficacy or side effects such as liver toxicity and bone marrow suppression. According to the ACR criteria, early diagnosis is essential for a successful management in order to treat patients as soon as possible avoiding late phase (disability) of the disease.

The attention of our group was recently focused on the development of a nanotechnological approach to treat and diagnose RA with a higher efficacy and specificity. This strategy is based on the use of polymeric biodegradable nanoparticles able to target in a specific manner the inflamed synovial tissue due to targeting molecules conjugated on the surface of these nanoparticles. Exploiting this strategy, their payload can be accumulated into the desired place avoiding toxic effects related to systemic administration.

In this research project, two different couples of nanoparticles have been produced: a couple of empty nanoparticles, with (tBNPs) and without (BNPs) the targeting molecule, and a couple of MTX loaded nanoparticles, with (tBNPs-MTX) and without (BNPs-MTX) the targeting molecule.

All different nanoparticles have been characterized by DLS, TEM, STEM and NanoTrack in order to assess their size distribution, diameter, PDI, charge and nanoparticles concentration. They showed an average diameter of about 150nm with a PDI of 0.3 and a slight negative charge of -6mV. These characteristics were designed for an ideal distribution in vivo, in particular the size is large enough to ensure high doses of the loaded compound and, at the same time, allow a good distribution within the body. Moreover, the low negative charge avoids the interaction with several positive basal membranes (like in kidneys and lungs) and in general with cells.

The biocompatibility of the shell's nanoparticles has been tested showing that empty nanoparticles, with and without the targeting molecule, did not show toxicity for cells. MTX

release has been measured demonstrating that 50% of the drug was still encapsulated into nanoparticles after 24h.

The importance of a targeting agent on nanoparticles' surface is still debated. Our data, obtained both *in vitro* and *in vivo* clearly evidenced the increased ability of tBNPs to selectively accumulate into inflamed synovial tissue. In particular, tBNPs showed a higher accumulation in the inflamed joints compared to BNPs in two different animal models.

Despite the differences seen in the animal models, it is evident that tBNPs are promising as a diagnostic delivery system able to potentially increase the accumulation of a diagnostic probe and, as a consequence, the sensitivity of several imaging techniques. Targeted nanobubbles through the synovial peptide will represent a potential probe for functional imaging using ultrasound, as well as targeted nanoparticles loaded with contrast agents may be useful in NMR or x-ray-based approaches.

The capacity of tBNP to accumulate in joints during the early phase of the inflammatory process, when no phenotypic evidence of the pathology is detectable, encourage our study to develop a diagnostic probe for early diagnosis. Moreover, the capacity to discriminate different degree of inflammation will provide the basis to use the same probe to follow the effectiveness of the therapy in use.

The core of the project was to demonstrate that tBNPs, which combine the active targeting with the nanoparticles features, could provide a new therapeutic approach through the selective accumulation of MTX in the inflamed synovial microenvironment. To reach this aim, tBNP-MTX efficacy has been first studied in CIA mouse model and then in AIA rat model. Results demonstrated that tBNPs-MTX showed similar outcome than free MTX, using the same total weekly dose but also reducing the dose of encapsulated MTX to 1/3, administering it once per week. Moreover, the therapeutic effects were also associated with a safe toxicological profile.

Part of this work has been dedicated to identifying the counterpart of the targeting molecule. Indeed, from the literature, it is known that the synovial homing peptide binds the microvasculature of the inflamed synovial tissue, although the bound molecule is not yet recognized. Co-staining immunofluorescence performed with the target molecule and markers of endothelial tissues evidenced that the target molecule localizes onto CD34+ cells. Cells expressing CD34 in synovial tissue are mainly progenitors of endothelial cells and this evidence was fundamental to first hypothesize and then demonstrate a different mechanism of action

of MTX once encapsulated into tBNPs. Due to the fact that nanoparticles impacted on endothelial cells, we speculate that MTX (initially isolated as a cytotoxic drug) could induce CD34+ cell death and, as a consequence, has an anti-neoangiogenic effect. On the contrary, free MTX usually plays its anti-inflammatory effect reducing the number of B and T cells and increasing adenine and adenosine into the extracellular space. The formation of new vessels is essential for leukocytes migration and synovial tissue infiltration; the reduction of leukocytes in synovial microenvironment brings to a reduction of the inflammatory process. This was particularly evident in an AIA rat model, where free MTX was ineffective. However, the formation of new vessels in synovial tissue was reduced using tBNP-MTX, preventing the onset of the pathology.

This work introduces an innovative approach to diagnose and treat RA, based on targeted polymeric nanoparticles able to deliver their payloads to the microvasculature of the inflamed synovial tissue. This nanotechnological system due to the active targeting shows enormous potential increasing sensitivity as a diagnostic tool and simultaneously enhancing therapeutic effects and reducing doses and related side effects. The focus of this study was to improve the management of patients affected by RA. However, several other articular pathologies, where neo-angiogenesis plays a pivotal role in the inflammatory process, can exploit the potential of tBNPs. Osteoarthritis is probably the first pathology where tBNPs can find application, indeed its treatment remains an unmet clinical need. Moreover, the ability of the targeting peptide to cross-react with mouse, rat and human inflamed synovial tissue suggest the possibility to extend the use of tBNPs to dogs and horses, in which articular disorders are common, in order to provide a new therapeutic approach and to collect several preclinical data before the first use in human.

6. References

- Abuchowski, a et al., 1977. Alteration of immunological properties of bovine serum albumin by covalent attachment of polyethylene glycol. *The Journal of biological chemistry*, 252(11), pp.3578–3581.
- Aceves-Avila, F.J. et al., 1998. Paleopathology in Osseous remains from the 16th century. A survey of rheumatic diseases. *Journal of Rheumatology*, 25(4), pp.776–782.
- Aggarwal, R. et al., 2009. Anti-citrullinated peptide antibody assays and their role in the diagnosis of rheumatoid arthritis. *Arthritis Care and Research*, 61(11), pp.1472–1483.
- Ahn, J.K. et al., 2008. Role of hypoxia-inducible factor-1 α in hypoxia-induced expressions of IL-8, MMP-1 and MMP-3 in rheumatoid fibroblast-like synoviocytes. *Rheumatology*, 47(6), pp.834–839.
- Ai, R. et al., 2016. Joint-specific DNA methylation and transcriptome signatures in rheumatoid arthritis identify distinct pathogenic processes. *Nature communications*, 7, p.11849.
- Aletaha, D. et al., 2010. 2010 Rheumatoid arthritis classification criteria: an American College of Rheumatology/European League Against Rheumatism collaborative initiative. *Arthritis Rheum*, 62(9), pp.2569–2581..
- Allen, J.B. et al., 1990. Rapid onset synovial inflammation and hyperplasia induced by transforming growth factor beta. *The Journal of experimental medicine*, 171(1), pp.231–47.
- Aragao-Santiago, L. et al., 2016. Compared in vivo toxicity in mice of lung delivered biodegradable and non-biodegradable nanoparticles. *Nanotoxicology*, 10(3), pp.292–302.
- Asahara, T., 1997. Isolation of Putative Progenitor Endothelial Cells for Angiogenesis. *Science*, 275(5302), pp.964–966.
- Asquith, D.L. et al., 2009. Animal models of rheumatoid arthritis. *European Journal of Immunology*, 39(8), pp.2040–2044.
- Banda, N.K. et al., 2006. Alternative complement pathway activation is essential for inflammation and joint destruction in the passive transfer model of collagen-induced arthritis. *Journal of immunology (Baltimore, Md. : 1950)*, 177(3), pp.1904–1912.
- Banda, N.K. et al., 2014. Essential role for the lectin pathway in collagen antibody-induced arthritis revealed through use of adenovirus programming complement inhibitor MAp44 expression. *Journal of immunology (Baltimore, Md. : 1950)*, 193(5), pp.2455–68.
- Banda, N.K. et al., 2007. Pathogenic Complement Activation in Collagen Antibody- Induced Arthritis in Mice Requires Amplification by the Alternative Pathway. *The Journal of*

- Immunology*, 179(6), pp.4101–4109.
- Banik, B.L., Fattah, P. & Brown, J.L., 2016. Polymeric nanoparticles: The future of nanomedicine. *Wiley Interdisciplinary Reviews: Nanomedicine and Nanobiotechnology*, 8(2), pp.271–299.
- Barenholz, Y., 2012. Doxil® - The first FDA-approved nano-drug: Lessons learned. *Journal of Controlled Release*, 160(2), pp.117–134.
- Bartok, B. & Firestein, G.S., 2011. Fibroblast-like synoviocytes: key effector cells in rheumatoid arthritis. *Immunol Rev.*, 233(1), pp.233–255.
- Beighton, P., Solomon, L. & Valkenburg, H. a, 1975. Rheumatoid arthritis in a rural South African Negro population. *Annals of the rheumatic diseases*, 34(2), pp.136–41.
- Benucci, M. et al., 2016. Costs associated with rheumatoid arthritis in Italy: past, present, and future. *ClinicoEconomics and outcomes research : CEOR*, 8, pp.33–41.
- Bergers, G., 2005. The role of pericytes in blood-vessel formation and maintenance. *Neuro-Oncology*, 7(4), pp.452–464.
- Bianco, A., Kostarelos, K. & Prato, M., 2011. Making carbon nanotubes biocompatible and biodegradable. *Chemical Communications*, 47(37), p.10182.
- Blanco, E., Shen, H. & Ferrari, M., 2015. Principles of nanoparticle design for overcoming biological barriers to drug delivery. *Nature Biotechnology*, 33(9), pp.941–951.
- Blüml, S. et al., 2011. Essential role of microRNA-155 in the pathogenesis of autoimmune arthritis in mice. *Arthritis and Rheumatism*, 63(5), pp.1281–1288.
- Boisseau, P. et al., 2005. *Vision Paper and a Basis for a Strategic Research Agenda for NanoMedicine*.
- Bosch, X., 2011. Dendrimers to treat rheumatoid arthritis. *ACS Nano*, 5(9), pp.6779–6785.
- Botsios, C., 2005. Safety of tumour necrosis factor and interleukin-1 blocking agents in rheumatic diseases. *Autoimmun Rev*, 4(3), pp.162–170.
- Bouta, E.M. et al., 2015. The role of the lymphatic system in inflammatory-erosive arthritis. *Seminars in Cell and Developmental Biology*, 38, pp.90–97.
- Brand, D.D., Latham, K.A. & Rosloniec, E.F., 2007. Collagen-induced arthritis. *Nature Protocols*, 2(5), pp.1269–1275.
- Brodeur, J.P. et al., 1991. Synovial fluid levels of complement SC5b-9 and fragment Bb are elevated in patients with rheumatoid arthritis. *Arthritis & Rheumatism*, 34(12), pp.1531–1537.

- Bugatti, S. et al., 2012. Assessment of synovitis to predict bone erosions in rheumatoid arthritis. *Therapeutic Advances in Musculoskeletal Disease*, 4(4), pp.235–244.
- Butler, D.M. et al., 1995. Modulation of proinflammatory cytokine release in rheumatoid synovial membrane cell cultures. Comparison of monoclonal anti TNF-alpha antibody with the interleukin-1 receptor antagonist. *Eur Cytokine Netw*, 6(4), pp.225–230.
- Campbell, J., Lowe, D. & Sleeman, M.A., 2011. Developing the next generation of monoclonal antibodies for the treatment of rheumatoid arthritis. *British Journal of Pharmacology*, 162(7), pp.1470–1484.
- Carver, L.A. & Schnitzer, J.E., 2003. Caveolae: mining little caves for new cancer targets. *Nature Reviews Cancer*, 3(8), pp.571–581.
- Cascão, R. et al., 2010. Neutrophils in rheumatoid arthritis: More than simple final effectors. *Autoimmunity Reviews*, 9(8), pp.531–535.
- Champion, J.A. & Mitragotri, S., 2006. Role of target geometry in phagocytosis. *Proceedings of the National Academy of Sciences of the United States of America*, 103(13), pp.4930–4.
- Chemin, K. et al., 2016. A Novel HLA-DRB1*10:01-Restricted T Cell Epitope from Citrullinated Type II Collagen Relevant to Rheumatoid Arthritis. *Arthritis and Rheumatology*, 68(5), pp.1124–1135.
- Chen, Y.F. et al., 2006. A systematic review of the effectiveness of adalimumab, etanercept and infliximab for the treatment of rheumatoid arthritis in adults and an economic evaluation of their cost-effectiveness. *Health Technol Assess*, 10(42), p.iii–iv, xi–xiii, 1-229.
- Cho, M.-L. et al., 2002. Cyclosporine inhibition of vascular endothelial growth factor production in rheumatoid synovial fibroblasts. *Arthritis and rheumatism*, 46(5), pp.1202–9.
- Consortium, T.W.T.C.C., 2007. Genome-wide association study of 14 000 cases of seven common diseases and 3 000 shared controls. *Nature*, 447(7145), pp.661–678.
- Cornish, A.L. et al., 2009. G-CSF and GM-CSF as therapeutic targets in rheumatoid arthritis. *Nature Reviews Rheumatology*, 5(10), pp.554–559.
- Danhier, F., Ansorena, E., et al., 2012. PLGA-based nanoparticles: An overview of biomedical applications. *Journal of Controlled Release*, 161(2), pp.505–522.
- Danhier, F., Pourcelle, V., et al., 2012. Targeting of tumor endothelium by RGD-grafted PLGA-nanoparticles. *Methods in Enzymology*, 508, pp.157–175.
- Danhier, F., Breton, A. Le & Préat, V., 2012. RGD-based strategies to target alpha(v) beta(3) integrin in cancer therapy and diagnosis. *Molecular Pharmaceutics*, 9(11), pp.2961–2973.

- Dans, L.F. et al., 1997. The prevalence of rheumatic diseases in a Filipino urban population: A WHO-ILAR COPCORD study. *Journal of Rheumatology*, 24(9), pp.1814–1819.
- Doherty, G.J. & McMahon, H.T., 2009. Mechanisms of Endocytosis. *Annual Review of Biochemistry*, 78(1), pp.857–902.
- Dowling, a et al., 2004. Nanoscience and nanotechnologies : opportunities and uncertainties. *London The Royal Society The Royal Academy of Engineering Report*, 46(July), pp.618–618.
- Drexler, K.E., 1986. Engines of Creation, The Coming Era of Nanotechnology. *Garden City*, 2017(1965), p.91109.
- Duque, G.A. & Descoteaux, A., 2014. Macrophage cytokines: Involvement in immunity and infectious diseases. *Frontiers in Immunology*, 5(OCT).
- Durigutto, P. et al., 2017. Targeted delivery of neutralizing anti-C5 antibody to renal endothelium prevents complement-dependent tissue damage. *Front. Immunol*, 8.
- Eatemadi, A. et al., 2014. Carbon nanotubes: properties, synthesis, purification, and medical applications. *Nanoscale Research Letters*, 9(1), p.393.
- Fang, C. et al., 2009. Functionalized nanoparticles with long-term stability in biological media. *Small*, 5(14), pp.1637–1641.
- Farokhzad, O.C. & Langer, R., 2009. Impact of nanotechnology on drug delivery. *ACS Nano*, 3(1), pp.16–20.
- Favalli, E.G. et al., 2012. The role of biologic agents in damage progression in rheumatoid arthritis: indirect comparison of data coming from randomized clinical trials. *Therapeutic Advances in Musculoskeletal Disease*, 4(4), pp.213–223.
- Ferrari, M., Onuoha, S.C. & Pitzalis, C., 2015. Trojan horses and guided missiles: targeted therapies in the war on arthritis. *Nature Reviews Rheumatology*, 11(6), pp.328–337.
- Firestein, G.S., 2013. Etiology and Pathogenesis of Rheumatoid Arthritis. *Kelley's Textbook of Rheumatology*, Ninth Edition, p.1059–1108.e5.
- Firestein, G.S., 2003. Evolving concepts of rheumatoid arthritis. *Nature*, 423(6937), pp.356–361.
- Firestein, G.S. et al., 1997. Somatic mutations in the p53 tumor suppressor gene in rheumatoid arthritis synovium. *Proceedings of the National Academy of Sciences of the United States of America*, 94(20), pp.10895–900.
- Fleischmann, R. et al., 2012. Placebo-Controlled Trial of Tofacitinib Monotherapy in

- Rheumatoid Arthritis. *New England Journal of Medicine*, 367(6), pp.495–507.
- Gabizon, a, Shmeeda, H. & Barenholz, Y., 2003. Pharmacokinetics of pegylated liposomal Doxorubicin: review of animal and human studies. *Clin.Pharmacokinet.*, 42(5), pp.419–436.
- Gabriel, S.E., 2008. Cardiovascular morbidity and mortality in rheumatoid arthritis. *The American journal of medicine*, 121(10 Suppl 1), pp.S9-14.
- Gerstner, C. et al., 2016. Functional and Structural Characterization of a Novel HLA-DRB1*04:01-Restricted α -Enolase T Cell Epitope in Rheumatoid Arthritis. *Frontiers in Immunology*, 7, p.494.
- Glantschnig, H. et al., 2003. M-CSF, TNFalpha and RANK ligand promote osteoclast survival by signaling through mTOR/S6 kinase. *Cell death and differentiation*, 10(10), pp.1165–1177.
- Gragnano, F. et al., 2017. The Role of von Willebrand Factor in Vascular Inflammation: From Pathogenesis to Targeted Therapy. *Mediators of Inflammation*, 2017.
- Gregersen, P.K., Silver, J. & Winchester, R.J., 1987. The shared epitope hypothesis. An approach to understanding the molecular genetics of susceptibility to rheumatoid arthritis. *Arthritis Rheum*, 30(11), pp.1205–1213.
- Griffiths, R.J., 1992. Characterisation and pharmacological sensitivity of antigen arthritis induced by methylated bovine serum albumin in the rat. *Agents Actions*, 35(1–2), pp.88–95.
- Hajishengallis, G., 2014. Periodontitis: from microbial immune subversion to systemic inflammation. *Nature Reviews Immunology*, 15(1), pp.30–44.
- Hamilton, A. et al., 2002. EORTC 10968: A phase I clinical and pharmacokinetic study of polyethylene glycol liposomal doxorubicin (Caelyx®, Doxil®) at a 6-week interval in patients with metastatic breast cancer. *Annals of Oncology*, 13(6), pp.910–918.
- Harush-Frenkel, O. et al., 2007. Targeting of nanoparticles to the clathrin-mediated endocytic pathway. *Biochemical and Biophysical Research Communications*, 353(1), pp.26–32.
- Harvey, J. et al., 1981. Rheumatoid arthritis in a Chippewa Band. I. Pilot screening study of disease prevalence. *Arthritis and rheumatism*, 24(5), pp.717–721.
- Hashizume, H. et al., 2000. Openings between defective endothelial cells explain tumor vessel leakiness. *American Journal of Pathology*, 156(4), pp.1363–1380.
- Helmick, C.G. et al., 2008. Estimates of the prevalence of arthritis and other rheumatic conditions in the United States. Part I. *Arthritis and Rheumatism*, 58(1), pp.15–25.

- Hu, C.-M.J. et al., 2011. Erythrocyte membrane-camouflaged polymeric nanoparticles as a biomimetic delivery platform. *Proceedings of the National Academy of Sciences*, 108(27), pp.10980–10985.
- Hu, C.M.J. & Zhang, L., 2012. Nanoparticle-based combination therapy toward overcoming drug resistance in cancer. *Biochemical Pharmacology*, 83(8), pp.1104–1111.
- Hu, Y. et al., 2013. Advances in research on animal models of rheumatoid arthritis. *Clin Rheumatol*, 32(2), pp.161–165.
- Huang, L. & Guo, S., 2011. Nanoparticles escaping RES and endosome: Challenges for siRNA delivery for cancer therapy. *Journal of Nanomaterials*, 2011.
- Huang, X. & Brazel, C.S., 2001. On the importance and mechanisms of burst release in matrix-controlled drug delivery systems. *Journal of Controlled Release*, 73(2–3), pp.121–136.
- Innala, L. et al., 2014. Age at onset determines severity and choice of treatment in early rheumatoid arthritis: a prospective study. *Arthritis research & therapy*, 16(2), p.R94.
- Isaacs, J.D., 2010. The changing face of rheumatoid arthritis: sustained remission for all? *Nat Rev Immunol*, 10(8), pp.605–611.
- Ivashkiv, L.B. & Hu, X., 2003. The JAK/STAT pathway in rheumatoid arthritis: Pathogenic or protective? *Arthritis and Rheumatism*, 48(8), pp.2092–2096.
- James, E.A. et al., 2010. HLA-DR1001 presents “altered-self” peptides derived from joint-associated proteins by accepting citrulline in three of its binding pockets. *Arthritis and Rheumatism*, 62(10), pp.2909–2918.
- Jimenez-Boj, E. et al., 2005. Interaction between Synovial Inflammatory Tissue and Bone Marrow in Rheumatoid Arthritis. *The Journal of Immunology*, 175(4), pp.2579–2588.
- Jing, F. & Choi, E.Y., 2016. Potential of Cells and Cytokines/Chemokines to Regulate Tertiary Lymphoid Structures in Human Diseases. *Immune Network*, 16(5), p.271.
- Johnston-Cox, H.A., Koupnova, M. & Ravid, K., 2012. A2 adenosine receptors and vascular pathologies. *Arteriosclerosis, Thrombosis, and Vascular Biology*, 32(4), pp.870–878.
- Jokerst, J. V et al., 2011. Nanoparticle PEGylation for imaging and therapy. *Nanomedicine*, 6(4), pp.715–728.
- Jung, E.-G. et al., 2015. Brazilin isolated from Caesalpinia sappan L. inhibits rheumatoid arthritis activity in a type-II collagen induced arthritis mouse model. *BMC Complementary and Alternative Medicine*, 15(1), p.124.
- Kelley, L.A. et al., 2015. The Phyre2 web portal for protein modeling, prediction and analysis.

- Nature Protocols*, 10(6), pp.845–858.
- Khachigian, L.M., 2006. Collagen antibody-induced arthritis. *Nature Protocols*, 1(5), pp.2512–2516.
- Kim, B.Y.S., Rutka, J.T. & Chan, W.C.W., 2010. Nanomedicine. *New England Journal of Medicine*, 363(25), pp.2434–2443.
- Kim, S.J., Park, Y. & Hong, H.J., 2005. Antibody engineering for the development of therapeutic antibodies. *Mol Cells*, 20(1), pp.17–29.
- Klareskog, L. et al., 1983. Role of T lymphocytes in collagen II induced arthritis in rats. *Clin Exp Immunol*, 51(1), pp.117–125.
- Klasen, I.S. et al., 1986. Joint inflammations and flare-up reactions in mice induced by a helper T cell clone. *Agents Actions*, 19(5–6), pp.331–334.
- Kohler, G. & Milstein, C., 1975. Continuous cultures of fused cells secreting antibody of predefined specificity. *Nature*, 256(5517), pp.495–497.
- Konisti, S., Kiriakidis, S. & Paleolog, E.M., 2013. Angiogenesis in rheumatoid arthritis. In *Angiogenesis and Vascularisation: Cellular and Molecular Mechanisms in Health and Diseases*. pp. 339–365.
- Krause, D.S. et al., 1996. CD34: structure, biology, and clinical utility. *Blood*, 87(1), pp.1–13.
- Kuhn, K.A. et al., 2006. Antibodies against citrullinated proteins enhance tissue injury in experimental autoimmune arthritis. *Journal of Clinical Investigation*, 116(4), pp.961–973.
- Kumari, A., Yadav, S.K. & Yadav, S.C., 2010. Biodegradable polymeric nanoparticles based drug delivery systems. *Colloids and Surfaces B: Biointerfaces*, 75(1), pp.1–18.
- Lainer-Carr, D. & Brahn, E., 2007. Angiogenesis inhibition as a therapeutic approach for inflammatory synovitis. *Nature clinical practice. Rheumatology*, 3(8), pp.434–42.
- Lange, F., 2005. Methotrexate ameliorates T cell dependent autoimmune arthritis and encephalomyelitis but not antibody induced or fibroblast induced arthritis. *Annals of the Rheumatic Diseases*, 64(4), pp.599–605.
- Lee, E.B. et al., 2014. Tofacitinib versus Methotrexate in Rheumatoid Arthritis. *New England Journal of Medicine*, 370(25), pp.2377–2386.
- Lee, L. et al., 2002. Identification of synovium-specific homing peptides by in vivo phage display selection. *Arthritis Rheum*, 46(8), pp.2109–2120.
- Lee, S.M. et al., 2013. Targeted chemo-photothermal treatments of rheumatoid arthritis using gold half-shell multifunctional nanoparticles. *ACS Nano*, 7(1), pp.50–57.

- Lim, A.Y.N., Gaffney, K. & Scott, D.G.I., 2005. Methotrexate-induced pancytopenia: Serious and under-reported? Our experience of 25 cases in 5 years. *Rheumatology*, 44(8), pp.1051–1055.
- Lin, J. et al., 2012. Cyr61 Induces IL-6 Production by Fibroblast-like Synoviocytes Promoting Th17 Differentiation in Rheumatoid Arthritis. *The Journal of Immunology*, 188(11), pp.5776–5784.
- Linton, S.M. & Morgan, B.P., 1999. Complement activation and inhibition in experimental models of arthritis. *Mol Immunol*, 36(13–14), pp.905–914.
- Liu, Y. et al., 2013. Epigenome-wide association data implicate DNA methylation as an intermediary of genetic risk in rheumatoid arthritis. *Nature biotechnology*, 31(2), pp.142–7.
- Lobo, E.D. & Balthasar, J.P., 2003. Pharmacokinetic-pharmacodynamic modeling of methotrexate-induced toxicity in mice. *Journal of Pharmaceutical Sciences*, 92(8), pp.1654–1664.
- LoBuglio, A.F. et al., 1989. Mouse/human chimeric monoclonal antibody in man: kinetics and immune response. *Proc Natl Acad Sci U S A*, 86(11), pp.4220–4224.
- Longmire, M., Choyke, P.L. & Kobayashi, H., 2008. Clearance properties of nano-sized particles and molecules as imaging agents: considerations and caveats. *Nanomedicine (London, England)*, 3(5), pp.703–17.
- Lu, X. & Kang, Y., 2010. Hypoxia and hypoxia-inducible factors (HIFs): master regulators of metastasis. *Clinical cancer research : an official journal of the American Association for Cancer Research*, 16(2), pp.5928–5935.
- Ma, X. & Xu, S., 2013. TNF inhibitor therapy for rheumatoid arthritis. *Biomedical reports*, 1(2), pp.177–184.
- MacGregor, A.J. et al., 2000. Characterizing the quantitative genetic contribution to rheumatoid arthritis using data from twins. *Arthritis & Rheumatism*, 43(1), pp.30–37.
- Macor, P. et al., 2012. Treatment of experimental arthritis by targeting synovial endothelium with a neutralizing recombinant antibody to C5. *Arthritis Rheum*, 64(8), pp.2559–2567.
- Maeda, H., Nakamura, H. & Fang, J., 2013. The EPR effect for macromolecular drug delivery to solid tumors: Improvement of tumor uptake, lowering of systemic toxicity, and distinct tumor imaging in vivo. *Advanced Drug Delivery Reviews*, 65(1), pp.71–79.
- Mahapatro, A. & Singh, D.K., 2011. Biodegradable nanoparticles are excellent vehicle for site

- directed in-vivo delivery of drugs and vaccines. *Journal of Nanobiotechnology*, 9(1), p.55.
- Makrygiannakis, D. et al., 2008. Smoking increases peptidylarginine deiminase 2 enzyme expression in human lungs and increases citrullination in BAL cells. *Annals of the rheumatic diseases*, 67(10), pp.1488–92.
- Malmström, V., Catrina, A.I. & Klareskog, L., 2016. The immunopathogenesis of seropositive rheumatoid arthritis: from triggering to targeting. *Nature Reviews Immunology*, 17(1), pp.60–75.
- Marrelli, A. et al., 2011. Angiogenesis in rheumatoid arthritis: A disease specific process or a common response to chronic inflammation? *Autoimmunity Reviews*, 10(10), pp.595–598.
- Matsumura, Y. & Maeda, H., 1986. A New Concept for Macromolecular Therapeutics in Cancer Chemotherapy: Mechanism of Tumoritropic Accumulation of Proteins and the Antitumor Agent Smancs. *Cancer Research*, 46(8), pp.6387–6392.
- McInnes, I.B. & Schett, G., 2011a. The pathogenesis of rheumatoid arthritis. *N Engl J Med*, 365(23), pp.2205–2219.
- McInnes, I.B. & Schett, G., 2011b. The pathogenesis of rheumatoid arthritis. *N Engl J Med*, 365(23), pp.2205–2219.
- Melnyk, V.O. et al., 1990. Synoviocytes synthesize, bind, and respond to basic fibroblast growth factor. *Arthritis & Rheumatism*, 33(4), pp.493–500.
- Mikuls, T.R. et al., 2009. Antibody responses to *Porphyromonas gingivalis* (*P. gingivalis*) in subjects with rheumatoid arthritis and periodontitis. *International Immunopharmacology*, 9(1), pp.38–42.
- Miossec, P., Korn, T. & Kuchroo, V.K., 2009. Interleukin-17 and Type 17 Helper T Cells. *New England Journal of Medicine*, 361(9), pp.888–898.
- Moghimi, S.M. & Patel, H.M., 1998. Serum-mediated recognition of liposomes by phagocytic cells of the reticuloendothelial system - The concept of tissue specificity. *Advanced Drug Delivery Reviews*, 32(1–2), pp.45–60.
- Mor, A., Abramson, S.B. & Pillinger, M.H., 2005. The fibroblast-like synovial cell in rheumatoid arthritis: A key player in inflammation and joint destruction. *Clinical Immunology*, 115(2), pp.118–128.
- Moran, N., 2005. *An ESF – European Medical Research Councils (EMRC) Forward Look report*,
- Morel, J.C.M. et al., 2002. Signal transduction pathways involved in rheumatoid arthritis synovial fibroblast interleukin-18-induced vascular cell adhesion molecule-1 expression.

- The Journal of biological chemistry, 277(38), pp.34679–34691.
- Mould, A.W. et al., 2003. Vegfb gene knockout mice display reduced pathology and synovial angiogenesis in both antigen-induced and collagen-induced models of arthritis. *Arthritis and Rheumatism*, 48(9), pp.2660–2669.
- Mundy, G.R., 2007. Osteoporosis and Inflammation. *Nutrition Reviews*, 65(SUPPL.3).
- Murthy, S.K., 2007. Nanoparticles in modern medicine: state of the art and future challenges. *International journal of nanomedicine*, 2(2), pp.129–41.
- Nadkarni, S., Mauri, C. & Ehrenstein, M.R., 2007. Anti-TNF-alpha therapy induces a distinct regulatory T cell population in patients with rheumatoid arthritis via TGF-beta. *J Exp Med*, 204(1), pp.33–39.
- Nehoff, H. et al., 2014. Nanomedicine for drug targeting: Strategies beyond the enhanced permeability and retention effect. *International Journal of Nanomedicine*, 9(1), pp.2539–2555.
- Nguyen, V.H. & Lee, B.J., 2017. Protein corona: A new approach for nanomedicine design. *International Journal of Nanomedicine*, 12, pp.3137–3151.
- Oh, P. et al., 2007. Live dynamic imaging of caveolae pumping targeted antibody rapidly and specifically across endothelium in the lung. *Nature biotechnology*, 25(3), pp.327–337.
- Olafsen, T. & Wu, A.M., 2010. Antibody vectors for imaging. *Semin Nucl Med*, 40(3), pp.167–181.
- Onuoha, S.C. et al., 2015. Rational Design of Antirheumatic Prodrugs Specific for Sites of Inflammation. *Arthritis & Rheumatology*, 67(10), pp.2661–2672.
- Le Ouay, B. & Stellacci, F., 2015. Antibacterial activity of silver nanoparticles: A surface science insight. *Nano Today*, 10(3), pp.339–354.
- Pablos, J.L. et al., 2003. Synoviocyte-Derived CXCL12 Is Displayed on Endothelium and Induces Angiogenesis in Rheumatoid Arthritis. *The Journal of Immunology*, 170(4), pp.2147–2152.
- Padyukov, L. et al., 2004. A gene-environment interaction between smoking and shared epitope genes in HLA-DR provides a high risk of seropositive rheumatoid arthritis. *Arthritis and Rheumatism*, 50(10), pp.3085–3092.
- Palframan, R. et al., 2009. Use of biofluorescence imaging to compare the distribution of certolizumab pegol, adalimumab, and infliximab in the inflamed paws of mice with collagen-induced arthritis. *Journal of Immunological Methods*, 348(1–2), pp.36–41.
- Pandita, D. et al., 2014. Dendrimers in drug delivery and targeting: Drug-dendrimer

- interactions and toxicity issues. *Journal of Pharmacy and Bioallied Sciences*, 6(3), p.139.
- Parodi, A. et al., 2012. Synthetic nanoparticles functionalized with biomimetic leukocyte membranes possess cell-like functions. *Nature Nanotechnology*, 8(1), pp.61–68.
- Pasut, G. & Veronese, F.M., 2012. State of the art in PEGylation: The great versatility achieved after forty years of research. *Journal of Controlled Release*, 161(2), pp.461–472.
- Pattni, B.S., Chupin, V. V. & Torchilin, V.P., 2015. New Developments in Liposomal Drug Delivery. *Chemical Reviews*, 115(19), pp.10938–10966.
- Pearson, C.M., 1956. Studies of polyarthritis and other lesions induced in rats by injection of mycobacterial adjuvant. I. General clinical and pathologic characteristics and some modifying factors. *Arthritis & Rheumatism*, 2(5).
- Peer, D. et al., 2007. Nanocarriers as an emerging platform for cancer therapy. *Nature Nanotechnology*, 2(12), pp.751–760.
- Peichev, M. et al., 2000. Expression of VEGFR-2 and AC133 by circulating human CD34(+) cells identifies a population of functional endothelial precursors. *Blood*, 95(3), pp.952–958.
- Perlman, H. et al., 2000. Bcl-2 Expression in Synovial Fibroblasts Is Essential for Maintaining Mitochondrial Homeostasis and Cell Viability. *J. Immunol.*, 164(10), pp.5227–5235.
- Perlman, H., Pagliari, L.J. & Volin, M. V, 2001. Regulation of apoptosis and cell cycle activity in rheumatoid arthritis. *Current molecular medicine*, 1(5), pp.597–608.
- Phillips, M.A., Gran, M.L. & Peppas, N.A., 2010. Targeted nanodelivery of drugs and diagnostics. *Nano Today*, 5(2), pp.143–159.
- Del Puente, a et al., 1989. High incidence and prevalence of rheumatoid arthritis in Pima Indians. *American journal of epidemiology*, 129(6), pp.1170–1178.
- Pusztaszeri, M.P., Seelentag, W. & Bosman, F.T., 2006. Immunohistochemical expression of endothelial markers CD31, CD34, von Willebrand factor, and Fli-1 in normal human tissues. *Immunohistochemical expression of endothelial markers CD31, CD34, von Willebrand factor, and Fli-1 in normal human tissues*, 54(4), pp.385–95.
- Raatz, Y. et al., 2012. Gene expression profiling and functional analysis of angiogenic markers in murine collagen-induced arthritis. *Arthritis Research & Therapy*, 14(4), p.R169.
- Radner, H. et al., 2014. Performance of the 2010 ACR/EULAR classification criteria for rheumatoid arthritis: a systematic literature review. *Annals of the Rheumatic Diseases*, 73(1), pp.114–123.
- Rangel-Moreno, J. et al., 2006. Inducible bronchus-associated lymphoid tissue (iBALT) in

- patients with pulmonary complications of rheumatoid arthritis. *Journal of Clinical Investigation*, 116(12), pp.3183–3194.
- Rau, R., 2002. Adalimumab (a fully human anti-tumour necrosis factor alpha monoclonal antibody) in the treatment of active rheumatoid arthritis: the initial results of five trials. *Annals of the rheumatic diseases*, 61 Suppl 2, p.ii70-3.
- Raychaudhuri, S. et al., 2012. Five amino acids in three HLA proteins explain most of the association between MHC and seropositive rheumatoid arthritis. *Nature genetics*, 44(3), pp.291–6.
- Reynisdottir, G. et al., 2014. Structural changes and antibody enrichment in the lungs are early features of anti-citrullinated protein antibody-positive rheumatoid arthritis. *Arthritis and Rheumatology*, 66(1), pp.31–39.
- Richards, D.A., Maruani, A. & Chudasama, V., 2017. Antibody fragments as nanoparticle targeting ligands: a step in the right direction. *Chem. Sci.*, 8(1), pp.63–77.
- Rieck, M. et al., 2007. Genetic variation in PTPN22 corresponds to altered function of T and B lymphocytes. *Journal of immunology (Baltimore, Md : 1950)*, 179(7), pp.4704–4710.
- Romao, V.C. et al., 2014. Three decades of low-dose methotrexate in rheumatoid arthritis: Can we predict toxicity? *Immunologic Research*, 60(2–3), pp.289–310.
- Rombouts, Y. et al., 2015. Anti-citrullinated protein antibodies acquire a pro-inflammatory Fc glycosylation phenotype prior to the onset of rheumatoid arthritis. *Annals of the rheumatic diseases*, 74(1), pp.234–41.
- Rothschild, B.M., Turner, K.R. & DeLuca, M.A., 1988. Symmetrical erosive peripheral polyarthritis in the Late Archaic Period of Alabama. *Science (New York, N.Y.)*, 241(4872), pp.1498–1501.
- Salmaso, S. & Caliceti, P., 2013. Stealth properties to improve therapeutic efficacy of drug nanocarriers. *Journal of drug delivery*, 2013, p.374252.
- Sanna, V., Pala, N. & Sechi, M., 2014. Targeted therapy using nanotechnology: Focus on cancer. *International Journal of Nanomedicine*, 9(1), pp.467–483.
- Scally, S.W. et al., 2013. A molecular basis for the association of the HLA-DRB1 locus, citrullination, and rheumatoid arthritis. *The Journal of experimental medicine*, 210(12), pp.2569–82.
- Schett, G. & Teitelbaum, S.L., 2009. Osteoclasts and Arthritis. *J Bone Miner Res*, 24(7), pp.1142–1146.

- Schroeder Jr., H.W. & Cavacini, L., 2010. Structure and function of immunoglobulins. *J Allergy Clin Immunol*, 125(2 Suppl 2), pp.S41-52.
- Schroff, R.W. et al., 1985. Human anti-murine immunoglobulin responses in patients receiving monoclonal antibody therapy. *Cancer Res*, 45(2), pp.879–885.
- Scott, D.L. & Kingsley, G.H., 2006. Tumor necrosis factor inhibitors for rheumatoid arthritis. *N Engl J Med*, 355(7), pp.704–712.
- Scott, D.L., Wolfe, F. & Huizinga, T.W., 2010. Rheumatoid arthritis. [Review]. *Lancet*, 376(England PT-Journal Article PT-Research Support, Non-U.S. Gov't PT-Review NO-(United Kingdom Arthritis Research UK) LG-English DC-20100927), pp.1094–1108.
- Seyler, T.M. et al., 2005. BLyS and APRIL in rheumatoid arthritis. *Journal of Clinical Investigation*, 115(11), pp.3083–3092.
- Shichikawa, K. et al., 1999. Changes in the incidence and prevalence of rheumatoid arthritis in Kamitonda, Wakayama, Japan, 1965-1996. *Annals of the rheumatic diseases*, 58(12), pp.751–6.
- Shin, J.M. et al., 2014. A hyaluronic acid–methotrexate conjugate for targeted therapy of rheumatoid arthritis. *Chemical Communications*, 50(57), p.7632.
- Shinde, C.G. et al., 2014. Methotrexate: A Gold Standard for Treatment of Rheumatoid Arthritis. *Journal of Pain & Palliative Care Pharmacotherapy*, 28(4), pp.351–358.
- Sidney, L.E. et al., 2014. Concise review: Evidence for CD34 as a common marker for diverse progenitors. *Stem Cells*, 32(6), pp.1380–1389.
- Silman, A.J. et al., 1993. Absence of rheumatoid arthritis in a rural Nigerian population. *Journal of Rheumatology*, 20(4), pp.618–622.
- Silman, A.J. et al., 1993. Twin concordance rates for rheumatoid arthritis: results from a nationwide study. *Br J Rheumatol*, 32(10), pp.903–907.
- Silman, A.J., Newman, J. & MacGregor, A.J., 1996. Cigarette smoking increases the risk of rheumatoid arthritis. Results from a nationwide study of disease-discordant twins. *Arthritis Rheum.*, 39(5), pp.732–5.
- Simon, L.C. & Sabliov, C.M., 2014. The effect of nanoparticle properties, detection method, delivery route and animal model on poly(lactic-co-glycolic) acid nanoparticles biodistribution in mice and rats. *Drug Metabolism Reviews*, 46(2), pp.128–141.
- Sjöberg, A. et al., 2005. The extracellular matrix and inflammation: Fibromodulin activates the classical pathway of complement by directly binding C1q. *Journal of Biological Chemistry*,

- 280(37), pp.32301–32308.
- Smijs, T.G. & Pavel, S., 2011. Titanium dioxide and zinc oxide nanoparticles in sunscreens: Focus on their safety and effectiveness. *Nanotechnology, Science and Applications*, 4(1), pp.95–112.
- Smolen, J.S. et al., 2007. New therapies for treatment of rheumatoid arthritis. *Lancet*, 370(9602), pp.1861–1874.
- Smolen, J.S., Aletaha, D. & McInnes, I.B., 2016. Rheumatoid arthritis. *The Lancet*, 388(10055), pp.2023–2038.
- Stahl, E.A. et al., 2010. Genome-wide association study meta-analysis identifies seven new rheumatoid arthritis risk loci. *Nature genetics*, 42(6), pp.508–14.
- Steichen, S.D., Caldorera-Moore, M. & Peppas, N.A., 2013. A review of current nanoparticle and targeting moieties for the delivery of cancer therapeutics. *European Journal of Pharmaceutical Sciences*, 48(3), pp.416–427.
- Stolt, P. et al., 2010. Silica exposure among male current smokers is associated with a high risk of developing ACPA-positive rheumatoid arthritis. *Annals of the rheumatic diseases*, 69(6), pp.1072–6.
- Storgard, C.M. et al., 1999. Decreased angiogenesis and arthritic disease in rabbits treated with an alphavbeta3 antagonist. *Journal of Clinical Investigation*, 103(1), pp.47–54.
- Sugiyama, D. et al., 2010. Impact of smoking as a risk factor for developing rheumatoid arthritis: a meta-analysis of observational studies. *Annals of the Rheumatic Diseases*, 69(1), pp.70–81.
- Suwannalai, P. et al., 2014. Low-avidity anticitrullinated protein antibodies (ACPA) are associated with a higher rate of joint destruction in rheumatoid arthritis. *Annals of the Rheumatic Diseases*, 73(1), pp.270–276.
- Swaak, A.J.G. et al., 1987. An analysis of the levels of complement components in the synovial fluid in rheumatic diseases. *Clinical Rheumatology*, 6(3), pp.350–357.
- Symmons, D. et al., 2002. The prevalence of rheumatoid arthritis in the United Kingdom: new estimates for a new century. *Rheumatology (Oxford, England)*, 41(7), pp.793–800.
- Szekanecz, Z. et al., 2009. Chemokines and angiogenesis in rheumatoid arthritis. *Frontiers in bioscience (Elite edition)*, 1, pp.44–51.
- Szekanecz, Z. & Koch, A.E., 2008. Vascular involvement in rheumatic diseases: “vascular rheumatology.” *Arthritis Research & Therapy*, 10(5), p.224.

- Taneja, V. et al., 2007. New humanized HLA-DR4-transgenic mice that mimic the sex bias of rheumatoid arthritis. *Arthritis and Rheumatism*, 56(1), pp.69–78.
- Taniguchi, N. & Others, 1974. On the basic concept of nanotechnology. *Proc. Intl. Conf. Prod. Eng. Tokyo, Part II, Japan Society of Precision Engineering*, pp.18–23.
- Tian, H. & Cronstein, B.N., 2007. Understanding the mechanisms of action of methotrexate: Implications for the treatment of rheumatoid arthritis. *Bulletin of the NYU Hospital for Joint Diseases*, 65(3), pp.168–173.
- Timmer, T.C.G. et al., 2007. Inflammation and ectopic lymphoid structures in rheumatoid arthritis synovial tissues dissected by genomics technology: Identification of the interleukin-7 signaling pathway in tissues with lymphoid neogenesis. *Arthritis and Rheumatism*, 56(8), pp.2492–2502.
- Todesco S, G.P.F., 2002. *Malattie Reumatiche*,
- Tolboom, T.C.A. et al., 2002. Invasive properties of fibroblast-like synoviocytes: correlation with growth characteristics and expression of MMP-1, MMP-3, and MMP-10. *Annals of the rheumatic diseases*, 61(11), pp.975–80.
- Too, C.L. et al., 2016. Occupational exposure to textile dust increases the risk of rheumatoid arthritis: results from a Malaysian population-based case-control study. *Annals of the rheumatic diseases*, 75(6), pp.997–1002.
- Toumey, C., 2009. Plenty of room, plenty of history. *Nature nanotechnology*, 4(12), pp.783–784.
- Trentham, D.E., Townes, A.S. & Kang, A.H., 1977. Autoimmunity to type II collagen an experimental model of arthritis. *J Exp Med*, 146(3), pp.857–868.
- Trouw, L.A., Pickering, M.C. & Blom, A.M., 2017. The complement system as a potential therapeutic target in rheumatic disease. *Nature reviews. Rheumatology*.
- Ulery, B.D., Nair, L.S. & Laurencin, C.T., 2011. Biomedical applications of biodegradable polymers. *Journal of Polymer Science, Part B: Polymer Physics*, 49(12), pp.832–864.
- van Vollenhoven, R.F. et al., 2012. Tofacitinib or Adalimumab versus Placebo in Rheumatoid Arthritis. *New England Journal of Medicine*, 367(6), pp.508–519.
- van Vollenhoven, R.F., 2009. Treatment of rheumatoid arthritis: state of the art 2009. *Nature Reviews Rheumatology*, 5(10), pp.531–541.
- Vries, M.H.M. et al., 2015. CXCL1 promotes arteriogenesis through enhanced monocyte recruitment into the peri-collateral space. *Angiogenesis*, 18(2), pp.163–171.

- Wang, Z. et al., 2000. Universal PCR amplification of mouse immunoglobulin gene variable regions: the design of degenerate primers and an assessment of the effect of DNA polymerase 3' to 5' exonuclease activity. *J Immunol Methods*, 233(1–2), pp.167–177.
- Wegner, N. et al., 2010. Peptidylarginine deiminase from *Porphyromonas gingivalis* citrullinates human fibrinogen and α-enolase: Implications for autoimmunity in rheumatoid Arthritis. *Arthritis and Rheumatism*, 62(9), pp.2662–2672.
- Whittle, S.L. & Hughes, R.A., 2004. Folate supplementation and methotrexate treatment in rheumatoid arthritis: a review. *Rheumatology (Oxford, England)*, 43(3), pp.267–71.
- Williams, A.S. et al., 1996. A single intra-articular injection of liposomally conjugated methotrexate suppresses joint inflammation in rat antigen-induced arthritis. *British journal of rheumatology*, 35(8), pp.719–24.
- Williams, A.S., 2001. Amelioration of rat antigen-induced arthritis by liposomally conjugated methotrexate is accompanied by down-regulation of cytokine mRNA expression. *Rheumatology*, 40(4), pp.375–383.
- Williams, R.O., Feldmann, M. & Maini, R.N., 1992. Anti-tumor necrosis factor ameliorates joint disease in murine collagen-induced arthritis. *Proceedings of the National Academy of Sciences*, 89(20), pp.9784–9788.
- Woodruff, T.M. et al., 2002. Antiarthritic activity of an orally active C5a receptor antagonist against antigen-induced monarticular arthritis in the rat. *Arthritis and Rheumatism*, 46(9), pp.2476–2485.
- Xu, W., Ling, P. & Zhang, T., 2013. Polymeric micelles, a promising drug delivery system to enhance bioavailability of poorly water-soluble drugs. *Journal of Drug Delivery*, 2013.
- Yamashita, A. et al., 2002. Fibroblast growth factor-2 determines severity of joint disease in adjuvant-induced arthritis in rats. *J Immunol*, 168(1), pp.450–457.
- Yameen, B. et al., 2014. Insight into nanoparticle cellular uptake and intracellular targeting. *Journal of Controlled Release*, 190, pp.485–499.
- Zeng, Q., Huang, S. & Chen, R., 1997. [10-year epidemiological study on rheumatic diseases in Shantou area]. *Zhonghua Nei Ke Za Zhi*, 36(3), pp.193–197.
- ZOLTÁN SZEKANECZ, TIMEA BESENYEI, GYÖRGY PARAGH, and A.E.K., 2009. Angiogenesis in rheumatoid arthritis. *Autoimmunity*, 42(7), pp.563–573.
- Zupan, J., Jeras, M. & Marc, J., 2013. Osteoimmunology and the influence of pro-inflammatory cytokines on osteoclasts. *Biochimia Medica*, 23(1), pp.43–63.

Acknowledgements

I would like to thank my mentor Paolo Macor Ph.D., who gave me the possibility to work in his laboratory allowing me to work as best I could. I thank also Professor Daniele Sblattero for his help and support.

Surely, I have to thank all the people working in this lab, it has been a pleasure to share this time with you.

I would like to thank Professor Jessica Bertrand for giving me the opportunity to spend part of this work in her laboratory at the University Hospital of Magdeburg, Experimental Orthopaedics Laboratory. Many thanks also to all the people in her laboratory.

Once again, I would like to thank:

Professor Claudio Tripodo and Beatrice Belmonte, who collaborated for the histological analyses; Stefania Biffi, who helped us with the study of biodistribution in rats; Professor Enzo Terreno, Paola Bardini and Giada Marini, who collaborated for the study of biodistribution in mice; Sabine Pietkiewicz for her kind help with the Imaging Flow Cytometer analysis; Professor Gabriele Pozzato, who collaborated for the blood analysis; Romina Oliva, who collaborated with the study of 3D modelling; Enrico Rampazzo for his help with TEM images and Annalisa Marcuzzi, who collaborated for the multiplex cytokine analysis.

